Contingency Analysis for Coupled Power-Water Networks

by

Brandon T. Gorman

A Dissertation Presented in Partial Fulfillment
of the Requirements for the Degree
Doctor of Philosophy

Approved April 2020 by the
Graduate Supervisory Committee:

Nathan Johnson, Chair
Thomas Seager
Mikhail Chester

ARIZONA STATE UNIVERSITY

May 2020

ABSTRACT

A mathematical approach was developed to evaluate the resilience of coupled power-water networks using a variant of contingency analysis adapted from electric transmission studies. In particular, the “what if” scenarios explored in power systems research were extended and applied for coupled power-water network research by evaluating how stressors and failures in the water network can propagate across system boundaries and into the electric network. Reduction in power system contingency reserves was the metric for determining violation of N-1 contingency reliability. Geospatial considerations were included using high-resolution, publicly available Geographic Information System data on infrastructure in the Phoenix Metropolitan Area that was used to generate a power network with 599 transmission lines and total generation capacity of 18.98 GW and a water network with 2,624 water network lines and capacity to serve up to 1.72M GPM of surface water. The steady-state model incorporated operating requirements for the power network—e.g., contingency reserves—and the water network—e.g., pressure ranges—while seeking to meet electric load and water demand. Interconnections developed between the infrastructures demonstrated how alternations to the system state and/or configuration of one network affect the other network, with results demonstrated through co-simulation of the power network and water network using OpenDSS and EPANET, respectively. Results indicate four key findings that help operators understand the interdependent behavior of the coupled power-water network: (i) two water failure scenarios (water flowing out of Waddell dam and CAP canal flowing west of Waddell dam) are critical to power-water network N-1 contingency reliability above 60% power system loading and at 100% water system demand, (ii) fast-starting natural gas generating units are necessary to maintain N-1 contingency reliability below 60% power system loading, (iii) Coolidge Station was the power plant to most frequently undergo a reduction in reserves amongst the water failure scenarios that cause a violation of N-1 reliability, (iv) power network vulnerability to water network failures was non-linear because it depends on the generating units that are dispatched, which can vary as line thermal limits or unit generation capacities are reached.

DEDICATION

I dedicate this to my mother and father for always believing in me.

ACKNOWLEDGEMENTS

I would personally like to thank my PhD advisor Dr. Nathan Johnson for his many years of dedication to my growth as an engineer and scientist. He has been a great role model professionally and intellectually. I would also like to personally thank Dr. Thomas Seager for bringing me into the RIPS team and always willing to engage in candid and insightful conversations.

This work was funded in part by the National Science Foundation (NSF) for the project entitled Resilience Simulation for Water, Power & Road Networks under award number 1441352 as part of the Resilient Interdependent Infrastructure Processes and Systems (RIPS) Type 2 program and in part by the United Stated Office of Naval Research (ONR) Defense University Research-to-Adoption (DURA) Initiative under award N00014-18-1-2393. Any opinions, findings, conclusions, or recommendations expressed in this material are those of the author and do not necessarily reflect those of the NSF or the ONR.

Maps throughout this Dissertation were created using ArcGIS® software by Esri. ArcGIS® and ArcMap™ are the intellectual property of Esri and are used herein under license. Copyright © Esri. All rights reserved. For more information about Esri® software, please visit www.esri.com.

TABLE OF CONTENTS

Page

APPENDIX Page

LIST OF TABLES

LIST OF FIGURES

Figure Page

Figure Page

Figure Page

Figure Page

NOMENCLATURE

Symbol	Units	Description	Symbol	Units	Description
$\boldsymbol{S}$	-	The set of all substations	$\boldsymbol{P_{tot,COM}}$	MW	Commercial sector power load of $\boldsymbol{P_{tot}}$
$\boldsymbol{T}$	-	The set of all tie line interconnections	$\boldsymbol{P_{tot,IND}}$	MW	Industrial sector power load of $\boldsymbol{P_{tot}}$
$\boldsymbol{G}$	-	The set of all non fast-starting generating units	$\boldsymbol{P_{tot,AGR}}$	MW	Agricultural sector power load of $\boldsymbol{P_{tot}}$
$\widehat{\boldsymbol{G}}$	-	The set of all fast-starting generating units	$\boldsymbol{P_{PMA,RES}}$	MW	Residential sector power load of $\boldsymbol{P_{PMA}}$
$\boldsymbol{B}$	-	The set of all transmission lines (branches)	$\boldsymbol{P_{PMA,COM}}$	MW	Commercial sector power load of $\boldsymbol{P_{PMA}}$
$\boldsymbol{U}$	-	The set of all water pumps	$\boldsymbol{P_{PMA,IND}}$	MW	Industrial sector power load of $\boldsymbol{P_{PMA}}$
$\boldsymbol{F_h^W}$	%	Average water demand factor for hour $\boldsymbol{h}$ of the year	$\boldsymbol{P_{PMA,AGR}}$	MW	Agricultural sector power load of $\boldsymbol{P_{PMA}}$
$\boldsymbol{F_m^W}$	%	Average water demand factor for month $\boldsymbol{m}$ of the year	$\boldsymbol{P_{s,init}}$	MW	Initial power load of $\boldsymbol{P_{PMA}}$ distributed to substation $\boldsymbol{s}$
$\boldsymbol{F_{m,h}^W}$	%	Average water demand factor for hour $\boldsymbol{h}$ of month $\boldsymbol{m}$	$\boldsymbol{P_{s,u}}$	MW	Power load of pump $\boldsymbol{u}$ at substation $\boldsymbol{s}$
$\boldsymbol{P_u}$	MW	Power consumption of pump $\boldsymbol{u}$	$\boldsymbol{P_{s,t}}$	MW	Power load of tie line $\boldsymbol{t}$ at substation $\boldsymbol{s}$
$\boldsymbol{H_u}$	ft	Head gain of pump $\boldsymbol{u}$	$\boldsymbol{P_s}$	MW	Final power load of $\boldsymbol{P_{PMA}}$ distributed to substation $\boldsymbol{s}$
$\boldsymbol{Q_u}$	GPM	Flow rate of pump $\boldsymbol{u}$	$\boldsymbol{P_b}$	MW	Power flow of transmission line $\boldsymbol{b}$ from bus 1 to bus 2

NOMENCLATURE

Symbol	Units	Description	Symbol	Units	Description
ϵ_u	-	System efficiency of pump u	$P_{b,max}$	MW	Thermal limit (normal rating) of transmission line b
SG	-	Specific gravity of water	P_g	MW	Power output of generating unit g
s_x	-	Total number of household occupants at substation s	$P_{g,min}$	MW	Minimum power output of generating unit g
s_e	-	Total number of employees at substation s	$P_{g,max}$	MW	Maximum power output of generating unit g
s_a	-	Total area units of agricultural land at substation s	$r_{g,max}$	MW/min	Maximum ramp rate of generating unit g
s_c	Ares	Total commercial land-use area at substation s	R_g	MW	10-minute reserves provided by generating unit g
s_i	Ares	Total industrial land-use area at substation s	uc_g	-	Commitment status of generating unit g
P_{APS}	MW	Total power load of APS service area	$\partial_{k,j}$	-	Relative distance from substation k to substation j
P_{SRP}	MW	Total power load of SRP service area	cr	-	Fraction of reserves allocated from second greatest unit contingency
P_{tot}	MW	Total power load of APS and SRP service area	$PTDF_{g,b}$	-	Power transfer distribution factor of generating unit g onto line b
P_{PMA}	MW	Total power load of PMA modeled area	$PTDF_{s,b}$	-	Power transfer distribution factor of substation s onto line b
$P_{tot,RES}$	MW	Residential sector power load of P_{tot}	$LODF_{o,b}$	-	Line outage distribution factor for line o onto line b

CHAPTER 1

INTRODUCTION

1.1 BRIEF HISTORY OF CRITICAL INFRASTRUCTURE

Infrastructure systems are critical to providing basic needs and an economy. Transportation systems enable movement of people, goods, and services, water supply systems deliver potable water to the public, facilitates sanitation for public health, and promotes industry, telecommunication systems eases the transfer of information and ideas, and energy systems powers our technology, promotes industry, and assists us in regulating our habitat. The notion of Critical Infrastructure was first defined in the US over 20 years ago as “those physical and cyber-based systems essential to the minimum operations of the economy and government,” by the Presidential Decision Directive No. 63 in 1998 [The White House, 1998]. The PDD-63 goes on to admit that “a result of advances in information technology and the necessity of improved efficiency, however, these infrastructures have become increasingly automated and interlinked,” which mobilized the need for improved protection of our critical infrastructure that has become increasingly interconnected. Maintaining and improving critical infrastructure protection requires an approach that is multi-discipline and multi-jurisdictional because our infrastructures are utilized by political, social, engineering, and other public-private entities.

For several decades, critical infrastructure protection has evolved through at least 8 phases of development that include recognition, natural disaster recovery, definitional phase, public-private cooperation, federalism, resilience, risk-informed decision-making, and cybersecurity and infrastructure [Lewis, 2020]. Risk analysis is currently the dominant approach to evaluating failure in engineering, and it includes risk assessment (e.g., a calculation of potential losses multiplied by their probability) and risk management. Traditional risk analysis, however, becomes less ideal for events that are low-probability and high-consequence (e.g., Black Swans), especially when hazards are nonlinear or when joint probabilities combine to produce an even greater impact [Park et al., 2012]. Critical infrastructure resilience offers an alternative to traditional risk analysis, however, resilience can be defined in many ways. Resilience may include an “ability to recover”, “ability to adapt”, “ability to withstand”, or “ability to absorb,” [Asubaie,

Alutaibi, & Marti, 2016] and may be parameterized using four properties including robustness, redundancy, resourcefulness, and rapidity [Bruneau et al., 2003]. This can include a process of sensing, anticipation, adaptation, and learning [Park et al., 2012]. Common amongst the many definitions of resilience are a capacity for absorption, adaptation, and restoration [Francis & Bekera, 2014]. The gradual adoption of resilience is an indication that traditional methodologies of critical infrastructure protection require further improvement and, potentially, new and different approaches such as the coupling of critical infrastructure systems in a single model

1.2 BRIEF HISTORY OF MODELING INTERCONNECTED INFRASTRUCTURE

The purpose of modeling and simulation for critical infrastructure protection is to analyze crisis scenarios, the technological performance of the critical infrastructure, the decision-making of crisis management, and the consequences. The assessment of the modeling and simulation of these scenarios provides information that may improve the crisis management and decision-making process for critical infrastructure planning and operations. Infrastructure models are essentially simplified representations of real-world infrastructure systems, however, engineers may develop formalized models that provide useful insights and actionable results. Critical infrastructure models may be evaluated in simulations with the goal to:

- Improve decision-making and strategizing for managing crisis and extreme events
- Assist operators in developing a course of action when facing real-time system disruptions and failure propagation
- Help planners improve system design by reducing frequency of disruptions, propagation of disruptions, and consequence of disruptions
- Train operators for engaging crisis scenarios with little to no cost to the real-world

Many types of dependences across infrastructure systems may exist, however, dependencies that are complex or hold latent effects may induce significant disruptions including cascading failures. One of the earliest attempts to classify interdependencies into four categories outlined as physical, cyber, geographic, and logical [Rinaldi, Peerenboom, & Kelly, 2001]. Physical interdependencies occur when one infrastructure depends on the physical output of another infrastructure. Cyber interdependencies occur when infrastructure depends on

information infrastructure. Geographic interdependencies occur when multiple infrastructures are in close proximity (thus susceptible to some natural disaster). Logical interdependencies occur when at least two infrastructures depends on the other (e.g., control, regulator) and not classified as physical, cyber, or geographic.

Approaches to modeling interdependent infrastructure can be categorized as empirical, agent-based, system dynamics, economic theory, network-based, and others including dynamic control system theory, Bayesian network, petri-net, and hierarchical holographic modeling [Ouyang, 2014]. Empirical approaches collect and process small and large interdependent critical infrastructure events, then statistically measure the significance of infrastructure interdependency [Luiijf et al., 2010; Chang, McDaniels, & Beaubien, 2009; McDaniels et al., 2007]. Such models are usually developed based on media reports and evaluated on a historical basis that can disregard low-probability, high-consequence events. Many empirical models were developed to investigate cascading failure to extreme events such as natural disasters [Rong, Han, & Liu, 2010; Bigger, Willingham, Krimgold, & Mili, 2009; Kajitani & Sagai, 2009]. Agent-based approaches consider critical infrastructure systems as a complex adaptive system (CAS) including decision-making processes in which collections of agents produce emergent behavior. These models are highly dependent on the assumed behavior of agents (i.e., model inputs) therefore difficult to theoretically justify, however a few agent-based models have been developed to study interdependencies [Dudenhoeffer, Permann, & Manic, 2006; Schoenwald, Barton, & Ehlen, 2004; North, 2001]. System dynamics approaches model infrastructure interdependencies as highly-interconnected CAS that produce feedback loops [Steinberg et al., 2011; Fair et al., 2007]. They can be used to model systems that are nonlinear and dynamic. Unfortunately, system dynamic models are not well-suited for modeling the technical operation of infrastructure assets because they require extensive calibration to be representative of real world infrastructure operation. Economic theory approaches model infrastructure interdependencies by economic relationships between infrastructure sectors using large-scale databases but cannot analyze component-level dynamics and can forego nonlinearities. Input-output economic models can be used to investigate the impact of natural hazards and systemic disruptions on industry and

economy in terms of markets [Crowther, Haimes, & Taub, 2007]. Network-based models simulate infrastructure as a collection of nodes and connections. Infrastructure assets are nodes that are connected together based on physical and relational characteristics. Thus, interdependencies can be represented as connections across infrastructure systems. Network-based models, however, can require excessive amounts of data for several reasons including creating a network topology, parameterizing components, and modeling decision-making process of real infrastructure operations. Network-based models come in two forms: topology-based or flow-based. Topology-based models investigate network connectivity and properties and flow-based models investigate the dynamics of flow throughout the network.

There are two types of computational architectures that can be used to model and simulate interconnected infrastructure systems: integrated and federated [Setola, Rosato, Kyriakides, & Rome, 2016]. Integrated modeling and simulation architectures consist of only one simulator for the entire system-of-systems. The integrated architecture is suitable for models with a high degree of abstraction. Alternatively, federated modeling and simulation architecture develop a communication software to interconnect domain-specific simulators. The federated architecture is usually more accurate on a domain basis because it uses specialized software for each domain. Most critical infrastructure models and simulates resulting from research projects are built on the federated architecture [Rome, Langeslag, & Usov 2014].

The coupling of infrastructures within an interconnected model may occur in three ways: simultaneous coupling, alternative iterative coupling, and externally coupling [Setola, Rosato, Kyriakides, & Rome, 2016]. Externally coupled models exchange data once per time step in both directions and is also known as a time-lagged approach. This method of data exchange is the least accurate but easiest to implement. Iterative coupled models exchange data per time step until a convergence criterion is met, then the simulation moves onto the next time step. This method is more accurate than externally coupled models but is more computationally expensive. Simultaneous coupling models represents the different infrastructures in a system of equations. This method can be the most complicated because all equations and processes must be internally consistent.

1.3 BRIEF BACKGROUND ON POWER AND WATER NETWORK OPERATIONS

Operation of the bulk electric power system balances three system-level properties in real-time: synchronous frequency, voltage, and thermal limits. The North American power grid consists of the Eastern, Western, Texas, and Quebec Interconnections that operate at a nominal synchronous frequency of 60 Hz. System frequency decreases when net load exceeds net generation, increases when net generation exceeds net load, and is maintained when net generation meets the net load. Power system assets are operated near rated voltages for safety and equipment longevity. ANSI range A standards dictate that voltage is only allowed to change +/- 5% away from nominal. Voltage magnitude decreases as current flows through components with impedance—i.e as power flows from source to sink—and increases as power is injected into the network. Assets that deviate from this frequency or their nominal operating voltages, or exceed their thermal limits are stressed and can be damaged. Water distribution and supply systems are operated to maintain minimum pressure, minimize water losses, and minimize water deficit for the large mass of the fluid flowing throughout the pipe and open-water systems. Pipe bursts can occur due to high pressures and water contamination intrusion and poor firefighting conditions can occur due to low pressures.

Physical (electric and hydraulic) properties can be represented using specialized software packages commonly used in industry and academia to simulate realistic infrastructure systems. Some commonly used commercial electric power network solvers include Siemens's PSSE, General Electric's PSLF, and PowerWorld Simulator, and open source solvers include EPRI's OpenDSS, MATLAB's MATPOWER and Simulink, and PNNL's GridLAB-D. Some commonly used water network solvers include Bentley Systems' WaterGEMS, the US Environmental Protection Agency's EPANET, DHI's MIKE URBAN+, the US Army Corps of Engineers' HEC-RAS and HEC-ResSim, and Innovyze's InfoWater. These network flow solvers enable numerous scopes of analysis that can include transient and steady-state analysis of infrastructure systems from small-scale (e.g., residential) to large-scale (e.g., regional) sized networks.

Optimal power flow (OPF) for electrical grid simulation has been studied in literature for around 100 years: minimizing cost of operation began in the 1930's; economic dispatch was performed using the equal incremental cost rule starting in the 1950's; solving nonlinear system using either nonlinear gradient methods or linear subproblems began in the 1960's; Newton's method, quadratic programming, and P-Q decomposition were used to solve dispatch of generating units starting the late 1960's [Huneault, 1991]; and classical economic dispatch was limited to real power optimization under loss constraints in the 1980's [Chowdhury, 1990]. P-Q decomposition works based on the assumption that phase angle primarily determines the flow of real power and that differences in voltage primarily determines the flow of reactive power [Coffrin, 2013], thus, real power can be solved as a linear problem and reactive power can be solved as a nonlinear problem separately and iteratively.

Modern deterministic OPF methods include a variety of linear programs that are continuous and mixed-integer, nonlinear programs that are continuous and mixed-integer, and quadratic programs using gradient methods, Newton's method, Simplex method, sequential programming, or interior point methods [Frank, 2012] are extensions of reliable OPF algorithms used since the 1960's whose output for nonlinear problems may be locally optimum but not globally optimum. Modern stochastic or non-deterministic OPF methods, however, include new techniques such as ant colony optimization, artificial neural networks, bacterial foraging algorithms, chaos optimization algorithms, evolutionary algorithms, particle swarm algorithms, simulated annealing, and tabu search that are shown to approach global optimality but with less efficiency than deterministic methods [Frank, 2012].

Conventional Security-Constrained OPF (SCOPF) approaches maintain system stability in post-contingency states, exclude some operational rules implemented by transmission system operators, and must decompose their optimization problems into subproblems because of large system sizes or large number of constraints [Capitanescu, 2016]. In the case of alternating current (AC) OPF, it is not suitable for real-time contingency analysis on large system sizes exceeding 10,000 buses or for highly constrained problems (which fail to converge); for instance, the "most comprehensive methodology for OPF" uses the ACOPF but is solved in "roughly 1

hour” [Capitanescu, 2016]. Thus, large systems may use the linear direct current (DC) model; for instance, the “most advanced risk-based OPF” adopts the DCOPF formulation [Capitanescu, 2016]. Therefore, DCOPF and ACOPF provide a tradeoff in computational cost, model complexity, and model accuracy and both have suitable uses in power systems modeling.

Optimal operation of pump and reservoirs for water supply and distribution systems is inherently a mixed-integer nonlinear problem (i.e., NP hard) [Fooladivanda & Taylor, 2015] but can categorized into 4 types of models: linear programming, nonlinear programming, dynamic programming, and computational intelligent [Ahamad, El-Shafie, Razali, & Mohamad, 2014]. Linear programming is a popular category used in many software packages because it is versatile for large scale systems and provides a feasible convergence to global optima. Nonlinear programming, however, is the most popular category because the operations and controls, thus the objective and constraint functions, for reservoir capacity, pumps, and demands are nonlinear. The most common types of nonlinear techniques include sequential linear programming, sequential quadratic programming, method of multipliers, and a generalization of the reduced gradient method. Stochastic dynamic programming has been previously developed to study water resource management in arid conditions of the Nebhana reservoir to meet irrigation water demand and minimum water levels [Alaya, Souissi, Tarhouni, Ncib, 2003]. Such dynamic programming formulations, however, have trouble with multiple state variables in the dimensionality problem, though attempts are being made to minimize the dimensionality problem including dynamic programming successive approximation, incremental dynamic programming, and discrete differential programming [Labadi, 2004]. Reservoir optimization algorithms have also been implemented using computational intelligent programs to find near-optimal solutions in a reasonable amount of time and may include genetic algorithms, simulated annealing, tabu search, particle swarm optimization, artificial neural networks, and fuzzy-logic [Ahamad, El-Shafie, Razali, & Mohamad, 2014].

1.4 CONTINGENCY ANALYSIS

Modern electric utilities use energy management systems (EMS) to monitor, visualize, control, and optimize the coordination of generation fleet, market operations, and transmission

systems. Various processes for electric operational planning can be performed under different temporal scales that attempt to forecast system states and stressors from 15-minute horizons with 5-second intervals to 6-month horizons with weekly intervals [Wood & Wollenberg, 2012]. Some of these processes are directly embedded in the EMS and are necessary to optimize economics and system reliability. Many important operational tools and analyses occur in the EMS including contingency analysis.

Contingency analysis nominally works on 2-day horizons with 10-minute intervals [Wood & Wollenberg, 2012], and attempts to identify system states and components that are critical—i.e., whose failure produces large perturbations—to normal operation. A cascading failure resulting in a region-wide blackout may be the most significant consequence of failure of a critical component. The North American Electric Reliability Corporation (NERC) has instituted the N-1 reliability rule for electric power systems in the U.S., which allows the failure of a single element of the bulk power system [NERC, 2007]. Other rules such as N-2 and N-1-1 can achieve a higher grade of reliability but are not commonly implemented.

Traditional electric power contingency analysis operates using the N-1 rule and is coupled with state estimator monitoring tool and (security constrained) economic dispatch. The monitoring tool communicates information about state of the system, with economic dispatch optimizing the system, and contingency analysis determining if a newly dispatched state is N-1 safe. The process for N-1 contingency analysis uses the network data from the state estimator and can undergo four steps: rank contingency severity of network elements and filter the highest priority contingencies, iterate through high priority elements and consider this single element offline, solve power flow for contingency scenario, and, at the end, perform Remedial Action Scheme (RAS) for contingency violations.

The naïve method for performing contingency analysis is to construct a realistic AC model of the network system, iterate through every element in the network, and consider the case that this element is offline. Solving this nonlinear and nonconvex problem using full enumeration of a large network is likely to be computationally infeasible for the necessary time interval. There are two possible solutions to the naïve method that hastes the process: linearize and vectorize

the model or perform a screening process of the contingency scenarios [Ejebe & Wollengberg, 1979].

The electric network can be linearized using a DC model. The DC model can use the power transfer distribution factor (PTDF) to approximate the real power change in branches given a change in transactional power between two sources and sinks—e.g., change in generation, change in load demand. The DC model can also use the line outage distribution factor (LODF) to approximate the real power change in branches given a change in real power for a single branch—i.e., a single branch goes offline. The limitation of the DC model is that it omits modeling the effects to reactive power and voltage stability.

Little work has been done in contingency analysis of water distribution systems. A large amount of work is done on the institutions and organizations that manage water systems that attempts to understand the trade-offs in risk—e.g., economics, quality—rather than operational post-contingency actions [Pollard et al., 2004]. However, contingency planning for water systems suggest that back-up water lines are a countermeasure to water contaminants [Clark & Deininger, 2000], improved real-time warning systems like chlorine residual monitoring should be implemented to prevent outbreaks [Hrudey, Hrudey, & Pollard, 200613], and sufficient water storage backup should be in place for extreme events—e.g., droughts [Central Valley Project an State Water Project, 2016; Bruins, 2000]. Contingency planning, however, occurs over longer time periods than the fast response 10-minute interval of electric power contingency analysis. First-order and second-order approximations of contingency analysis of 5 tanks in a 92-node water network are accurate only up to a 40% perturbation in tank head-levels [Yeung, Judi, Daniel, 2017].

1.5 RESEARCH OBJECTIVES

The goal of this dissertation is to characterize how interdependencies between power and water infrastructure can increase the incidence of system-wide failures. To focus this goal into an actional piece of work of reasonable scope, this dissertation focuses on answering the question of how vulnerable is the Phoenix Metropolitan Area power and water infrastructure

systems to interdependencies? It does so by answering two specific sub-questions in the investigation performed in Chapter 2. The sub-questions are listed below:

1. How do stressors propagate across interconnected power and water networks?
2. What are the independent and dependent variable for investigating the propagation of stressors across interconnected power-water networks?
3. How do interdependencies affect reliability in a case study of the Phoenix Metropolitan Area?

The analysis performed in Chapter 2 simulates an interconnected power-water network of the Phoenix Metropolitan Area in the Resilient Infrastructure Simulation Environment (RISE). This version of RISE was developed in a federated architecture that has OpenDSS for the power flow solver and EPANET for the water hydraulic solver, and data exchange between the two solvers occurred in an integrated coupling process. This model evaluated the N-1 contingency reliability of the power network due to water network failure scenarios from lower to upper bounds of their respective power system loadings and water system demand levels.

CHAPTER 2

QUANTIFYING RELIABILITY OF COUPLED POWER-WATER NETWORKS USING CONTINGENCY ANALYSIS

2.1 INTRODUCTION

Electric power and water supply infrastructure are inextricably linked [Dai et al., 2018; IEA, 2016; U.S. DOE, 2014; U.S. DOE, 2006]. Approximately 4% of annual global electricity supply is used to pump water from underground sources, transport water, treat water for drinking, and treat water for placement back into the environment [IEA, 2016]. Similarly, about 9% of global water supplied for human use is withdrawn annually for hydroelectricity generation and cooling of thermoelectric power plants [IEA, 2016]. Such connections suggest that disturbances in one infrastructure may affect the other infrastructure. History shows this is true. Since 2000, there have been 42 incidents of power plant curtailment or shutdown due to high water temperature or insufficient water availability in the United States [OpenEI, n.d.]. Further, estimates indicate that 347 coal-fired power plants are vulnerable to water-shortages throughout 43 states in the U.S. [U.S. DOE, 2010]. Looking globally, approximately one-half of worldwide capacity of thermal power plants are in water-stressed areas [Kressig, Byers, Friedrich, & Luo, 2018]. In 2016, water shortages in Kenya forced the electrical reserve margin to a low point of 4.4%, compared to the mandated target of 15% [Otuki, 2017]. In 2016, India curtailed or shut down 18 thermal power plants and lost 14 TWh of generation due to water shortages [Luo, 2017]. In 2017, Hurricanes Irma and Maria demonstrated a strong, nonlinear, and interdependent relationship between power and water infrastructure in the post-disaster recovery of Puerto Rico [Sarker & Lester, 2019]. These vulnerabilities and shortages can become more pronounced in countries experiencing high population growth, increased urbanization, and increased water scarcity. India is classified as water-stressed, China and the Middle East are experiencing water constraints [IEA, 2016], and 61 countries are expected to become highly water-stressed by 2040 [Luo, Young, & Reig, 2015]. This global challenge may hit metropolitan areas the hardest when noting that one in four large cities are currently water-stressed [Mcdonald et al., 2014] and an estimated 40% of the global population is expected to live in water-stressed areas by 2050 [WWAP, 2014].

Anticipating, preventing, and mitigating challenges of insufficient power and water availability can be improved through a study of coupled infrastructure processes and systems.

Research into coupled infrastructure systems has increased over the past ten years with motivation from catastrophic failures following extreme weather events [Zimmerman, Zhu, de Leon, &, Guo, 2017; Guidotti et al., 2016; Pregnolato et al., 2016, Wilbanks, Fernandez, & Allen, 2015; Ouyang, 2014; Chang et al., 2013; Johansson & Hassel, 2010; McDaniels et al., 2008]. Methodological approaches are varied to address different goals with varying fidelity and accuracy of infrastructure data. Interdependent infrastructure models have been generated using abstract networks with power-law node degree distributions (e.g., preferential attachment) for analysis of tipping points that cause cascading failure [Zhang, Yang, & Lall, 2016; Chen, Du, Cao, & Zhou, 2015; Chen et al. 2015; Brummitt, D'Souza, & Leicht, 2012; Svendsen & Walthusen, 2007]. In cases using real or realistic power networks, the underlying physics is often simplified by omitting alternating current power flow and hydraulic fluid flow [Zio & Sansavini, 2011; Lee, Mitchell, & Wallace, 2007]. Other research has investigated specific stressors, such as population growth and climate change, that result in reduced power generation capacity [Craig & Feng, 2016; Liu, Tang, Voisin, & Cui, 2016; Van Vliet, Sheffeld, Wiberg, & Wood, 2016; Van Vliet, Wiberg, Leduc, & Riahi, 2016; Voisin et al., 2016; Bartos & Chester, 2015; Van Vliet et al., 2012], reduced power line ampacity [Bartos et al., 2016], and increased water consumption [Liao, Hall, & Eyre, 2016; Scanlon, Duncan, & Reedy, 2013; Koch & Vögel, 2009].

Despite the rapid pace of resilience and coupled infrastructure analyses, there is presently no study exploring if reduced water availability can affect power generation reliability at maintaining N-1 contingency requirements. In the abstract, contingency analysis simulates "what if" scenarios of a network operations under stress. Previous work has attempted to approximate the effect of water-shortage on power system reliability using a simplified metric: reserve margin percent of aggregate peak load [Voisin et al., 2018]. This simplified metric, however, omits the real-time frequency and voltage controls maintained by North American Electric Reliability Corporation (NERC) balancing authorities including, but not limited to, N-1 contingency analysis. For example, real-time operations of balancing authorities included shedding loads for

approximately seven hours during an extreme cold weather event that occurred in New Mexico and Texas in 2011 [FERC & NERC, 2011; Potomac Economics, 2011]. This work introduces methods, a case study for a metropolitan area, and conducts simulations to investigate the reliability of a power network coupled to a vulnerable water network during real-time operation. Separate steady-state models for electric power and water are completed in OpenDSS (power) and EPANET (water) solvers [EPRI, 2016; U.S. EPA, 2008], respectively, are then interconnected to create a coupled network using the Resilient Infrastructure Simulation Environment (RISE) using Python 3.7. Major contributions of this work include:

- Methodology for simulating steady-state, coupled power-water networks that express the mathematical relationships of real, interdependent components and systems.
- Process for using publicly available datasets to construct realistic electric transmission and water supply networks for metropolitan areas
- Operational models for the Phoenix Metropolitan Area power and water networks with applications in power only, water only, and interconnected power-water analysis

2.2 METHODS FOR COUPLED POWER-WATER CONTINGENCY ANALYSIS

Contingency analysis of coupled power-water networks consists of three parts shown in Fig. 1: generating a coupled power-water network model, simulating operational changes, and running contingency analysis of the power-water network. The network model is comprised of infrastructure system topology, locations, and ratings of assets. Operational changes include power demands, water demands, and component failures.

Contingency analysis begins by simulating a water failure scenario and then resolving the updated water network state (i.e., flows and pressures). This, in turn, affects the power consumption of water pumps that are used to update the power network state (i.e., unit commitment and dispatch). The effect of water loss is then simulated for generating units to examine a potential deficit in cooling-water, with any generating units that must reduce output or be shut down counting as a reduction of contingency reserves. If operating contingency reserves drop below the required amount of N-1 contingency reserves determined by electric utility operating procedures, then the system is no longer N-1 contingency reliable and is deemed

vulnerable. This methodology analyzes how stressors on a water network propagate to the adjoined power network, and remains different from traditional N-X contingency analysis because the approach in Fig. 1 analyzes a continuous range of operation for cooling water-constrained generating units (i.e., partly loaded units) instead of simulating only discrete on/off operating states for X number of units.

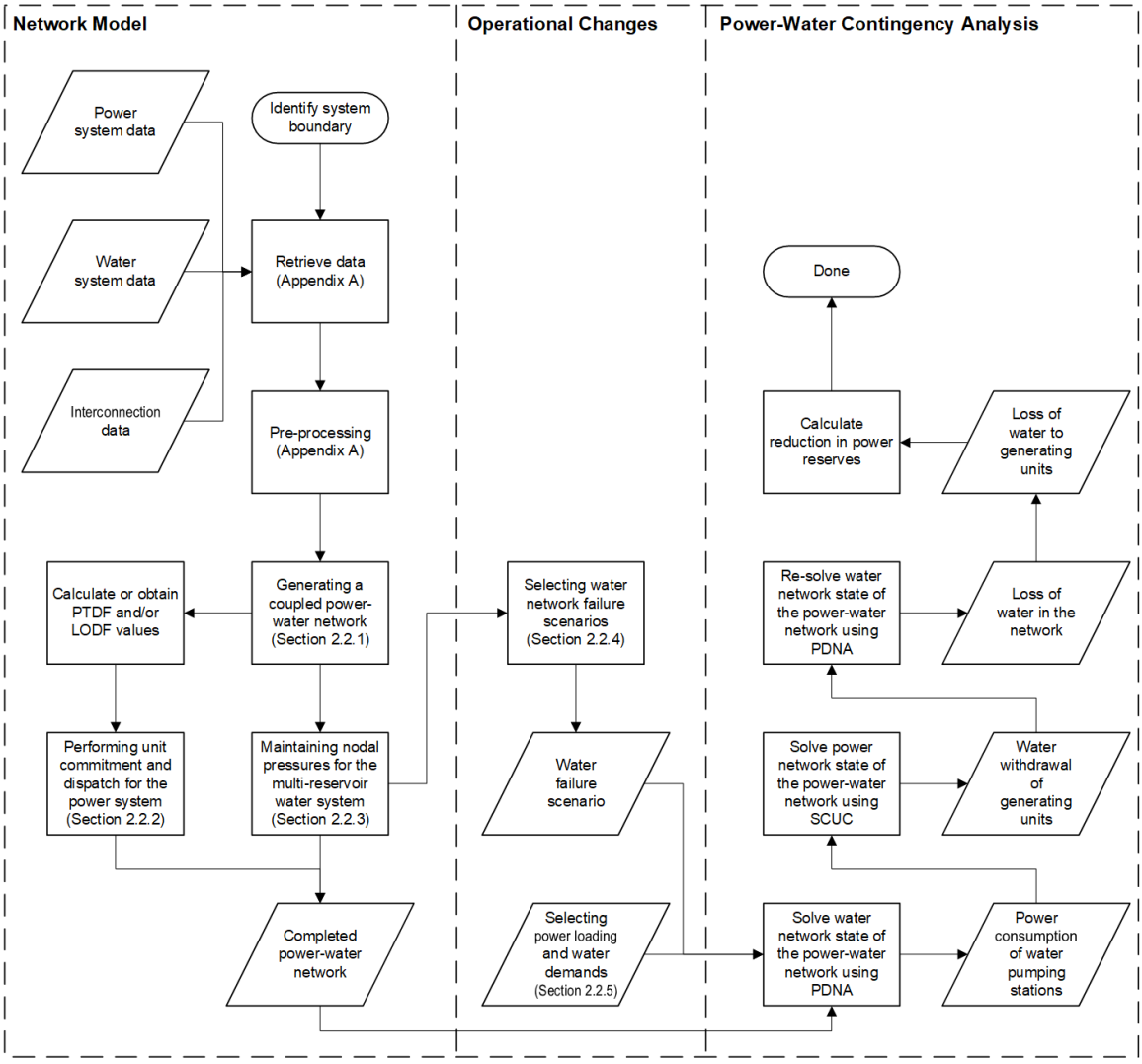

Figure 1: Process for Contingency Analysis of Coupled Power-Water Networks

Water deficits occur at nodal junctions during power-water contingency analysis. The nodal junctions may have multiple sinks that require water demand, including municipalities and generating units. A junction that is water-constrained may need to prioritize serving water demands to some sinks over others. The power-water contingency analysis methodology used

here assumes best case operation for power system reliability—i.e., cooling-water for dispatched generating unit output has the highest priority, cooling-water for generating unit contingency reserves has second priority, and then municipalities have the lowest priority. Additionally, cooling-water for contingency reserves prioritizes generating units that require the least amount of cooling-water per unit of power output which ensures that the most amount of reserves are retained.

2.2.1 GENERATING A COUPLED POWER-WATER NETWORK

A power network and water network were generated as depicted in Figs. 2 and 3, respectively, for the Phoenix Metropolitan Area (PMA) comprised of Maricopa and Pinal counties in Arizona and served by Arizona Public Service (APS) and Salt River Project (SRP) electric power utilities. The coupled power-water network is given in two figures, rather than a single figure, due to the complexity of each network. The data and process for generating the power network, the water network, and the interconnections are provided in Supplementary Information. Creating a coupled network is often challenging for researchers, and hence limits scientific study, due to the lack of co-located power network and water network data [Bloomfield et al., 2017; Chopra & Khanna, 2015; Ouyang, 2014; Wang, Hong, & Chen, 2011]. Fig. 2 of the power network shows a total of 599 transmission lines (390 69 kV, 33 115 kV, 141 230 kV, 1 345 kV, 34 500 kV), 429 substations, 64 generating units, and 184 transformers (not depicted). A total of 23 generating units are thermoelectric plants with an aggregate capacity of 5.9 GW that can withdraw water for cooling up to 400.0 thousand GPM. Fig. 3 of the water network shows a total of 2,624 surface water connections, 2,449 junctions, 3 reservoirs/dams, and 3 pumping stations. The pumping stations have an aggregate capacity of 109,000 horsepower

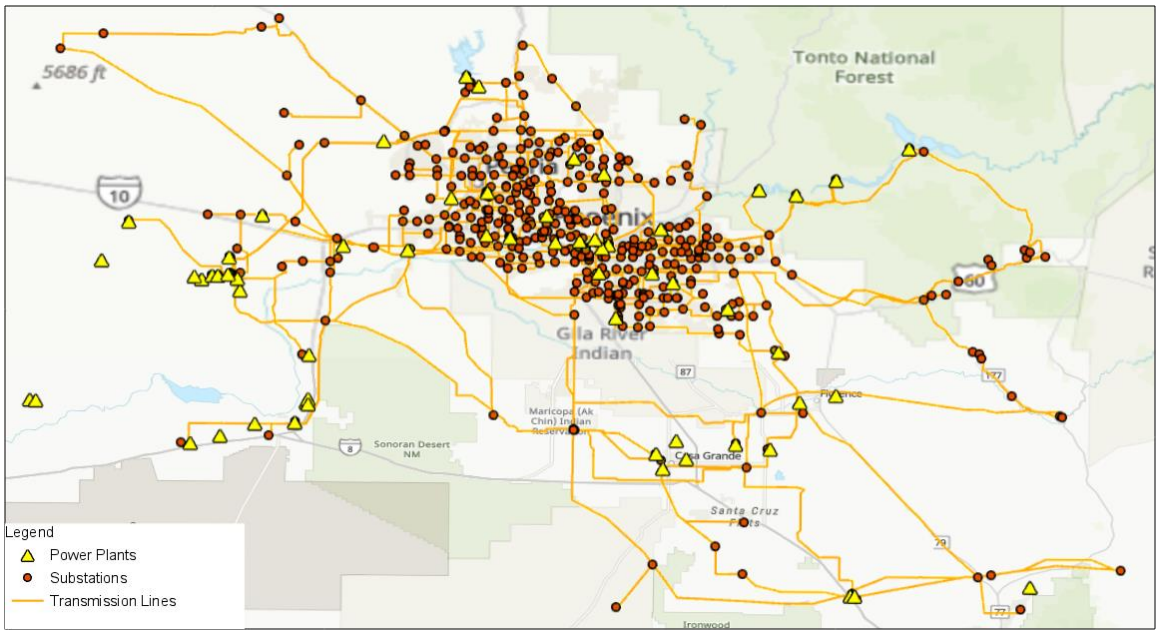

Figure 2: Case Study Power Network

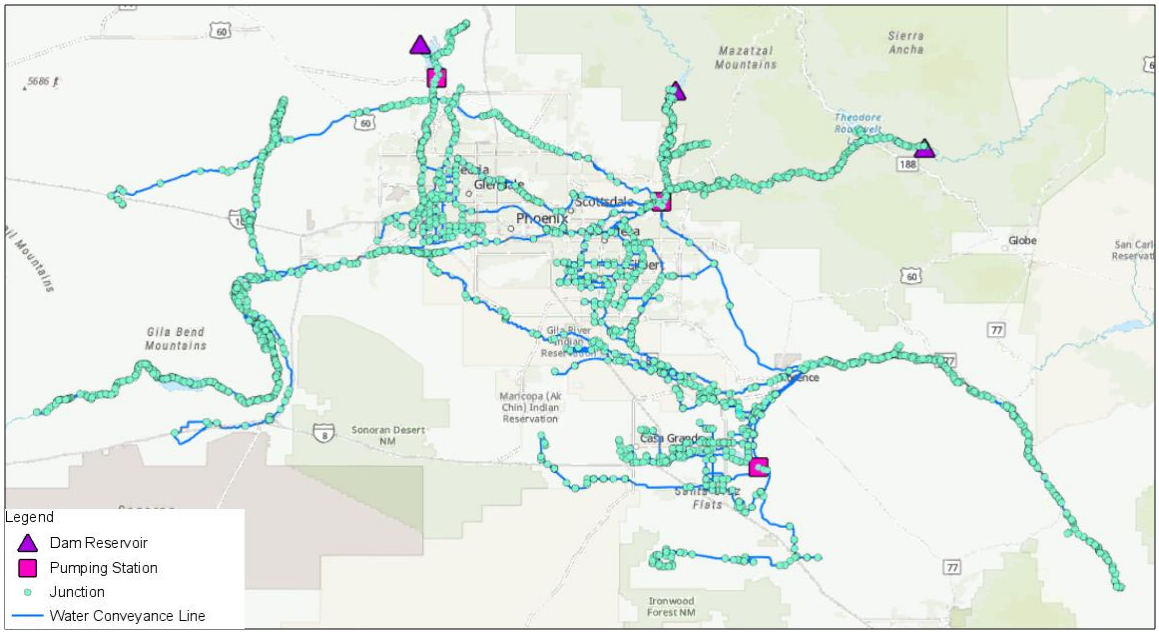

Figure 3: Case Study Water Network

2.2.2 PERFORMING UNIT COMMITMENT AND DISPATCH FOR THE POWER SYSTEM

Security constrained unit commitment (SCUC) and economic dispatch is commonly solved as an optimization program that may include binary variables, linear equations, nonlinear equations, stochastic processes, and more [Padhy, 2004]. The optimization program decides

which generating units should be online and their associated set points with respect to a set of equations that can target economic constraints, reliability constraints (e.g., contingency planning), or reduced uncertainty over some time horizon (e.g., day-ahead). The SCUC uses a mixed-integer linear program written in Eqs. 1 to 13 to prevent violation of line thermal limits (at normal and emergency ratings) and requires that reserves be available to respond to any single contingency (i.e., N-1 contingency). Losses are not included because real power losses were small relative to total system load. This introduces an error of 4% that was similar to other studies that ignored losses [Farivar, Chen, & Low, 2013].

Power transfer distribution factors (PTDF) were used to track changes in branch power flow and the associated effect on maintaining normal line ratings within thermal limits. Line outage distribution factors (LODF) were used to track how power flow is redistributed across active branches in the network in the event of a line contingency, and hence maintain emergency line ratings.

The APS and SRP utilities are 2 of 12 electric utilities participating the Southwest Reserve Sharing Group (SRSG) that share contingency reserves to maximize generator dispatch efficiency. The operating procedure for contingency reserves amongst the SRSG depends on the real-time operating state of each of the 12 members that, unfortunately, is not included in this PMA model [Southwest Reserve Sharing Group, 2017]. Therefore, an alternative operating procedure for contingency reserves was used that's implemented by Southwest Power Pool's and ISO New England's, two major bulk electric system operators in the US [Southwest Power Pool, 2015; ISO New England, 2019]. The SCUC allocates contingency reserves equal to 100% the most severe single contingency and 50% of the second greatest contingency. This methodology, however, is only solvable up to 93% power system loading. Thus, the 50% of the second greatest contingency was linearly reduced from 50% to 17% for power system loadings from 93% to 100% using a fraction scalar (cr).

The transmission system was constructed using available public data sets [Homeland Infrastructure Foundation-Level Data, 2019; WECC, 2019]. These data sets were not curated for the purpose of steady-state power flow simulations, unlike the well-documented test cases

provided by IEEE. Thus, the topology of the power network (See Appendix A.1), the parameterization of the components (e.g., line thermal ratings) (See Appendix A.1), and the allocation of loads to the substations (See Appendix A.1) were estimations of real system operation. These assumptions were combined to generate a flow-driven power network that can be solved in traditional power system solvers and, thus, modeled using the SCUC. This modeled power system while it meets numerous constraints based on topology, parameterization, loads, and/or reliability requirements, however, the SCUC cannot output a solution in some cases. Therefore, one of the three assumptions must be relaxed to output a solution. The topology and parameterization were based on high-quality curated data from HIFLD and WECC which are widely used in many domains, while the allocation of loads to the substations was developed in this paper using Thiessen polygons and GIS based data. Therefore, to maintain consistency with other work that also use the HIFLD and WECC data sets, substation loads were relaxed by re-allocating them to nearby substation if necessary to solve the SCUC.

The SCUC objective function given in Eq. 1 minimizes the re-allocation of power load (P) from substation k to substation j, and each re-allocation is weighted using the distance (∂) from substation k to substation j (i.e., the function minimizes re-allocation to nearby substations),

$$\min\left(\sum_k \sum_j \partial_{k,j} \left| P_{k,j} \right|\right) \text{ for each } k, j \text{ in } S \quad (1)$$

Eq. 2 maintains that re-allocation of power load (P) from substation k to substation j is equal to the negative of the re-allocation of power load (P) from substation j to substation k,

$$P_{k,j} = -P_{j,k} \text{ for each } k, j \text{ in } S \quad (2)$$

Eq. 3 updates the power load (P) of substation s from its initial value ($P_{s,init}$) using the sum of all re-allocations to each substation k,

$$P_s = P_{s,init} - \sum_k P_{s,k} \text{ for each } s, k \text{ in } S \quad (3)$$

Eq. 4 sets total system-wide generation, the sum of power output (P) by committed (uc) each generating unit g, equal to total system load, the sum of initial power load of each substation s ($P_{s,init}$), the power consumption of each water pumping plant u at each substation s ($P_{s,u}$), and the net power flow (imports – exports) of each tie line t at each substation s ($P_{s,t}$),

$$\sum_g \left(uc_g \cdot P_g\right) = \sum_s \left(P_{s,init} + P_{s,u} + P_{s,t}\right) \text{ for each } g \text{ in } G \cup \hat{G}, s \text{ in } S, u \text{ in } U, \text{ and } t \text{ in } T \quad (4)$$

Eq. 5 maintains that the power output (P) by committed (uc) generating unit g is bounded between minimum ($P_{g,min}$) and maximum ($P_{g,max}$) output,

$$uc_g \cdot P_{g,min} \leq uc_g \cdot P_g \leq uc_g \cdot P_{g,max} \text{ for each } g \text{ in } G \cup \hat{G} \quad (5)$$

Eq. 6 maintains that the 10-minute contingency reserves (R) allocated from committed (uc) non fast-starting generating unit g does not exceed maximum output ($P_{g,max}$),

$$R_g \leq uc_g \cdot \left(P_{g,max} - P_g\right) \text{ for each } g \text{ in } G \quad (6)$$

Eq. 7 maintains that the 10-minute contingency reserves (R) allocated from fast-starting generating unit g does not exceed maximum output ($P_{g,max}$),

$$R_g \leq P_{g,max} - P_g \text{for each } g \text{ in } \hat{G} \quad (7)$$

Eq. 8 maintains that the 10-minute contingency reserves (R) allocated from committed (uc) non fast-starting generating unit g does not exceed 10-minutes of its maximum ramp rate ($\dot{r}$),

$$R_g \leq uc_g \cdot 10 \cdot \dot{r}_{g,max} \text{ for each } g \text{ in } G \quad (8)$$

Eq. 9 maintains that the 10-minute contingency reserves (R) allocated from fast-starting generating unit g does not exceed 10-minutes of its maximum ramp rate ($\dot{r}$),

$$R_g \leq 10 \cdot \dot{r}_{g,max} \text{ for each } g \text{ in } \hat{G} \quad (9)$$

Eq. 10 maintains that total 10-minute contingency reserves (R) is at least 100% of generator i with the greatest amount of dispatch and reserves plus a fraction (cr) of generator j with the second greatest amount of dispatch and reserves,

$$\sum_g R_g \geq uc_i \cdot (P_i + R_i) + cr \cdot max\{uc_j \cdot \left(P_j + R_j\right)\} \quad (10)$$

$$\text{for all } g \text{ in } G \cup \hat{G} \text{ and for all } j \text{ in } \left(G \cup \hat{G}\right) \backslash \{i\}$$

$$\text{where } u_i \cdot (P_i + R_i) = max\{uc_h \cdot (P_h + R_h)\} \text{ for all } h \text{ in } G \cup \hat{G}$$

Eq. 11 sets the power flow (P) of line b equal to the summed PTDFs of each generating unit g to line b plus the summed PTDFs of each updated substation s to line b,

$$P_b = \sum_g \left(uc_g \cdot P_g \cdot PTDF_{g,b}\right) + \sum_s \left(\left(P_s + P_{s,u} + P_{s,t}\right) \cdot PTDF_{s,b}\right) \quad (11)$$

$$\text{for each } b \text{ in } B, g \text{ in } G \cup \hat{G}, \text{ and } s \text{ in } S$$

Eq. 12 maintains that the thermal power flow (P) of line b is bounded between minimum ($-P_{b,max}$) and maximum ($P_{b,max}$) normal limits,

$$-P_{b,max} \leq P_b \leq P_{b,max} \text{ for each } b \text{ in } B \quad (12)$$

And Eq. 13 maintains that the thermal power flow (P) of line b plus the LODF of any line o to line b is bounded between minimum and maximum emergency limits (assumed to be 150% of normal limits),

$$1.5 \cdot P_{b,max} \leq P_b + P_o \cdot LODF_{o,b} \leq 1.5 \cdot P_{b,max} \text{ for each } b, o \text{ in } B \quad (13)$$

The LODF values for transmission line 10297 are shown in Fig. 4 with all 599 transmission lines categorically graphed along the x-axis. A positive LODF indicates that power flow in 10297 will decrease in the event of the line outage identified at the x-axis and a negative value indicates that power flow will increase. The selected line is a 230 kV line between Mesa and Apache Junction and has the largest mean LODF, which can be interpreted as the transmission line with the most dependence on other lines—i.e., outages in other lines can significantly change the power flow across line 10297. Line 10285, a terminal 230 kV line going south in Arlington Valley, had the smallest mean LODF which can be interpreted as the transmission line with least dependence on other lines. Line 10285 had the smallest mean LODF because it had an LODF value of 0 (no dependence) for all lines, except for itself (LODF of 1 for itself, per definition of LODF).

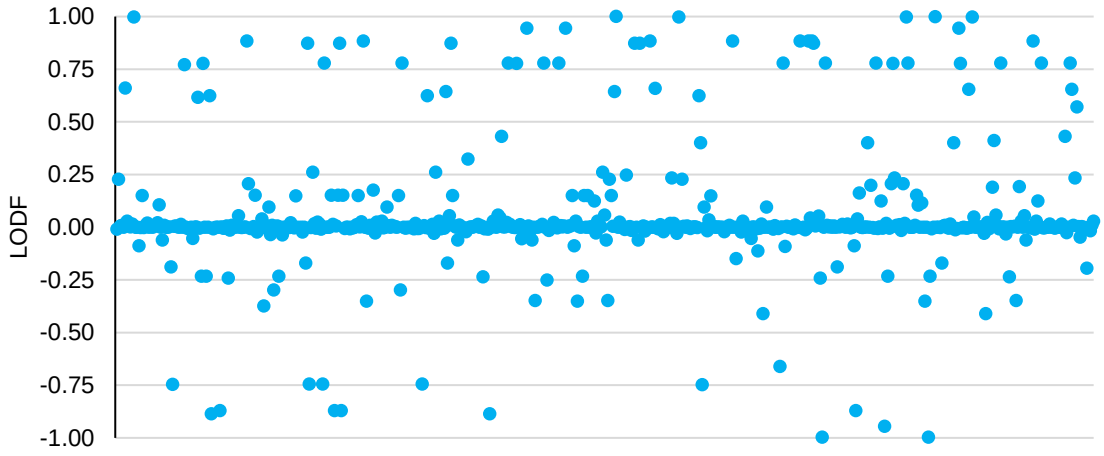

Figure 4: LODF Values for Line 10297 (230 kV Line Between Mesa and Apache Junction)

2.2.3 MAINTAINING NODAL PRESSURES IN THE MULTI-RESERVOIR WATER SYSTEM

EPANET was used as the water hydraulic solver. EPANET uses junction water demand as inputs and outputs junction pressure values, this assumes that all water demand is met—i.e., there are no water deficits. Given that this work needs to quantify deficits, a modified version of the pressure-deficient network algorithm (PDNA) [Ang and Jowitt, 2006] was implemented around EPANET, shown in Fig. 5, that outputs junction water deficits if minimum junction pressures are not met for multi-reservoir water networks. The PDNA was modified through the inclusion of 4 additional steps that are indicated by dashed borders. The non-modified PDNA algorithm makes no distinction between reservoirs supplying the water network, however, the interconnected power-water network has multiple reservoirs of two types: groundwater and dam reservoirs.

The first 2 additional steps were used to model the groundwater reservoirs that supply the municipalities. Prior to simulating EPANET junction demands at 0, an additional step connected the groundwater reservoirs to their municipalities using a pressure breaker valve with a setting of 0 pressure loss. This ensured that the groundwater reservoirs did not withdraw water from the water system (reservoirs at lower elevations can withdraw water from reservoirs from reservoirs at higher elevations in EPANET), which would negatively affect junction head levels. After the PDNA identified demand junctions with greater head levels than their minimum, an additional step re-connected groundwater reservoirs to their municipalities using flow control valves set to supply the municipality with the modeled amount of groundwater flow.

The last 2 additional steps were used to disable real reservoirs (i.e., groundwater and dam reservoirs) withdrawing water from the water system that would negatively affect junction head levels. After the PDNA determined that no junctions are withdrawing more than required demand, an additional step determined if any real reservoirs withdrawing water from the water system and, if so, are then disabled in the network and the PDNA re-runs from the beginning with the updated operation of real reservoirs. If no junctions were withdrawing more than required demand and no real reservoirs were withdrawing water from the water system, then the water network was considered solved. In summary, the purpose of the PDNA is to model multiple

groundwater and dam reservoirs that supply the water network to meet the demands of junctions at a minimum allowable pressure.

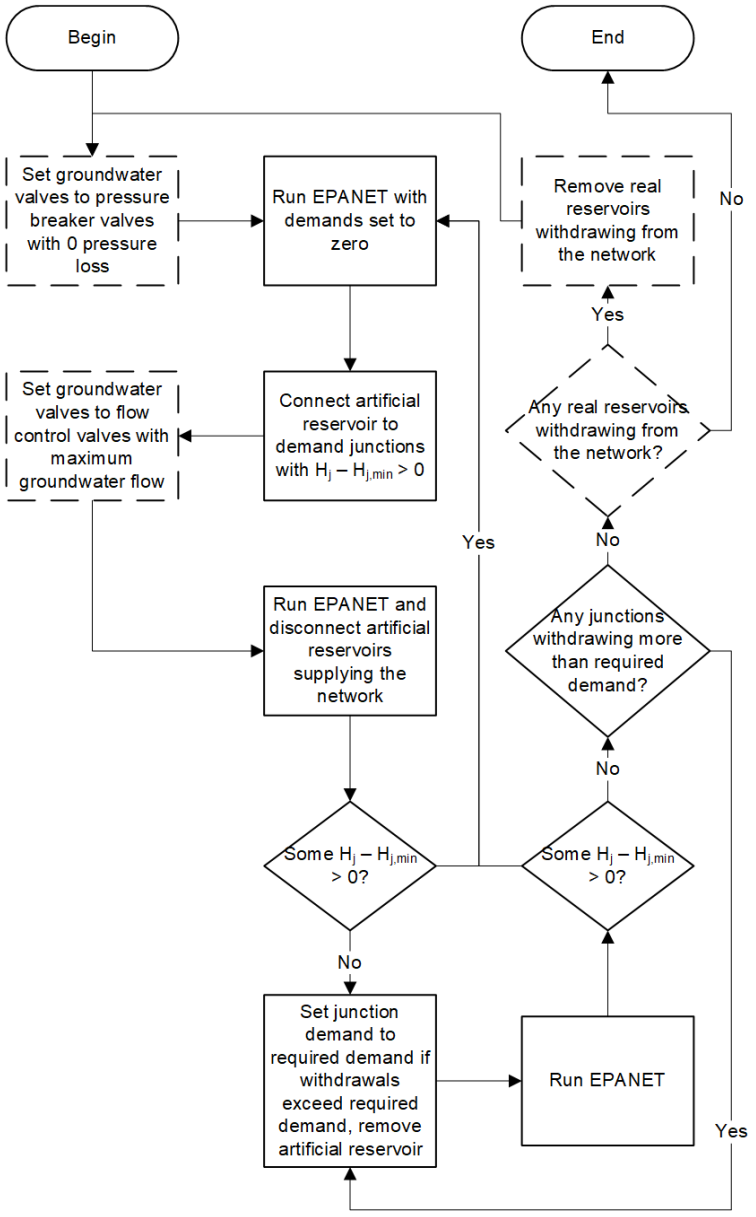

Figure 5: Multi-Reservoir Pressure-Deficient Network Algorithm for EPANET

2.2.4 SELECTING WATER NETWORK FAILURE SCENARIOS

The PDNA was used to identify critical water lines in the water network by performing a failure analysis of the water network lines during maximum water system demand. Water failure analysis at maximum water system demand captures the worst-case deficits for each simulated

water line failure, and if the worst-case deficit is 0 then the water line failure is inconsequential. The modeled medium-sized water supply network contained 2,624 lines, however, many of these lines are redundant in a water line failure analysis because many lines create a path (in Graph theory) in which all the nodes have a degree of 2. If along this path there are no properties that affect the flow of water (e.g., supply, demand, or pressure), then the failure of any line along this path is equivalent to any other line along this path because lines along this path can be concatenated into a single line with no change in water network simulation results. For example, 2 connecting canal sections of length 500 ft. can be combined into a single canal section of length 1000 ft. if their interconnecting junction does not change water demand or pressure. Therefore, it is possible to reduce the number of lines to analyze in the water line failure analysis with no loss of information.

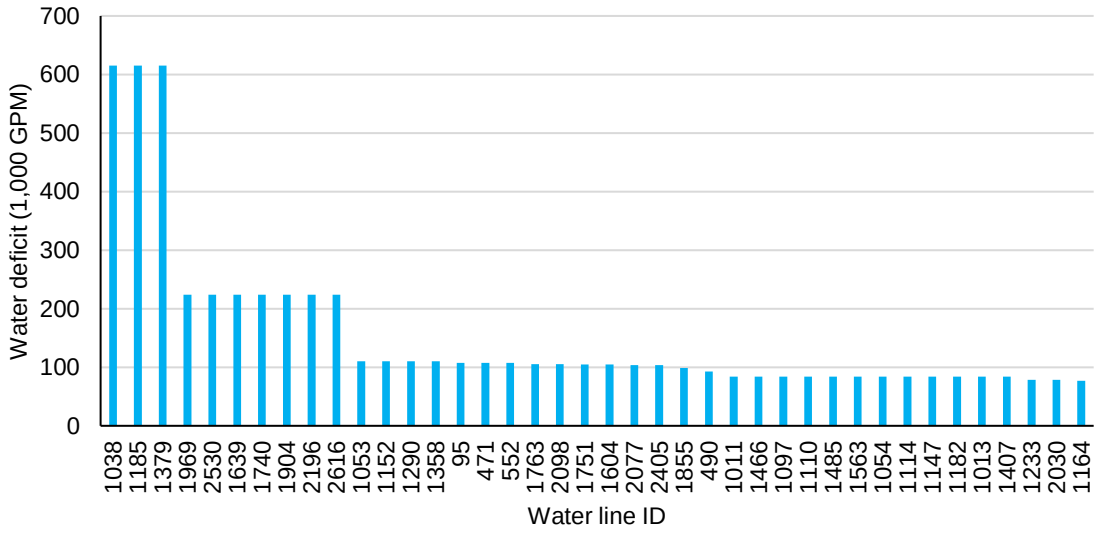

Figure 6: Total Water Deficits Due to Water Line Failure

The number of water lines to analyze was reduced to 942 by only selecting lines connected to a municipal junction, power plant junction, pumping station, or a junction node with a degree of at least 3 (defined as a hub node for current purposes). Water lines not connected to a node with a degree of 3 will have an upstream line connected to a municipal junction, power plant junction, pumping station, or a hub node. Fig. 6 shows results of the top 40 water line

failures that caused the largest water deficits. Complete results for all 139 water line failures that caused water deficits (i.e., the other 803 lines cause no water deficits) are reported in Table 13.

Table 1: Selected Water Line Failure Scenarios

Water Line ID	Water Line Failure Scenario	Affected Area
1038	1	Salt River feeding into Salt-Gila Pumping Station
1969	2	Water flow exiting Waddell Dam
1053	3	Water flow exiting Bartlett Dam
471	4	Roosevelt Canal between Queen Creek and Chandler
1763	5	CAP Canal in Paradise Valley (1)
2077	6	Agua Fria River south of Waddell Dam
1855	7	Water flow feeding into Peoria
490	8	Water flow feeding into Chandler
1011	9	Verde River south of Bartlett Dam
1233	10	Salt River south fork downstream Salt-Gila Pumping Station
2030	11	Hassayampa River north of CAP Canal
1164	12	Water flow feeding into Mesa
1026	13	Water flow feeding into Kyrene Gas Plant and Guadalupe
128	14	CAP Canal south of Florence
194	15	CAP Canal east of Queen Creek
1081	16	Southern Canal in northeast Mesa
1136	17	South fork after water line 1233
1349	18	CAP Canal in Paradise Valley (2)
192	19	South of Santan Mountains
787	20	West of Santan Mountains
1886	21	Gila River confluence in South Avondale
1673	22	Gila River southwest of Buckeye Valley
2021	23	South of Arlington Valley
1689	24	Hassayampa River north of Gila River
2617	25	Hassayampa River south of CAP Canal
2180	26	CAP Canal west of Waddell Dam
2488	27	Arlington Canal to Hassayampa River
71	28	Canal in southeast Gilbert
1967	29	Agua Fria River south of Sun City
920	30	Canal east of Coolidge (pre-fork)
950	31	Canal east of Coolidge (post-fork)

Water line failures 1038, 1185, and 1379 are equivalent and produced the largest deficits of water because they cut off water flow from the Bartlett Dam and Theodore Roosevelt Dam reservoirs incoming from the Verde and Salt Rivers, respectively. Lines failures 1969, 2530, 1639, 1740, 1904, 2196, and 2616 are equivalent and cut off water flow from the Waddell Dam reservoir. Lines failures 1053, 1152, 1290, and 1358 are equivalent and cut off water flow from the Bartlett Dam reservoir. Line failures 95, 471, and 552 are equivalent and cut off flow in the Roosevelt Canal between Queen Creek and Chandler, AZ. Line failures 1763, 2098, 1751, and 1604 are equivalent cut off flow in the CAP Canal near Paradise Valley, AZ. Many water line

failures comprised an equivalent set, and a single line is chosen from this set. A total of 31 unique water line failure scenarios that cause at least 10,000 GPM of total water deficit were identified for use in the power-water contingency analysis and are listed in Table 1 above and shown in Figs. 24 to 54 in Appendix C with black lines indicating the water network and red lines indicating the simulated failure scenario and its equivalent set.

2.2.5 SELECTING POWER LOADING AND WATER DEMANDS

A sensitivity analysis on 51 power system loadings, 4 water system demands, 31 water line failure scenarios, and 2 natural gas fast-starting configurations were used to investigate the reliability of the coupled PMA power-water network over two different assumptions: that all the natural gas units are fast-starting units or none are. The assumption that all the natural gas units are fast-start units is the best-case scenario in this analysis because fast-start units can provide contingency reserves even while the unit is offline, and the assumption that no natural gas units are fast-start is the worse-case scenario. Uniformly spaced values of 2.0% (62.1 MW) intervals from lower bound to upper bound power system loading were used in the sensitivity analysis. Power system loadings were analyzed using a higher resolution than water system demands because the water system demand added 43.6 MW of load onto the power system at 100% water system demand, which is equivalent to a 1.4% change in the bounded power system load. Therefore, the power system is lightly stressed by the water system interconnections in terms of megawatts, however, the stress in terms of cooling water supply interconnections remains under water failure scenarios is unknown. Table 2 defines the lower and upper bounds for the PMA power system loading (in single-phase power units) after implementing the top-down methodology on the total APS and SRP power system loading that's described in Appendix A, and Table 3 defines the corresponding bounds for PMA water system demands.

Table 2: Power System Loading Reference

Power System Loading (%)	Total PMA Power System Load (MW)	Total APS and SRP Power System Load (MW)	Comment
100	4,800.5	5448.7	Maximum total power load
0	1,696.4	1894.0	Minimum total power load

Table 3: Water System Demand Reference

Water System Demand (%)	Total PMA Water System Demand (GPM)	Comment
100	1,727,655	Maximum total water demand
0	215,640	Minimum total water demand

2.3 IMPACT OF WATER NETWORK FAILURES ON POWER NETWORK RELIABILITY

Initially dispatched reserves (prior to water failure scenarios) and sensitivity analysis results for the coupled PMA power-water network are reported in the heatmaps shown Figs. 7 and 8, respectively. The x-axis indicates 51 power system loadings from the lower to upper bounds, and the y-axis indicates 4 different water system demands and whether all the natural gas units are fast-start (all fs) or none (no fs).

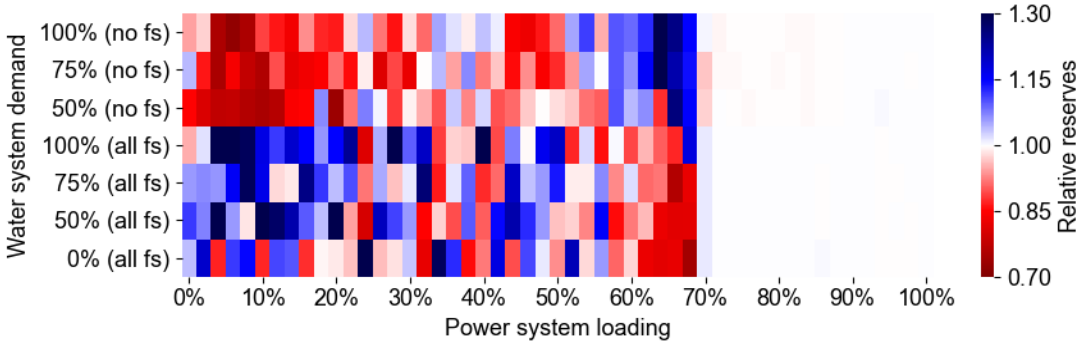

Figure 7: Variation in Initially Dispatched Contingency Reserves Across 51 Power System Loadings

Figure 7 shows the variation in dispatched reserves as water system demand and natural gas fast-start configuration were changed while keeping power system loading constant. This heatmap displays the initially dispatched reserves for each cell relative to the average value across all cells at the same power system loading value. For instance, dark blue at 6% power system loading and 100% water system demand (all fs) indicates that dispatched reserves at this operating point were 32% higher than the average value for all 6% power loadings, and the dark red at 6% power loading and 100% water system demand (no fs) indicates that dispatched reserves were 72% of the average. Dispatched reserves varied greatly between the no fs and all

fs configurations and, to a lesser extent, due to changes in water system demand. Somewhere below power system loading of 60%, more reserves, on average, were dispatched for the all fs configuration compared to the no fs configuration. Between 55% and 70% power system loadings, more reserves, on average, were dispatched for the no fs configuration when compared to the all fs configuration. There was almost no variation in the amount of reserves dispatched for power system loadings above 70% because the SCUC frequently dispatched 1,624 MW of reserves—i.e., the maximum reported amount. This maximum reported amount corresponds to the N-1 reserves needed to meet the capacity of 100% of the largest unit (Palo Verde Nuclear) and 50% of the 2nd largest unit (Santan Natural Gas). Thus, the transition that occurs from 60% to 70% power system loading is due to the complete dispatch of these two largest units.

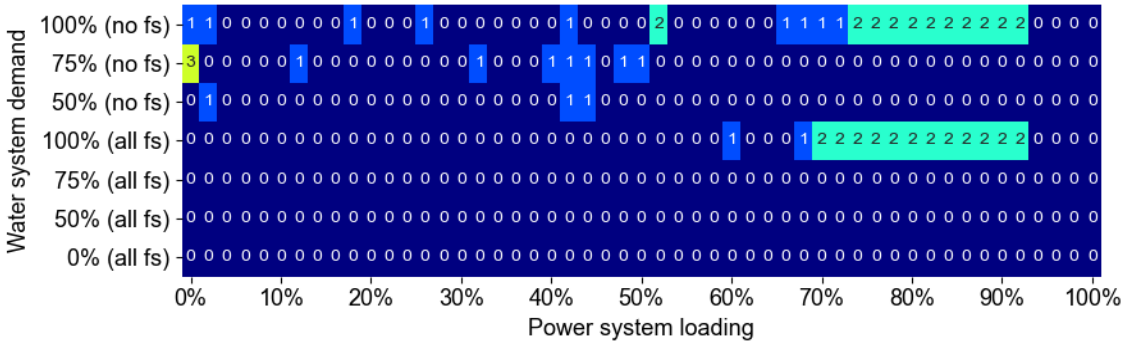

Figure 8: Number of N-1 Contingency Analysis Violations Across 51 Power System Loadings, 4 Water System Demands, and 2 Natural Gas Unit Fast-Start Configurations

The heatmap for Fig. 8 displays the number of water failure scenarios that violated N-1 contingency reliability in the coupled power-water network out of the total of 31 scenarios. When assuming all fs configuration, there were no violations of N-1 contingency reliability for water system demands at 75% and below, however, at 100% water system demand there were violations at 60% power system loadings and above. When assuming no fs configuration, there were several violations of N-1 contingency reliability between 0% and 50% power system loading at 50% and 75% water system demand, and between 0% and 92% power system loadings at 100% water system demand. When contrasting the all fs and no fs configurations, there were no violations below 60% when assuming all fs compared to the several violations in the same operating region for no fs. This corresponds with Fig. 7 in which the no fs configuration, on

average, had less dispatched reserves compared to the all fs configuration and this indicates that the power-water network is more vulnerable for power system loadings lower than 60% when no natural gas units were of fast-start configuration. In addition, at 60% power system loading there are no violations for the no fs configuration compared to the 1 violation for the all fs configuration, and at 70% and 72% power system loadings there was 1 violation for the no fs configuration compared to the 2 violations for the all fs configuration. This indicates that the power-water network was more vulnerable above 60% power system loading when all the natural gas units were of fast-start configuration.

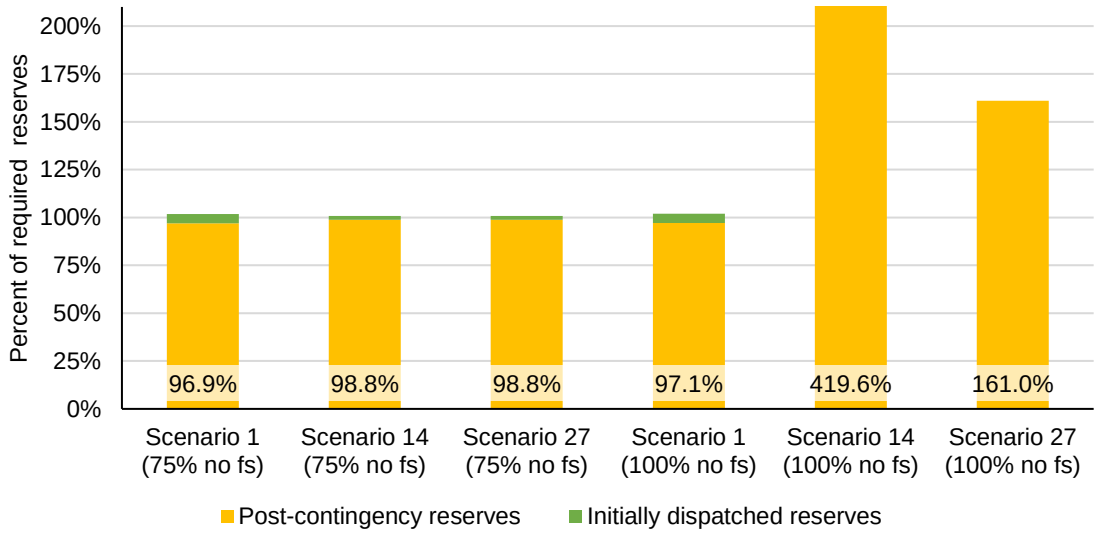

Figure 9: Comparing Water Failure Scenarios 1, 14, and 27 at 0% Power System Loading (with Water System Demand and Fast-Start Configuration Noted below the X-axis)

At 0% power system loading and under the no fs configuration, 3 violations occurred at 75% water system demand compared the 1 at 100% water system. Unintuitively, the power-water network was more vulnerable at the lower water system demand state. Fig. 9 above depicts the pre- and post-contingency reserves of the three water failure scenarios (1, 14, and 27) that violated N-1 contingency reliability at these 75% and 100% water system demands. At 75% water system demand, the initially dispatched reserves for these three scenarios were at or slightly above their required amounts but after the water failure scenario and being cooling water constrained (i.e., post-contingency reserves) they drop slightly below their required amounts. At

100% water system demand, however, scenarios 14 and 27 were initially dispatched much greater reserves (449.3% and 161.0% of their required amounts, respectively) and did not undergo a sufficient reduction in reserves to cause the same N-1 violations that occurred in the 75% water system demand case.

Returning to Fig 8., all 50 violations of N-1 contingency reliability at power system loadings 60% and greater occurred due to water failure scenarios 2 and 26. Scenarios 2 and 26, however, did not cause any violations for any power system loadings lower than 60%. This indicates that scenarios 2 and 26 were critical to the reliability of the power-water network at the higher power system loads. At power system loadings 58% and lower, 10 different water failure scenarios contributed to the 20 violations that occurred in this operating region, and scenario 1 contributed 10 of these violations amongst the 50%, 75%, and 100% water system demands. This indicates for the no fs configuration that scenario 1 was critical to the reliability of the power network at the lower power system loads but also that any other water failure scenario may cause a violation of N-1 reliability in this operating region.

and 11 depict scenario 1's reserves and violations that compares 75% and 100% water system demands for the no fs configuration, and Figs. 12 to 15 depict scenarios 2 and 26's reserves and violations that compares the no fs and all fs configurations during 100% water system demand. All other water failure scenarios that caused violation of N-1 contingency analysis is depicted in Fig. 55 to 63 in Appendix C. These figures have blue bars (primary Y-axis) that indicate reserves are in excess of their required amount—i.e., N-1 reliability is maintained—and red bars (primary Y-axis) that indicate reserves do not meet their required amount—i.e., N-1 reliability is violated. Despite the values for the primary Y-axis regularly reaching 500% and higher, the primary Y-axis is capped at 100% exceeding required reserves to provide greater visibility when reserves are less than required (which never drops below a value of -25%). The yellow dots (secondary Y-axis) indicate the percentage of reserves available after units are cooling water constrained due to water failure scenarios (i.e., post-contingency reserves) relative to initially dispatched reserves.

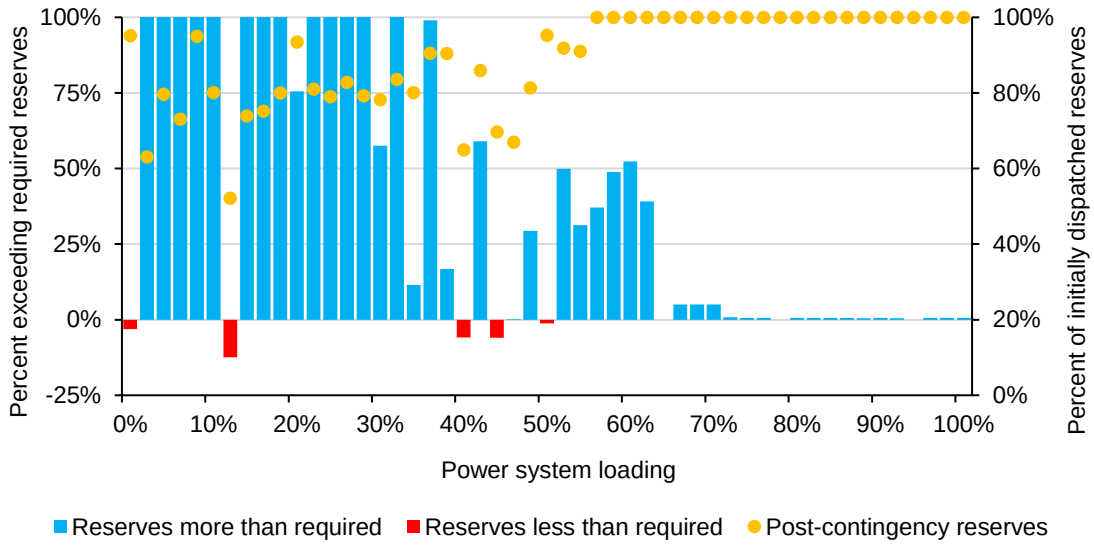

Figure 10: Contingency Reserves During Water Failure Scenario 1 at 75% Water System Demand and Assuming No Fs

Based on prior observations that water failure scenarios 1, 2, and 26 are critical, Figs. 10

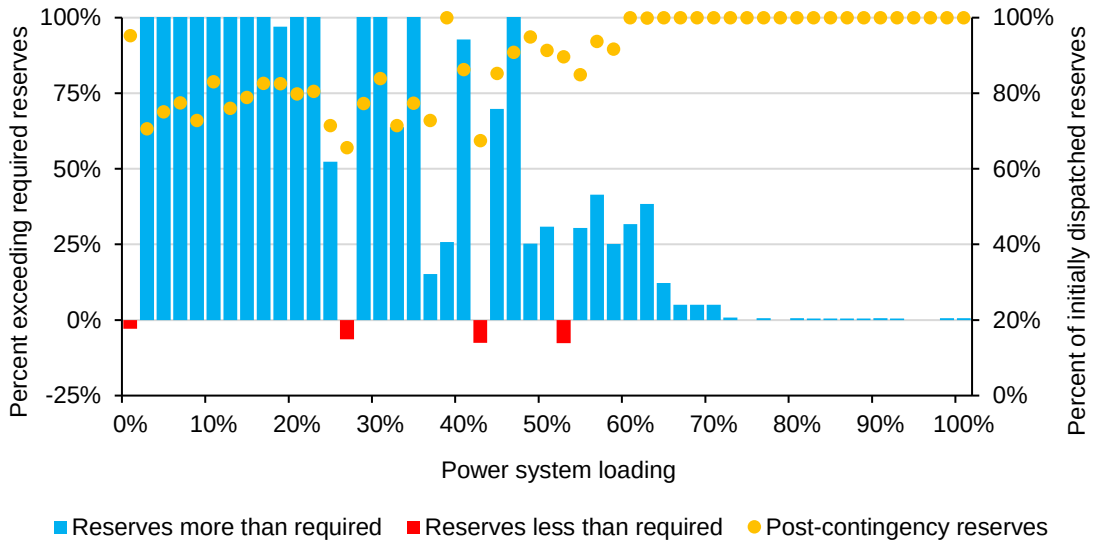

Figure 11: Contingency Reserves During Water Failure Scenario 1 at 100% Water System Demand and Assuming No Fs

Figure 10 depicts that water failure scenario 1 violated N-1 contingency reliability at 5 power system loadings during 75% water system demand for the no fs configuration, and Fig. 11 depicts that scenario 1 violated N-1 reliability at 4 power system loadings during 100% water system demand for the no fs configuration. However, there is no easily identifiable trend to the

violations in both cases. At 0% power system loading, post-contingency reserves are 95% of initially dispatched reserves for the 75% and 100% water system demands yet do not meet required reserves. Despite maintaining 95% of initially dispatched reserves, the power-water network violated N-1 contingency reliability at the 0% power system loading. Compared to 2% power system loading, post-contingency reserves are 63% and 71% of initially dispatched reserves for the 75% and 100% water system demands, respectively. While maintaining a lower percentage of reserves, the 2% power system loading simulations here still greatly exceed required reserves and maintains N-1 reliability. It's not uncommon to greatly exceed required reserves at one power system loading but have less than required reserves at an adjacent power system loading—e.g., 50% and 52% power system loadings in Fig. 10 and 42% and 44% power system loadings in Fig. 11—due to the changing commitment and dispatch from the SCUC.

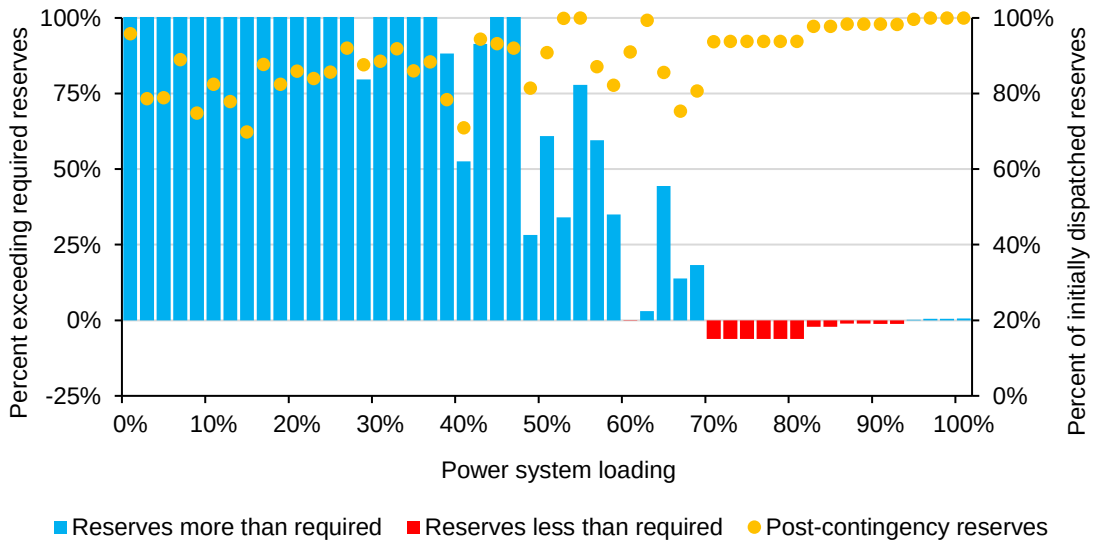

Figure 12: Contingency Reserves During Water Failure Scenario 2 at 100% Water System Demand and Assuming All Fs

Figure 12 depicts that water failure scenario 2 violated N-1 contingency reliability between 70% and 92% power system loadings during 100% water system demand for the all fs configuration, and Fig. 13 depicts the violations that occurred between 66% and 92% power system loadings at the same water system demand for the no fs configuration. In addition to this, Fig. 13 drops to 78% of required reserves at 72% and 74% power system loading while Fig. 12

only drops to 94% of required reserves in the same power system loadings. This may indicate that the no fs configuration leaves the power-water network more vulnerable to water failure scenario 2 when compared to the all fs configuration.

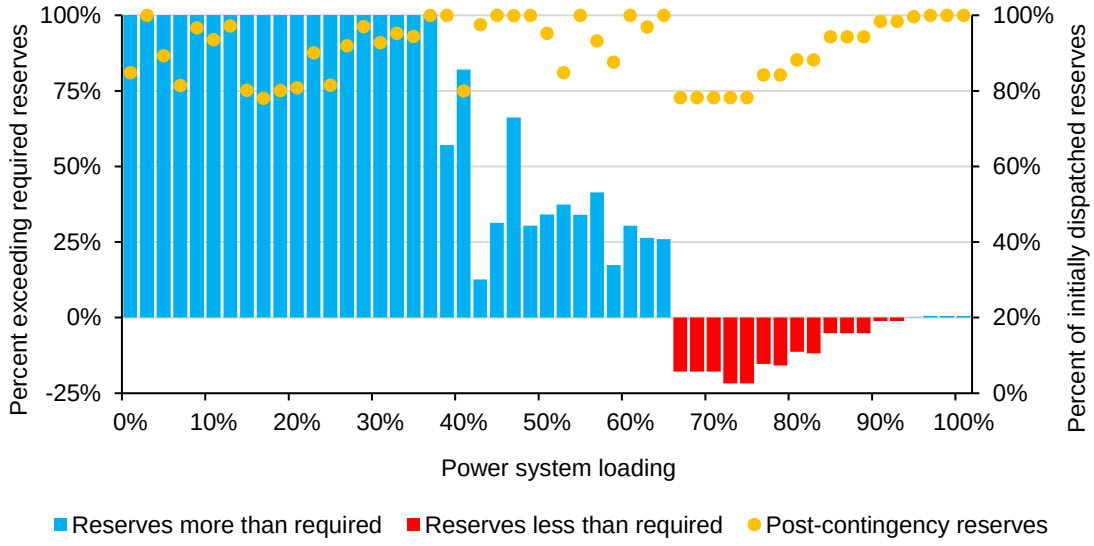

Figure 13: Contingency Reserves During Water Failure Scenario 2 at 100% Water System Demand and Assuming No Fs

Figure 14 depicts that water failure scenario 26 violated N-1 contingency reliability between 68% and 92% power system loadings during 100% water system demand for the all fs configuration, and Fig. 15 depicts the violations that occurred between 74% and 92% power system loadings at the same water system demand for the no fs configuration. This may indicate that the all fs assumption leaves the power-water network more vulnerable to water failure scenario 26 when compared to the no fs configuration. Under the all fs configuration, initially dispatched reserves exactly equal required reserves from 68% to 84% power system loading, therefore any amount of reduced reserves violated contingency reliability—i.e., the power system dispatch is tightly optimized, thus susceptible to any cooling-water deficits. Under the no fs configuration, initially dispatched reserves exactly equal required reserves only at 74% power system loading, otherwise initially dispatched reserves were greater than required reserves which allowed a safe margin for a reduction in reserves. The no fs configuration, however, did not undergo any reduction in reserves from 68% to 72% power system loading whereas the all fs

configuration did undergo reductions. Therefore, differences in the units committed and dispatched between the no fs and the all fs configurations may have resulted in cooling-water disruptions for the all fs configuration that did not occur in the no fs configuration.

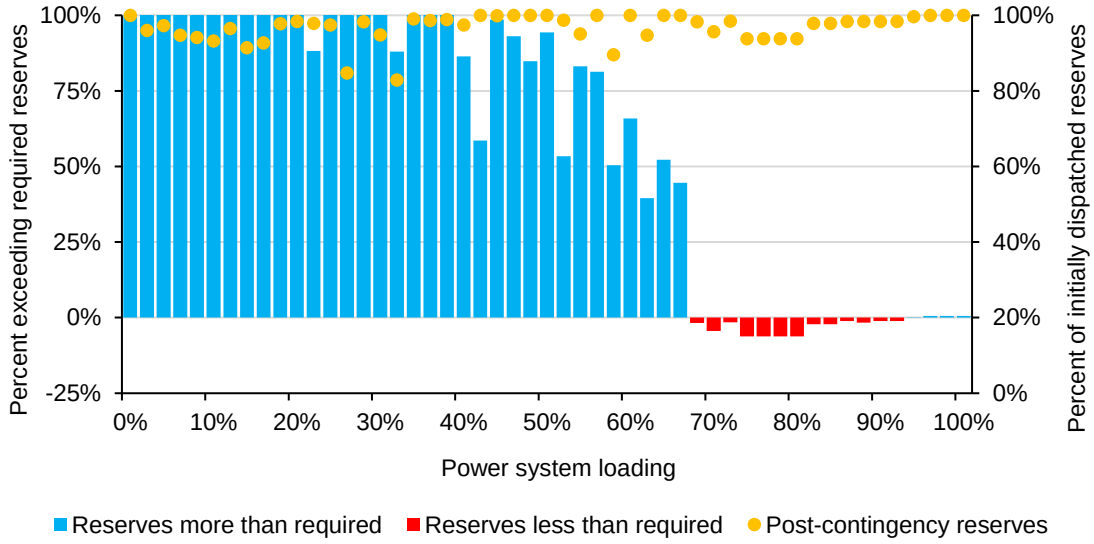

Figure 14: Contingency Reserves During Water Failure Scenario 26 at 100% Water System Demand and Assuming All Fs

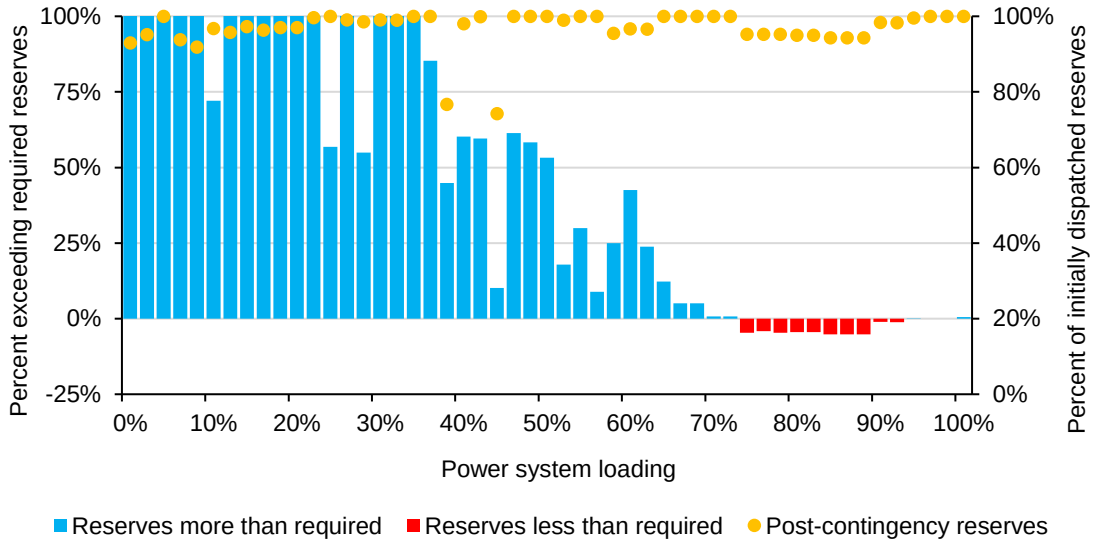

Figure 15: Contingency Reserves During Water Failure Scenario 26 at 100% Water System Demand and Assuming No Fs

All reduction in reserves that occurred for the 68%, 70%, and 72% power system loading during the 100% water system demand for the all fs configuration were due to a reduction in

reserves at natural gas unit 40013—i.e., Harquahala Generating Project. No reserves were lost at the same power system loading and water system demand for the no fs configuration. Figure 16 depicts the reduction in reserves at Harquahala Generating Project for these the three power system loadings.

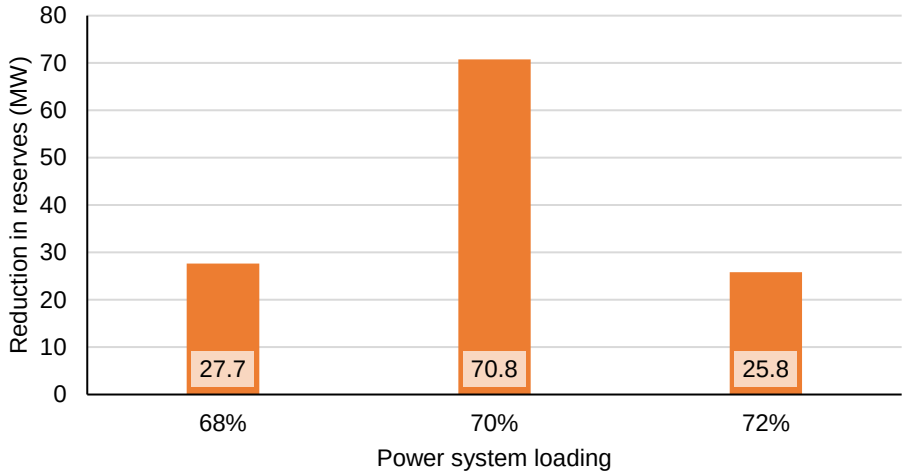

Figure 16: Reduction in Reserves at Harquahala Generating Project During Water Failure Scenario 26 at 100% Water System Demand and Assuming All Fs

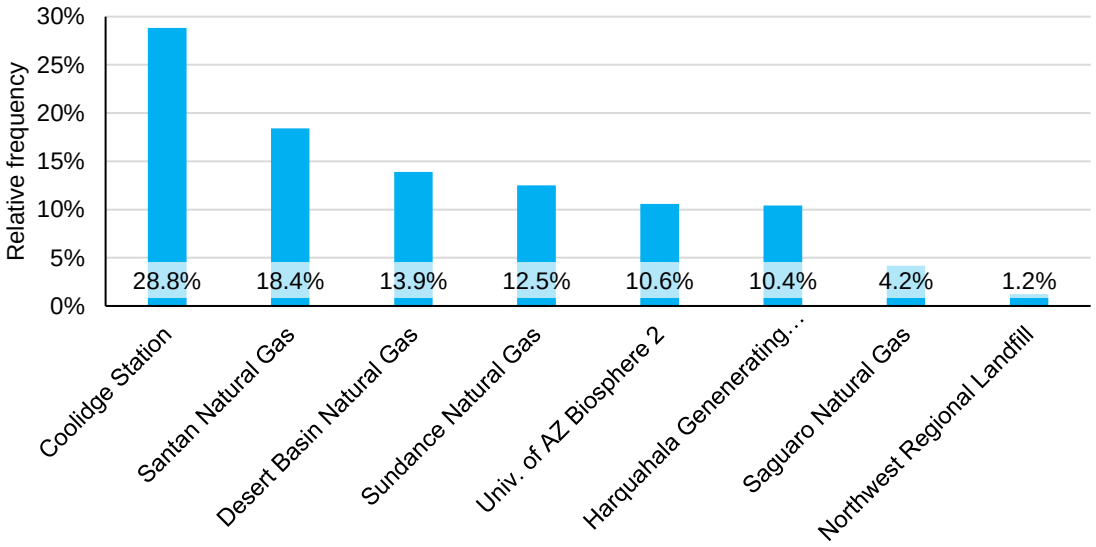

Figure 17: Distribution for Generating Units That Undergo Reduction in Reserves

Figure 17 identifies the frequency that generating units undergo a reduction in reserves when any unit undergoes a reduction in reserves. This frequency data is generated from data

collected from scenarios 2 and 26 under water system demand 100% for the all fs configuration, scenarios 1, 21, and 29 under water system demand 50% for the no fs configuration, scenarios 1, 4, 9, 14, and 27 under water system demand 75% for the no fs configuration, and scenarios 1, 2, 3, 8, 18, and 26 under water system demand 100% for the no fs configuration. These scenarios were chosen because they contributed to the violations depicted in Fig. 8. Coolidge Station undergoes 28.8% of all instances of reduced reserves and was the most frequent of the 8 units that undergo reduced reserves.

2.4 CONCLUSIONS

This work separately modeled an electric power network and water supply network serving the urban area within the Phoenix Metropolitan Area—i.e., Maricopa and Pinal counties. Their operation is simulated in a realistic network flows model in which the power system is dispatched to serve power loads and maintain N-1 contingency reliability, and the water system met water demands while maintaining required pressure levels. A proposed methodology for power-water contingency analysis was performed by analyzing the effect of 31 water failure scenarios on power system reliability across many power and water operational states—e.g. system load. When assuming that all natural gas generating units are fast-starting, the coupled power-water network's N-1 reliability was found to be vulnerable to 2 water failure scenarios above 60% power system loading at high water system demand of 100%. When assuming no natural gas generating units are fast-starting, the power-water network was vulnerable to many water failure scenarios below 60% power system loading at water system demands of 75% and 100% and vulnerable to 2 water failure scenarios above 60% power system loading at 100% water system demand.

A water failure analysis at 100% water system demand was performed on 942 canal sections after screening all 2,624 canal sections in the water supply network. The 31 water failure scenarios that were unique and caused the greatest amount of water deficits in the water failure analysis were chosen for use in the power-water contingency analysis investigation. Results indicate that 2 water failure scenarios violated N-1 contingency reliability when assuming all fast-starting, and that 10 water failure scenarios violated reliability when assuming no fast-starting. At

power system loadings 60% and above, 2 water failure scenarios commonly caused violations and are identified as critical: scenarios 2 (water flow out of Waddell dam) and 26 (CAP canal west of Waddell Dam). At power system loadings below 60% and when assuming no fs, 1 water failure scenario commonly caused violations and is identified as critical: scenario 1 (Salt River feeding water into the Salt-Gila Pumping Station). Noting, however, that there are numerous other water failure scenarios that cause violations of N-1 reliability at 75% and 100% water system demand when assuming no fs.

It's possible for lower water system demands to be vulnerable to more water failure scenarios than higher demands as demonstrated at 0% power system demand by the 75% and 100% water system demand assuming no fs. The former is vulnerable to water failure scenarios 1, 14, and 27 and the latter only vulnerable to water failure scenario 1. The 75% water system demand case dispatches only enough contingency reserves to exactly meet required reserves so that any reduction in reserves causes violation, while the 100% case dispatches at least 160% of required reserves for scenarios 14 and 27. It's also possible that having all fast-starting generating units is more vulnerable than having no fast-starting as demonstrated at 100% water system demand by the 68%-72% power system demands. The power-water undergoes reduction in reserves at Harquahala Generating Project when assuming all fast-starting while no reduction in reserves occurs when assuming no fast-starting.

Frequency analysis of 13 water failure scenarios that caused a violation of N-1 contingency reliability at 75% and 100% water system demand indicates that there were 8 generating units that undergo a reduction in reserves. The units that undergo a reduction in reserves from highest to lowest frequency include: Coolidge Station, Santan Natural Gas, and Desert Basin Natural Gas, Harquahala Generating Station, Sundance Natural Gas, University of Arizona Biosphere 2, Saguaro Natural Gas, and Northwest Regional Landfill. Future work may be done to identify the generating units undergoing reduced reserved, sourcing them to their water junction, and evaluating the water system vulnerabilities that affect that generating unit's junction. Other work may explore the effect of allocating larger amounts of reserves during dispatch, which

provides an allowable margin of reduction in reserves and potentially reducing the number of N-1 contingency reliability violations.

CHAPTER 3

CONCLUSIONS

It's been over 20 years since the US identified the need for improving the protection of interlinked critical infrastructure in Presidential Decision Directive No. 63. Since then there have been numerous disasters and extreme events including the February 2011 cold weather event in the United States, the 2016 water shortages in Kenya, the 2016 curtailment of thermal power plants in India, and the 2017 hurricane extreme events in Puerto Rico that demonstrate cross infrastructure dependencies are critical to public wellness and safety. While resiliency for civil infrastructure systems has undergone gradual adoption and numerous models and simulations of interconnected infrastructure system have been created, there remains no unified or codified definition, process, or methodology for investigating the vulnerabilities of interdependent infrastructure systems. Previous works in coupled power and water systems are insufficient for modeling and simulating the operation of these systems in real-time scenarios because they're constrained by at least one of the three following limitations: time scale is too long, system boundary is too small, or model is too abstract. Hydrological network models focus on long time periods (e.g., years) in which power plant capacity or reserve margin of the power system decrease over decades. These investigations are useful to planners for system expansion, however, provide little guidance for operators to respond to emergencies in minutes. Many real-time network flow models are sized below one substation service area which may not even include a single power plant. Graph network models focus on topological properties of networks and may not fully represent electric power flow determined by the complex behavior of heterogenous components operating in the network. These limitations diverge from the reality of power system operators (i.e., balancing authorities) that must respond to contingencies within a 10-minute time period for their operating area (i.e., numerous substations) while constrained by voltage ratings, thermal limits, generating unit characteristics (e.g., ramp rates), and more.

Chapter 2 examined the dynamic complexity of an interconnected electric transmission network and water supply network when subjected to normal operating stress (i.e., power system loading, water system demand), failure (i.e., water failure scenario), and under two configurations

for the generation fleet (i.e., all or no natural gas units are fast-start) and dispatched to meet the numerous operating and reliability constraints for the power (e.g., allocation of contingency reserves) and water (e.g., pressure levels) systems. This highly constrained and stressed model simulated the emergent behavior in which localized water failure scenarios propagated across infrastructure systems to disrupt the operational reliability of the power system. Results identified range of power system loadings and water system demands in which the water system failures affected the power system, but also specified critical water system failure scenarios, the generating units that most frequently undergo a reduction in contingency reserves, and the potential trends in the power system dispatch that increase vulnerability. The results are explicit enough to be immediately actionable for power and water system operators serving the Phoenix Metropolitan Area.

The results from Chapter 2 indicate several key findings. Changes in water system demand or natural gas fast-start configuration had little to no effect on the amount of reserves dispatched by the security-constrained unit and commitment (SCUC) optimization program for power loadings greater than 70% because the two largest generating units are dispatched to maximum capacity. Natural gas units with fast-start capability were necessary to maintain N-1 contingency reliability of the PMA power network for power system loadings less than 60% because the SCUC dispatched less contingency reserves, on average, when assuming no natural gas units were of fast-start configuration for power system loadings less than 60%. When assuming that all natural gas units were of fast-start configuration, power network N-1 reliability was negatively affected during water failure scenarios when water system demands were greater than 75%. Water failure scenarios 2 (water flow exiting Waddell Dam) and 26 (CAP canal west of Waddell Dam) were critical to N-1 reliability for power loadings above 60%. When assuming that no natural gas units were of fast-start configuration, water failure scenario 1 (Salt River feeding into Salt-Gila Pumping Station) was critical to N-1 reliability for power loadings less than 60%. The Coolidge Station was the most frequent power plant to undergo reduced contingency reserves when N-1 reliability was violated, while Santan Natural Gas and Desert Basin Natural Gas were second and third, respectively, most frequent. Based on these results, power and water

system operators can direct their attention these infrastructure assets critical to reliability. However, when assuming no fast-start configuration, 9 other water failure scenarios also caused the violation of N-1 reliability for power loadings less than 60% without any indication of a trend, therefore, in this operating region, it is suggested that an analysis by full enumeration of water failure scenarios is performed because any scenario may negatively affect N-1 reliability.

How do stressors propagate across interconnected power and water? Stressors in interconnected infrastructure systems can propagate across systems primarily because the nonlinear behaviors of complex infrastructure systems obscure their origins and effects. We can reveal some of these latent stressors by modeling and simulating the interconnected infrastructures. Currently, however, water system and power system operators maintain separated operational practices, conceding the potential for stressors to propagate across infrastructure systems because they remain hidden. With improved data collection and sharing, more accurate infrastructure modeling and broader modeling of systems of infrastructures, and inclusion of the realistic operating procedures (e.g., constraints) of the critical infrastructures we can better understand the simultaneous operation of our combined infrastructure systems under stressors and system states not yet considered. This work demonstrates that localized failures in water supply systems can lead to a reduction in reserves available at power generating facilities needed to maintain N-1 contingency reliability of power systems, and that some water failure scenarios are only critical in certain operating regions (e.g., power system loadings).

What are the independent and dependent variables for investigating the propagation of stressors across interconnected power-water networks? The work done in this dissertation investigated the effects of stress across power-water interconnections that include the power system dependence on cooling water for the generation fleet and the water system dependence on electric power for the pumping stations. Two independent variables that stress the interconnected network daily were loadings of the power system and demands of the water system, however, two additional independent variables also affected propagation of stress across the power-water infrastructure including water canal failures and whether the natural gas units were of fast-start configuration or not. One hypothesis is that higher power system loadings and

higher water system demands would increase the propagation of failure. Results confirm that there is truth to this, however, it's not directly correlated. Power system loadings greater than 92% showed no signs of violating N-1 contingency reliability, however, the region between 65% and 92% power loading most frequently showed the most violations at high water system demands. Secondly, that vulnerability at medium (50%) water system demands and greater depends largely on the fast-start configuration of the natural gas generating units. While there are over 2,500 water line connections in the water supply network, only 3 unique sections of the were network were found to be critical (Scenarios 1, 2, and 26). These critical sections were identified after performing a water failure analysis and then the full power-water contingency analysis. Only 8 of the 64 generating units undergo reduced reserves whenever the power-water network violated N-1 contingency analysis. Therefore, the investigation reveals that while power system loadings and water system demands matter, so too do the water failure scenarios in the water network, the fast-start configuration of the natural gas units, and the dispatched output and reserves from generating units in the power network.

How do interdependencies affect reliability in a case study of the Phoenix Metropolitan Area? Chapter 2 used the most recent publicly available data on the power and water infrastructure in the Phoenix Metropolitan Area to simulate an interconnected power-water network and it indicated several cases in which the power system N-1 contingency reliability is susceptible to water system failures. A total of 11,067 power-water simulations were performed across 51 power system loading states, 4 water system demand states, 31 water failure scenarios, and 2 natural gas fast-starting configuration and 70 simulations resulted in a violation of N-1 contingency analysis for the power system. Statistically, this is only 0.006% of simulations, however, these cases can result in the unlikely propagation of failure from the water to the power system that would otherwise remain hidden from traditional risk analysis methods. It's precisely the low-probability, high-consequence extreme events that pose significant threat to critical infrastructure protection. With this in mind, it's urged that power and water system operators engage in a collective effort to better understand the dependences and interconnections that occur between their two systems. The current analysis identified five observations that can help

operators understand the interdependent behavior of the coupled power and water system in the Phoenix Metropolitan Area:

- When power system loadings were above 60%, power system reliability was only negatively affected by water failure scenarios 2 and 26.
- When power system loadings were below 60%, power system reliability was only negatively affected when the natural gas units were not fast-start configuration. Primarily because the fast-start configuration allows excess of contingency reserves to be dispatched at this lower power system operating region.
- When power system loadings were below 60%, power system reliability was most negatively affected by water failure scenario 1 but can also be affected by any of the other water failure scenarios.
- Power system vulnerability differs for power system loadings below 60% to above 60% because the largest and second largest generating units gradually become dispatched to their maximum capacity, requiring the peak amount of contingency reserves.
- When N-1 contingency reliability is negatively affected, the generating unit that most frequently undergoes a reduction in reserves is Coolidge Stations, with Santan Natural Gas, Desert Basin Natural Gas, and Sundance Natural Gas in second, third, and fourth place.

This dissertation improves our understanding of interconnected electric transmission and water supply networks serving a metropolitan area based on the operational practices used by engineers for real-time situational awareness and response. This dissertation contributes towards scientific literature by providing and implementing a methodology for generating case studies of realistic power and water networks for metropolitan areas from the publicly available US data set and anywhere else similar data sets are available, evaluating failure scenarios that begin in the water network and propagate to across infrastructure systems to negatively affect the power network, identifying a set of independent and dependent variables for investigating contingency

analysis for power-water networks, and identifying specific infrastructure components/assets that are otherwise hidden to power and water system operators and potentially pose a threat to power-water network reliability. This model and its output improve the sensing capabilities of operators and planners, thus providing power system decision-makers with information to better withstand and absorb water failure scenarios across the breadth of many power load and water demand states. Overall, the realistic interconnected power-water model improves scientists' and engineers' capacity to sense and anticipate propagation of vulnerabilities across infrastructures through a low-cost simulation and learning environment, and adapt current operating procedures for power and water engineers that are currently done separately after learning. This output should encourage more sharing of information for operator and planners between the power and water systems, especially in the Phoenix Metropolitan Area.

REFERENCES

Ahmad, A., El-Shafie, A., Razali, S. F. M., & Mohamad, Z. S. (2014). Reservoir Optimization in Water Resources: a Review. Water Resources Management, 28(11), 3391–3405. doi:10.1007/s11269-014-0700-5

Alaya, A. & Souissi, A. & Tarhouni, J. & Ncib, K. (2003). Optimization of Nebhana Reservoir Water Allocation by Stochastic Dynamic Programming. Water Resources Management. 17. 259-272. 10.1023/A:1024721507339.

Alsubaie, A., Alutaibi, K., & Martí, J. (2016). Resilience Assessment of Interdependent Critical Infrastructure. Lecture Notes in Computer Science, 43–55. doi:10.1007/978-3-319-33331-1_4

Ang, W. K., & Jowitt, P. W. (2006). Solution for Water Distribution Systems under Pressure-Deficient Conditions. Journal of Water Resources Planning and Management, 132(3), 175–182. doi:10.1061/(asce)0733-9496(2006)132:3(175)–7. doi:10.1109/tpwrs.1986.4335006

Bartos, M., Chester, M., Johnson, N., Gorman, B., Eisenberg, D., Linkov, I., & Bates, M. (2016). Impacts of rising air temperatures on electric transmission ampacity and peak electricity load in the United States. Environmental Research Letters, 11(11), 114008. doi:10.1088/1748-9326/11/11/114008

Bartos, M. D., & Chester, M. V. (2015). Impacts of climate change on electric power supply in the Western United States. Nature Climate Change, 5(8), 748–752. doi:10.1038/nclimate2648

Bigger, J. E., Willingham, M. G., Krimgold, F., & Mili, L. (2009). Consequences of critical infrastructure interdependencies: lessons from the 2004 hurricane season in Florida. International Journal of Critical Infrastructures, 5(3), 199. doi:10.1504/ijcis.2009.024871

Bloomfield, R. E., Popov, P., Salako, K., Stankovic, V., & Wright, D. (2017). Preliminary interdependency analysis: An approach to support critical-infrastructure risk-assessment. Reliability Engineering & System Safety, 167, 198–217. doi:10.1016/j.ress.2017.05.030

Brummitt, C. D., D'Souza, R. M., & Leicht, E. A. (2012). Suppressing cascades of load in interdependent networks. Proceedings of the National Academy of Sciences, 109(12), E680–E689. https://doi.org/10.1073/pnas.1110586109

Bruneau, M., Chang, S. E., Eguchi, R. T., Lee, G. C., O'Rourke, T. D., Reinhorn, A. M., … von Winterfeldt, D. (2003). A Framework to Quantitatively Assess and Enhance the Seismic Resilience of Communities. Earthquake Spectra, 19(4), 733–752. doi:10.1193/1.1623497

Bruins, H. J. (2000). Proactive Contingency Planning vis-à-vis Declining Water Security in the 21st Century. Journal of contingencies and crisis management, 8(2). 63-72.

Capitanescu, F. (2016). Critical review of recent advances and further developments needed in AC optimal power flow. Electric Power Systems Research, 136, 57–68. doi:10.1016/j.epsr.2016.02.008

Central Arizona Project. (2012). Cap Pumping Stations. [PDF file] Retrieved from http://web.sahra.arizona.edu/education2/hwr213/docs/Unit1Wk4/Hwr203_CAPslides.pdf

Central Valley Project and State Water Project. (2016). 2016 Drought Contingency Plan for Water Project Operations. Retrieved from http://www.water.ca.gov/waterconditions/docs/2016-DroughtContingencyPlan-CVP-SWPOperations-Feb-Nov_1.19.16-FINAL.pdf

Chang, S. E., McDaniels, T., & Beaubien, C. (2009). Societal Impacts of Infrastructure Failure Interdependencies: Building an Empirical Knowledge Base. TCLEE 2009. doi:10.1061/41050(357)66

Chang, S. E., McDaniels, T., Fox, J., Dhariwal, R., & Longstaff, H. (2013). Toward Disaster-Resilient Cities: Characterizing Resilience of Infrastructure Systems with Expert Judgments. Risk Analysis, 34(3), 416–434. doi:10.1111/risa.12133

Chen, Z., Du, W. B., Cao, X. Bin, & Zhou, X. L. (2015). Cascading failure of interdependent networks with different coupling preference under targeted attack. Chaos, Solitons and Fractals, 80, 7–12. https://doi.org/10.1016/j.chaos.2015.03.005

Chen, Y.-Z., Huang, Z.-G., Zhang, H.-F., Eisenberg, D., Seager, T. P., & Lai, Y.-C. (2015). Extreme events in multilayer, interdependent complex networks and control. Scientific Reports, 5, 17277. https://doi.org/10.1038/srep17277

Chopra, S. S., & Khanna, V. (2015). Interconnectedness and interdependencies of critical infrastructures in the US economy: Implications for resilience. Physica A: Statistical Mechanics and Its Applications, 436, 865–877. doi:10.1016/j.physa.2015.05.091

Chowdhury, B. H., & Rahman, S. (1990). A review of recent advances in economic dispatch. IEEE Transactions on Power Systems, 5(4), 1248–1259. doi:10.1109/59.99376

Chin, D. A. (2013). Water-Resources Engineering (3rd ed.). Upper Saddle River, NJ: Pearson Education, Inc.

City of Phoenix Water Services Department. (2011). 2011 Water Resource Plan. Retrieved from https://www.phoenix.gov/waterservicessite/Documents/wsd2011wrp.pdf

Clark, R. M., & Deininger, R. A. (2000). Protecting the nation's critical infrastructure: The vulnerability of US water supply systems. Journal of contingencies and crisis management, 8(2), 73-80.

Coffrin, C., & Van Hentenryck, P. (2014). A Linear-Programming Approximation of AC Power Flows. INFORMS Journal on Computing, 26(4), 718–734. doi:10.1287/ijoc.2014.0594

Craig, C. A., & Feng, S. (2016). An examination of electricity generation by utility organizations in the Southeast United States. Energy, 116, 601–608. doi:10.1016/j.energy.2016.10.013

Crowther, K. G., Haimes, Y. Y., & Taub, G. (2007). Systemic Valuation of Strategic Preparedness Through Application of the Inoperability Input-Output Model with Lessons Learned from Hurricane Katrina. Risk Analysis, 27(5), 1345–1364. doi:10.1111/j.1539-6924.2007.00965.x

Dai, J., Wu, S., Han, G., Weinberg, J., Xie, X., Wu, X., … Yang, Q. (2018). Water-energy nexus: A review of methods and tools for macro-assessment. Applied Energy, 210, 393–408. doi:10.1016/j.apenergy.2017.08.243

Dudenhoeffer, D., Permann, M., & Manic, M. (2006). CIMS: A Framework for Infrastructure Interdependency Modeling and Analysis. Proceedings of the 2006 Winter Simulation Conference. doi:10.1109/wsc.2006.323119

Ejebe, G. C. & Wollengberg, B. F. (1979). Automatic contingency selection. IEEE Transactions on Power Apparatus and Systems, (1), 97-109

EPRI. (2016). [Software]. OpenDSS (Version 7.6.5.64). Retrieved from http://smartgrid.epri.com/SimulationTool.aspx

IEA. (2016). World Energy Outlook 2016. doi:10.1787/weo-2016-en

Fair, J. M., LeClaire, R. J., Wilson, M. L., Turk, A. L., DeLand, S. M., Powell, D. R., … Izraelevitz, D. (2007). An Integrated Simulation of Pandemic Influenza Evolution, Mitigation and Infrastructure Response. 2007 IEEE Conference on Technologies for Homeland Security. doi:10.1109/ths.2007.370052

Farivar, M., Chen, L., & Low, S. (2013). Equilibrium and dynamics of local voltage control in distribution systems. 52nd IEEE Conference on Decision and Control. doi:10.1109/cdc.2013.6760555

FERC & NERC. (2011). Report on Outages and Curtailments During the Southwest Cold Weather Event of February 1-5, 2011. Retrieved from https://www.ferc.gov/legal/staff-reports/08-16-11-report.pdf

Fooladivanda, D., & Taylor, J. A. (2015). Optimal pump scheduling and water flow in water distribution networks. 2015 54th IEEE Conference on Decision and Control (CDC). doi:10.1109/cdc.2015.7403043

Francis, R., & Bekera, B. (2014). A metric and frameworks for resilience analysis of engineered and infrastructure systems. Reliability Engineering & System Safety, 121, 90–103. doi:10.1016/j.ress.2013.07.004

Frank, S., Steponavice, I., & Rebennack, S. (2012). Optimal power flow: a bibliographic survey I. Energy Systems, 3(3), 221–258. doi:10.1007/s12667-012-0056-y

Frank, S., Steponavice, I., & Rebennack, S. (2012). Optimal power flow: a bibliographic survey II. Energy Systems, 3(3), 259–289. doi:10.1007/s12667-012-0057-x

Freihoefer, A., Mason, D., Jahnke, P., Dubas, L., & Hutchinson, K. (2009). Regional Groundwater Flow Model of the Salt River Valley Phoenix Active Management Area Model Update and Calibration. Retrieved from http://www.azwater.gov/AzDWR/Hydrology/Modeling/documents/SRV8306_Model_Report.pdf

Gonzalez-Salazar, M. A., Kirsten, T., & Prchlik, L. (2018). Review of the operational flexibility and emissions of gas- and coal-fired power plants in a future with growing renewables. Renewable and Sustainable Energy Reviews, 82, 1497–1513. doi:10.1016/j.rser.2017.05.278

Guidotti, R., Chmielewski, H., Unnikrishnan, V., Gardoni, P., McAllister, T., & van de Lindt, J. (2016). Modeling the resilience of critical infrastructure: the role of network dependencies. Sustainable and Resilient Infrastructure, 1(3-4), 153–168. doi:10.1080/23789689.2016.1254999

Homeland Infrastructure Foundation-Level Data. (2019). Electric Power Transmission Lines [Data file]. Retrieved from https://gii.dhs.gov/hifld/content/hifld-data-catalog on October 7, 2019

Homeland Infrastructure Foundation-Level Data. (2019). Power Plants [Data file]. Retrieved from https://gii.dhs.gov/hifld/content/hifld-data-catalog on October 7, 2019

Hrudey, S. E., Hrudey, E. J., & Pollard, S. J. (2006). Risk management for assuring safe drinking water. Environment International, 32(8), 948-95

Huneault, M., & Galiana, F. D. (1991). A survey of the optimal power flow literature. IEEE Transactions on Power Systems, 6(2), 762–770. doi:10.1109/59.76723

ISO New England. (2019). ISO New England Operating Procedure No. 8 Operating Reserve and Regulation. Retrieved from https://www.iso-ne.com/static-assets/documents/rules_proceds/operating/isone/op8/op8_rto_final.pdf

Johansson, J., & Hassel, H. (2010). An approach for modelling interdependent infrastructures in the context of vulnerability analysis. Reliability Engineering & System Safety, 95(12), 1335–1344. doi:10.1016/j.ress.2010.06.010

Kajitani, Y., & Sagai, S. (2009). Modelling the interdependencies of critical infrastructures during natural disasters: a case of supply, communication and transportation infrastructures. International Journal of Critical Infrastructures, 5(1/2), 38. doi:10.1504/ijcis.2009.022848

Koch, H., & Vögele, S. (2009). Dynamic modelling of water demand, water availability and adaptation strategies for power plants to global change. Ecological Economics, 68(7), 2031–2039. doi:10.1016/j.ecolecon.2009.02.015

Kressig, A., Byers, L., Friedrich, J., & Luo, T. (2018, April 11). Water Stress Threatens Nearly Half the World's Thermal Power Plant Capacity. World Resources Institute. Retrieved from http://www.wri.org/blog/2018/04/water-stress-threatens-nearly-half-world-s-thermal-power-plant-capacity

Labadie, J. W. (2004). Optimal Operation of Multireservoir Systems: State-of-the-Art Review. Journal of Water Resources Planning and Management, 130(2), 93–111. doi:10.1061/(asce)0733-9496(2004)130:2(93)

Lee, E. E., Mitchell, J. E., & Wallace, W. A. (2007). Restoration of Services in Interdependent Infastructure Systems: A Network Flows Approach. IEEE Transactions on Systems, Man, and Cybernetics, 37(6), 1303–1317. https://doi.org/10.1109/TSMC.2007.905849

Lewis, T. G. (2020). Critical Infrastructure Protection in Homeland Security: Defending a networked nation. John Wiley & Sons Inc.

Liao, X., Hall, J. W., & Eyre, N. (2016). Water use in China's thermoelectric power sector. Global Environmental Change, 41, 142–152. doi:10.1016/j.gloenvcha.2016.09.007

Liu, X., Tang, Q., Voisin, N., & Cui, H. (2016). Projected impacts of climate change on hydropower potential in China. Hydrology and Earth System Sciences Discussions, 1–30. doi:10.5194/hess-2016-41

Luiijf, H. A. M., Nieuwenhuijs, A. H., Klaver, M. H. A., Eeten, M. J. G. V., & Cruz, E. (2010). Empirical findings on European critical infrastructure dependencies. International Journal of System of Systems Engineering, 2(1), 3. doi:10.1504/ijsse.2010.035378

Luo, T. (2017, July 26). Droughts and Blackouts: How Water Shortages Cost India Enough Energy to Power Sri Lanka. World Resources Institute. Retrieved from http://www.wri.org/blog/2017/07/droughts-and-blackouts-how-water-shortages-cost-india-enough-energy-power-sri-lanka

Luo, T., Young, R., Reig, P. (2016). Aqueduct Projected Water Stress Country Rankings. Retrieved from http://www.wri.org/sites/default/files/aqueduct-water-stress-country-rankings-technical-note.pdf

Macknick, J., Newmark, R., Heath, G., & Hallett, K. C. (2012). Operational water consumption and withdrawal factors for electricity generating technologies: a review of existing literature. Environmental Research Letters, 7(4), 045802. doi:10.1088/1748-9326/7/4/045802

Maricopa Association of Governments. (2019). 2017/2018 Arizona COG/MPO Employer Database [Data file]. Accessible from https://geo.azmag.gov/maps/azemployment/

McDaniels, T., Chang, S., Cole, D., Mikawoz, J., & Longstaff, H. (2008). Fostering resilience to extreme events within infrastructure systems: Characterizing decision contexts for mitigation and adaptation. Global Environmental Change, 18(2), 310–318. doi:10.1016/j.gloenvcha.2008.03.001

McDaniels, T., Chang, S., Peterson, K., Mikawoz, J., & Reed, D. (2007). Empirical Framework for Characterizing Infrastructure Failure Interdependencies. Journal of Infrastructure Systems, 13(3), 175–184. doi:10.1061/(asce)1076-0342(2007)13:3(175)

McDonald, R. I., Weber, K., Padowski, J., Flörke, M., Schneider, C., Green, P. A., … Montgomery, M. (2014). Water on an urban planet: Urbanization and the reach of urban water infrastructure. Global Environmental Change, 27, 96–105. doi:10.1016/j.gloenvcha.2014.04.022

Mizgalewicz, P. J. (1991). An analysis of monthly water demand in Phoenix, Arizona. (Masters Thesis). Retrieved from http://www.ce.utexas.edu/prof/maidment/GISHYDRO/pawel/phoenix/x2v6a.pdf

National Atlas of the United States. (2013). Cities and Towns of the United States, 2014. National Atlas of the United States. Available at https://purl.stanford.edu/bx729wr3020

NERC. (2007). Reliability Concepts Version 1.0.2. Retrieved from http://www.nerc.com/files/concepts_v1.0.2.pdf

North, M. J. (2001). Toward Strength and Stability. Social Science Computer Review, 19(3), 307–323. doi:10.1177/089443930101900306

OpenEI. (n.d.). [Data table] Powerplant Curtailments. Retrieved from http://en.openei.org/wiki/Powerplant_Curtailments

Otuki, N. (2017, May 15). Spare power capacity falls to 7-year low. Business Daily. Retrieved from https://www.businessdailyafrica.com/news/Spare-power-capacity-falls-7year-low--/539546-3927358-pxwuk2/index.html

Ouyang, M. (2014). Review on modeling and simulation of interdependent critical infrastructure systems. Reliability Engineering and System Safety, 121, 43–60. https://doi.org/10.1016/j.ress.2013.06.040

Pala, O., Wilson, D., Bent, R., Linger, S., & Arnold, J. (2014). Accuracy of Service Area Estimation Methods Used for Critical Infrastructure Recovery. Lecture Notes in Computer Science, 173–191. doi:10.1007/978-3-662-45355-1_12

Park, J., Seager, T. P., Rao, P. S. C., Convertino, M., & Linkov, I. (2012). Integrating Risk and Resilience Approaches to Catastrophe Management in Engineering Systems. Risk Analysis, 33(3), 356–367. doi:10.1111/j.1539-6924.2012.01885.x

Pollard, S. J., Strutt, J. E., MacGillivray, B. H., Hamilton, P. D., & Hrudey, S. E. (2004). Risk analysis and management in the water utility sector: a review of drivers, tools and techniques. Process Safety and Environmental Protection, 82(6), 453-462.

Potomac Economics. (2011). Investigation of the ERCOT Energy Emergency Alert Level 3 on February 2, 2011. Retrieved from http://www.ercot.com/content/meetings/tac/keydocs/2011/0505/09._IMM_Report_Events_020211.pdf

Pregnolato, M., Ford, A., Robson, C., Glenis, V., Barr, S., & Dawson, R. (2016). Assessing urban strategies for reducing the impacts of extreme weather on infrastructure networks. Royal Society Open Science, 3(5), 160023. doi:10.1098/rsos.160023

Rinaldi, S. M., Peerenboom, J. P., & Kelly, T. K. (2001). Identifying, understanding, and analyzing critical infrastructure interdependencies. IEEE Control Systems, 21(6), 11–25. doi:10.1109/37.969131

Robinius, M., Stein, F. ter, Schwane, A., & Stolten, D. (2017). A Top-Down Spatially Resolved Electrical Load Model. Energies, 10(3), 361. doi:10.3390/en10030361

Rome, E., Langeslag, P., & Usov, A. (2014). Federated Modelling and Simulation for Critical Infrastructure Protection. Networks of Networks: The Last Frontier of Complexity, 225–253. doi:10.1007/978-3-319-03518-5_11

Rong, M., Han, C., & Liu, L. (2010). Critical Infrastructure Failure Interdependencies in the 2008 Chinese Winter Storms. 2010 International Conference on Management and Service Science. doi:10.1109/icmss.2010.5576239

Sarker, P., & Lester, H. D. (2019). Post-Disaster Recovery Associations of Power Systems Dependent Critical Infrastructures. Infrastructures, 4(2), 30. doi:10.3390/infrastructures4020030

Scanlon, B. R., Duncan, I., & Reedy, R. C. (2013). Drought and the water–energy nexus in Texas. Environmental Research Letters, 8(4), 045033. doi:10.1088/1748-9326/8/4/045033

Schoenwald, D. A., Barton, D. C., & Ehlen, M. A. (2004). An agent-based simulation laboratory for economics and infrastructure interdependency. Proceedings of the 2004 American Control Conference. doi:10.23919/acc.2004.1386752

Setola, R., Rosato, V., Kyriakides, E., & Rome, E. (Eds.). (2016). Managing the Complexity of Critical Infrastructures. Studies in Systems, Decision and Control. doi:10.1007/978-3-319-51043-9

Singh, A., Eser, P., Chokani, N., & Abhari, R. S. (2015). Improved modelling of demand and generation in high resolution simulations of interconnected power systems. 2015 12th International Conference on the European Energy Market (EEM). doi:10.1109/eem.2015.7216689

Southwest Power Pool. (2015). Operating Criteria: Revision 1.3. Retrieved from https://spp.org/documents/49959/spp%20operating%20criteria%20and%20appendices%20v1.3%204_27_2017.pdf

Southwest Reserve Sharing Group. (2017). Participation Agreement. Retrieved from https://5041bd21-7d6a-45c6-8837-e6980babf476.filesusr.com/ugd/537731_817eaa839a7f4a40ace76ce7c24e67d5.pdf

Steinberg, Laura and Santella, Nicholas and Zoli, Corri, Baton Rouge Post-Katrina: The Role of Critical Infrastructure Modeling in Promoting Resilience (February 15, 2011). Homeland Security Affairs, Vol. 7, Article 7, February 2011. Available at SSRN: https://ssrn.com/abstract=2004532

Svendsen, N. K., & Wolthusen, S. D. (2007). Connectivity models of interdependency in mixed-type critical infrastructure networks. Information Security Technical Report, 12(1), 44–55. https://doi.org/10.1016/j.istr.2007.02.005

Tucson Water. (2016). 2016 Annual Water Quality Report. [PDF file]. Retrieved from https://toua.net/wp-content/uploads/2016_Annual_Water_Quality_Report_Main_1.pdf

U.S. Census Bureau. (2019). American Community Survey 2017 5-year estimates block group [Data file]. Retrieved from https://www2.census.gov/geo/tiger/TIGER_DP/2017ACS/

USDA. (2019). 2018 National Cropland Data Layer [Data file]. Retrieved from https://www.nass.usda.gov/Research_and_Science/Cropland/Release/

USDA. (1939). *Flow of Water in Irrigation and Similar Canals*. Washington, DC: Scobey, F. C. Retrieved from https://naldc.nal.usda.gov/download/CAT86200647/PDF

U.S. DOE. (2014). The Water-Energy Nexus: Challenges and Opportunities. Retrieved from https://www.energy.gov/sites/prod/files/2014/07/f17/Water%20Energy%20Nexus%20Full%20Report%20July%202014.pdf

U.S. DOE. (2010). Water Vulnerabilities for Existing Coal-fired Power Plants. Retrieved from http://www.ipd.anl.gov/anlpubs/2010/08/67687.pdf

U.S. DOE. (2006). Energy Demands on Water Resources. Retrieved from http://www.circleofblue.org/wp-content/uploads/2010/09/121-RptToCongress-EWwEIAcomments-FINAL2.pdf

U.S. EIA. (2019). U.S. Electric System Operating Data [Data file]. Retrieved from https://www.eia.gov/opendata/bulkfiles.php

U.S. EIA. (2017). Electricity: Components of Net Demand, 2014 [Table file]. Retrieved from https://www.eia.gov/consumption/manufacturing/data/2014/pdf/table11_1.pdf

U.S. EIA. (2017). Sales of Electricity to Ultimate Customers by End-Use Sector [Table]. Retrieved from https://www.eia.gov/electricity/annual/html/epa_02_08.html

U.S. EPA. (2008). [Software]. EPANET (Version 2.00.12). Retrieved from https://www.epa.gov/water-research/epanet

USGS. (2019). National Hydrography Dataset Plus High Resolution [Data file]. Retrieved from https://viewer.nationalmap.gov/basic/?basemap=b1&category=nhd&title=NHD%20View

USGS. (2019). NED 1/3 arc-second 2013 1x1 degree ArcGrid [Data file]. Retrieved from https://viewer.nationalmap.gov/basic/

USGS. (2018). Water Use Data for Arizona [Table]. Available at https://waterdata.usgs.gov/az/nwis/water_use?format=html_table&rdb_compression=file&wu_area=County&wu_year=2015&wu_county=013%2C021&wu_category=ALL&wu_county_nms=Maricopa%2BCounty%252CPinal%2BCounty

Van Vliet, M. T. H., Sheffield, J., Wiberg, D., & Wood, E. F. (2016). Impacts of recent drought and warm years on water resources and electricity supply worldwide. Environmental Research Letters, 11(12), 124021. doi:10.1088/1748-9326/11/12/124021

Van Vliet, M. T. H., Wiberg, D., Leduc, S., & Riahi, K. (2016). Power-generation system vulnerability and adaptation to changes in climate and water resources. Nature Climate Change, 6(4), 375–380. doi:10.1038/nclimate2903

Van Vliet, M. T. H., Yearsley, J. R., Ludwig, F., Vögele, S., Lettenmaier, D. P., & Kabat, P. (2012). Vulnerability of US and European electricity supply to climate change. Nature Climate Change, 2(9), 676–681. doi:10.1038/nclimate1546

Voisin, N., Kintner-Meyer, M., Wu, D., Skaggs, R., Fu, T., Zhou, T., … Kraucunas, I. (2018). Opportunities for Joint Water–Energy Management: Sensitivity of the 2010 Western U.S. Electricity Grid Operations to Climate Oscillations. Bulletin of the American Meteorological Society, 99(2), 299–312. doi:10.1175/bams-d-16-0253.1

Voisin, N., Kintner-Meyer, M., Skaggs, R., Nguyen, T., Wu, D., Dirks, J., Xie, Y., Hejazi, M. (2016). Vulnerability of the US western electric grid to hydro-climatological conditions: How bad can it get? Energy, 115, 1–12. doi:10.1016/j.energy.2016.08.059

Wallace, W. A., Mendonça, D., Lee, E. E., Mitchell, J. E., & Chow, J. H. (2003). Managing Disruptions to Critical Interdependent Infrastructures in the Context of the 2001 World Trade Center Attack. Beyond September 11th: An Account of Post-Disaster Research. https://doi.org/10.1109/icsmc.2004.1401165

Wang Fangdong, Lin Han, Wang Fangdong, & Wen Buying. (2010). Substation optimization planning based on the improved orientation strategy of Voronoi diagram. The 2nd International Conference on Information Science and Engineering. doi:10.1109/icise.2010.5688695

Wang, S., Hong, L., & Chen, X. (2012). Vulnerability analysis of interdependent infrastructure systems: A methodological framework. Physica A: Statistical Mechanics and Its Applications, 391(11), 3323–3335. doi:10.1016/j.physa.2011.12.043

WECC. (2019). 2019 Heavy Summer 3a base case [Data file]. Available at https://www.wecc.org/Pages/home.aspx

The White House. (1998, May 22). Presidential Decision Directive/NSC-63. Federation of American Scientists. Retrieved from https://fas.org/irp/offdocs/pdd/pdd-63.htm

Wilbanks, T., Fernandez, S., & Allen, M. (2015). Meeting Challenges in Understanding Impacts of Extreme Weather Events on Connected Infrastructures. Environment, 57(4). doi:10.1080/00139157.2015.1048134

Wood, A. J., & Wollenberg, B. F. (2012). Power Generation, Operation, and Control. John Wiley & Sons.

WWAP. (2014). The United Nations World Water Development Report 2014: Water and Energy. Retrieved from http://unesdoc.unesco.org/images/0022/002257/225741E.pdf

Yeung, E., Judi, D. R., & Daniel, W. B. (2017). Contingency analysis of water distribution networks using quadratic sensitivity functions. 2017 American Control Conference (ACC). doi:10.23919/acc.2017.7962958

Zhang, Y., Yang, N., & Lall, U. (2016). Modeling and simulation of the vulnerability of interdependent power-water infrastructure networks to cascading failures. Journal of Systems Science and Systems Engineering, 25(1), 102–118. doi:10.1007/s11518-016-5295-3

Zimmerman, R., Zhu, Q., de Leon, F., & Guo, Z. (2017). Conceptual Modeling Framework to Integrate Resilient and Interdependent Infrastructure in Extreme Weather. Journal of Infrastructure Systems, 23(4), 04017034. doi:10.1061/(asce)is.1943-555x.0000394

Zio, E., & Sansavini, G. (2011). Modeling interdependent network systems for identifying cascade-safe operating margins. IEEE Transactions on Reliability, 60(1), 94–101. https://doi.org/10.1109/TR.2010.2104211

APPENDIX A

SUPPLEMENTARY INFORMATION FOR QUANTIFYING RELIABILITY OF COUPLED POWER-WATER NETWORKS USING CONTINGENCY ANALYSIS

A.1 POWER NETWORK

The power network topology is based on publicly available 2019 U.S. transmission line and power plant data retrieved from Homeland Infrastructure Foundation-Level Data (HIFLD) [Homeland Infrastructure Foundation-Level Data, 2019]. The 2019 transmission line and power plant data sets contained 83,207 lines and 11,085 plants, respectively, and geographically exceeds the chosen Phoenix Metropolitan Area (PMA) of interest. HIFLD transmissions lines and power plants located outside the geographic boundary enveloping Maricopa and Pinal counties were filtered out. This enveloping area is similar to a rectangle and was used because strictly adhering to the Maricopa and Pinal county boundaries excluded a few transmission lines that looped outside the county boundaries. The resulting HIFLD transmission line within the Maricopa and Pinal county envelope are depicted in Fig. 18 below. This enveloping area was also used for the water network to maintain consistency.

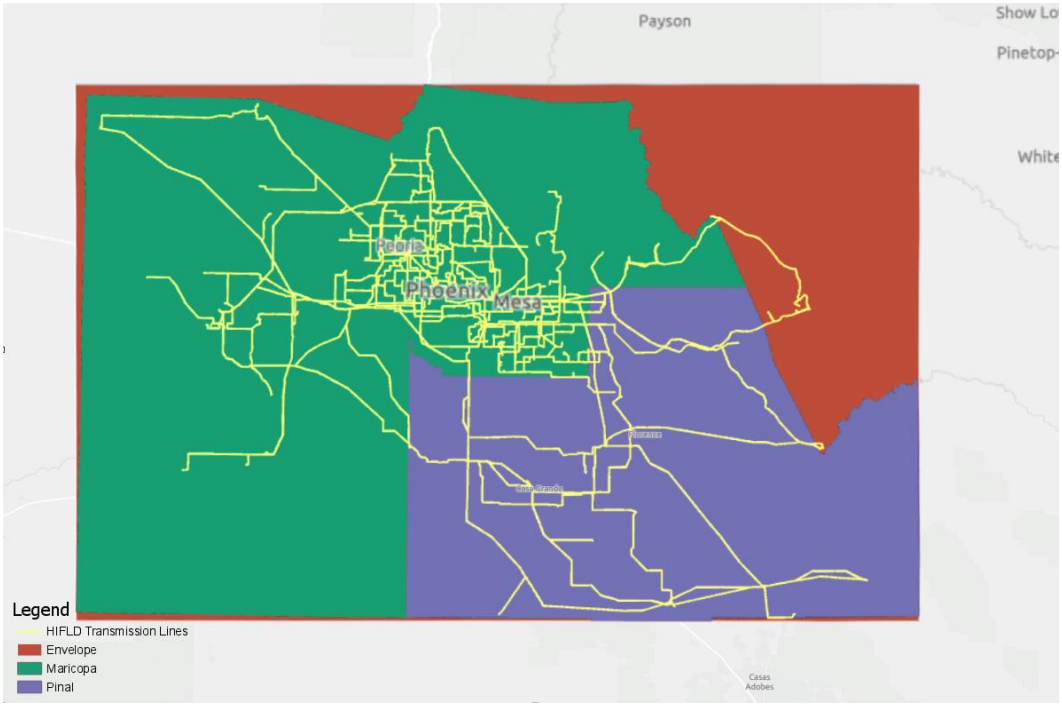

Figure 18: HIFLD Transmission Line System Within the PMA Boundary

While the HIFLD data is very comprehensive, there are some gaps in data, and the HIFLD team provided a list of 7 disconnected line segments to omit from the PMA investigation

that are given in Table 4 [M. Tuttle, personal communication, October 10, 2019]. Invalid voltages of 79 lines were fixed by setting their voltages to the highest value of neighboring buses.

Table 4: Omitted HIFLD Transmission Lines

Transmission ID
300431
300439
304980
306768
307165
312587
313239

Table 5: APS and SRP Interchange Balancing Authorities

Balancing Authority
California Independent System Operator (CISO)
Lost Angeles Department of Water and Power (LDWP)
New Harquahala Generating Company (HGMA)
Public Service Company of New Mexico (PNM)
WAPA – Desert Southwest Region (WALC)
WAPA – Rocky Mountain Region (WACM)
Arlington Valley (DEAA)
Gila River Power (GRMA)
Imperial Irrigation District (IID)
PacifiCorp East (PACE)
Tucson Electric Power (TEPC)

Power system load was modeled using a top-down methodology that takes total system load and spatially distributed load to substations in the PMA region using Eqs. 14-23. Similar methodologies for approximating the distribution of aggregate power loads were used elsewhere [Robinius, Stein, Schwane, & Stolten, 2017; Singh, Eser, Chokani, & Abhari, 2015]. The availability of high-quality real data for the top-down method makes it the better option over bottom-up methods. Total system load of the Arizona Public Service (APS) and Salt River Project (SRP) balancing authorities were combined and then disaggregated into four sectors: total residential load, total commercial load, total industrial load, and total agricultural load. The total loads of the four sectors were then converted into four respective sector loads for PMA the region, then these four PMA sectoral loads were distributed to substations in the PMA region. APS and SRP power system generation, load, and 11 balancing authority (listed in Table 5) interchange values for the 8760 hours of 2017 were obtained from EIA's electric system operating

data [U.S. EIA, 2019], with 2017 chosen because it's the most recent year that had the most complete data set. The EIA operating system hourly data is provided in GMT and were adjusted to local Arizona time by shifting time by negative 7 hours.

The total electric load of APS (P_{APS}) and SRP (P_{SRP}) was combined (P_{tot}) in Eq. 14 and then disaggregated as 44.1% residential load ($P_{tot,RES}$) in Eq. 15, 38.2% commercial load ($P_{tot,COM}$) in Eq. 16, and 17.7% industrial load ($P_{tot,IND}$) based on 2017 EIA sector power consumption data for Arizona [U.S. EIA, 2017], and the agricultural load ($P_{tot,AGR}$) was taken as 10.9% of $P_{tot,IND}$ based on 2014 Western U.S. regional data in Eqs. 17 and 18 [U.S. EIA, 2017].

$$P_{tot} = P_{APS} + P_{SRP} \tag{14}$$

$$P_{tot,RES} = 0.441 \cdot P_{tot} \tag{15}$$

$$P_{tot,COM} = 0.382 \cdot P_{tot} \tag{16}$$

$$P_{tot,IND} = 0.177 \cdot 0.881 \cdot P_{tot} \tag{17}$$

$$P_{tot,AGR} = 0.177 \cdot 0.109 \cdot P_{tot} \tag{18}$$

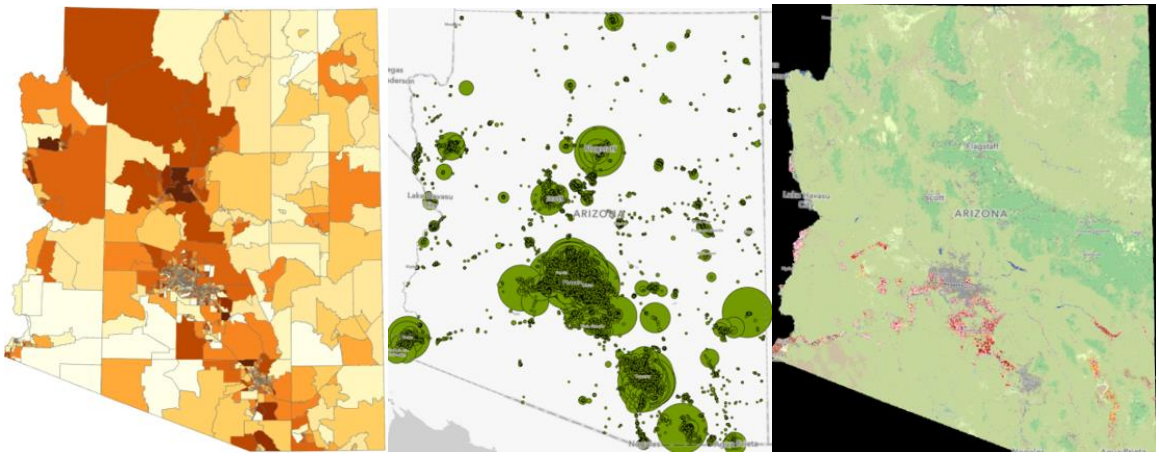

Figure 19: ACS Block Group Household Occupancy (Left), MAG Number of Employees (Center), and USDA Agricultural Cropland Area (Right)

Three data sources for Arizona household occupancy, number of employees, and agricultural cropland area were used for modeling distribution of power system loads to substations. Residential load was modeled using the 2017 5-year American Community Survey

block group data [U.S. Census Bureau, 2019]. Commercial and industrial loads were modeled using 2018 Maricopa Association of Governments employee data [Maricopa Association of Governments, 2019]. Agricultural loads were modeled using 2018 Cropland Data Layer [USDA, 2019]. All three are depicted in Fig. 19 above.

The 2017 5-year American Community Survey block group data set indicates that the PMA region contains 86.7% of the total household occupancy in the APS and SRP region, therefore PMA residential load ($P_{PMA,RES}$) is modeled to comprise 86.7% of $P_{tot,RES}$ in Eq. 19.

$$P_{PMA,RES} = 0.867 \cdot P_{tot,RES} \tag{19}$$

The 2018 Maricopa Association of Governments employee data set indicates that the PMA region contains 88.1% of employees in the APS and SRP region, therefore PMA commercial and industrial loads ($P_{PMA,COM}$ and $P_{PMA,IND}$) are modeled to comprise 88.1% of $P_{tot,COM}$ and $P_{tot,IND}$ in Eqs. 20 and 21.

$$P_{PMA,COM} = 0.881 \cdot P_{tot,COM} \tag{20}$$

$$P_{PMA,IND} = 0.881 \cdot P_{\alpha,IND} \tag{21}$$

The 2018 Cropland Data Layer indicates that the PMA region contains 60.3% of total agricultural crop land area in the APS and SRP region (based on the 50 types of agricultural products identified in Table 14), therefore PMA agricultural load ($P_{PMA,AGR}$) is modeled to comprise 60.3% of $P_{tot,AGR}$ in Eq. 22.

$$P_{PMA,AGR} = 0.603 \cdot P_{tot,AGR} \tag{22}$$

Thiessen polygons have been used to estimate substation service area [Pala et al., 2014; Fangdong, Han, Fangdong, & Buying, 2010], therefore were used to estimate service area for individual substations for the PMA power network model. The thiessen polygon for the PMA boundary is depicted in Fig. 20 below. The number of total household occupants (s_x), of employees (s_e), and crop land area (s_a) for each substation (s) service area were taken from the data sets used in Eqs. 19 to 22. In addition to this, Maricopa and Pinal counties provide 2018 and 2012 land use data, respectively, that designate land for commercial and industrial use. Commercial and industrial land (s_c and s_i) areas were taken for each substation service area in

Ares units (which are equal to about 1076 square-feet). Therefore, Eq. 23 was used to calculate each substation load (P_s) from the PMA's residential, commercial, industrial, and agricultural loads. The resulting distribution of power load to each substation for each sector are visualized as a heatmap in Figs. 64 to 67.

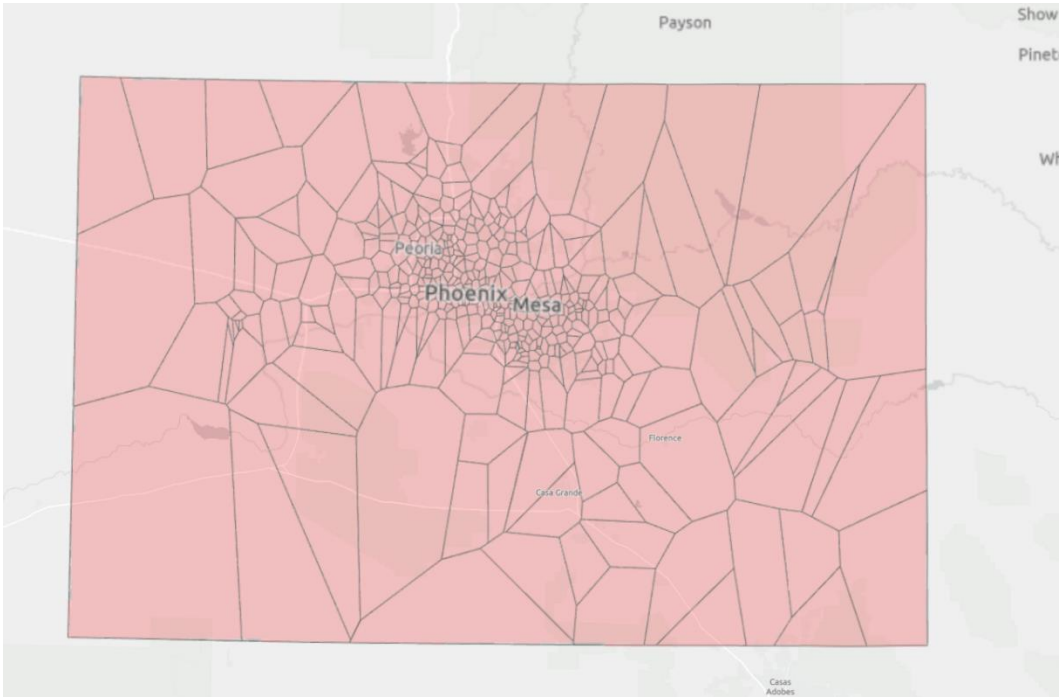

Figure 20: Thiessen Polygon for Representing PMA Substation Service Area

$$P_{s,init} = P_{PMA,RES} \cdot \frac{s_x}{\sum_s(s_x)} + P_{PMA,COM} \cdot \frac{s_e \cdot s_c}{\sum_s(s_e \cdot s_c)} + P_{PMA,IND} \cdot \frac{s_e \cdot s_i}{\sum_s(s_e \cdot s_i)} + P_{PMA,AGR} \cdot \frac{s_a}{\sum_s(s_a)} \quad (23)$$

Balancing authority tie lines are not specified in the HIFLD data set, nor are readily available. Therefore, tie lines for the 11 balancing authorities are approximated based on the high voltage lines between control areas—e.g., high voltage lines crossing between California and APS territory are likely CISO tie lines. While 10 balancing authorities have a distinct control area from the APS and SRP control area, the same cannot be said for WALC which surrounds the APS and SRP control area. It is assumed that WALC tie lines comprise all the tie lines entering and exiting the PMA region. The tie line substations for the 11 balancing authorities and their respective weighted allocation of interchange at that substation are provided in Tables 15 and 16, where the weighted allocation is proportional to line voltage.

Minimum generation and generating unit ramp rates are based on percentage of unit capacity shown in Table 6 [Gonzalez-Salazar, Kirsten, & Prchlik, 2018]. Solar photovoltaic units were assumed to have no minimum generation and no ramping capacity. Landfill units were assumed to have values equivalent to bioenergy type units.

Table 6: Minimum Generation and Ramp Rates

Unit Type	Minimum Generation (%)	Ramp Rate (%/min)
Hydroelectric	5	15
Landfill gas	50	2
Natural gas	20	8
Nuclear	50	2
Solar photovoltaic	0	0
Solar thermal	25	7

Table 7: Transmission Line Parameters

Voltage (kV)	Thermal Limit (MW)	R (per-unit/MI)	X (per-unit/MI)	Susceptance (per-unit/MI)
69	40.93	0.21169	0.66629	5.71645
115	50.66	0.16335	0.74380	5.82038
138	50.66	0.16335	0.74380	5.82038
230	233.79	0.08361	0.68006	5.94453
345	269.37	0.05698	0.61112	6.90143
500	838.87	0.02640	0.59981	7.82508

Table 8: Transformer Parameters

Low Voltage (kV)	High Voltage (kV)	Thermal Limit (MW)	R (per-unit)	X (per-unit)
69	115	35.67	0.00217	0.07166
69	230	64.94	0.00156	0.07916
69	500	85.80	0.00121	0.10285
115	230	86.08	0.00100	0.04351
230	345	193.72	0.00055	0.04579
230	500	289.87	0.00072	0.07312
345	500	302.44	0.00012	0.01160

The Western Electricity Coordinating Council (WECC) compiles steady-state and dynamic base cases of their interconnection system. While the WECC network data was not used for this model, because the WECC base cases do not contain sufficient geographic data to spatially locate assets, component parameters from the 2019 WECC Heavy Summer base case [WECC, 2019] were used to model the thermal limits, resistance, reactance, and susceptance values of the transmission lines and transformers based on the line and transformer voltage

ratings provided in the HIFLD data set. The average values of APS and SRP transmission lines and transformers for each voltage rating in the WECC base case are provided in Tables 7 and 8.

A.2 WATER NETWORK

The water network topology was based on publicly available 2018 U.S. National Hydrography Dataset Plus High Resolution vector data from the U.S. Geological Survey (USGS) for hydrologic unit codes 1505, 1506, and 1507 [USGS, 2019]. The combined 1505, 1506, 1507 vector data is depicted in Fig. 21 below surrounding the envelope and contained a total of 276,865 network lines that far exceeded the resolution of data for the water supply network model in this work. Indications of missing data in Fig. 21 are due to limitations of visualizations and rendering of the ArcGIS software.

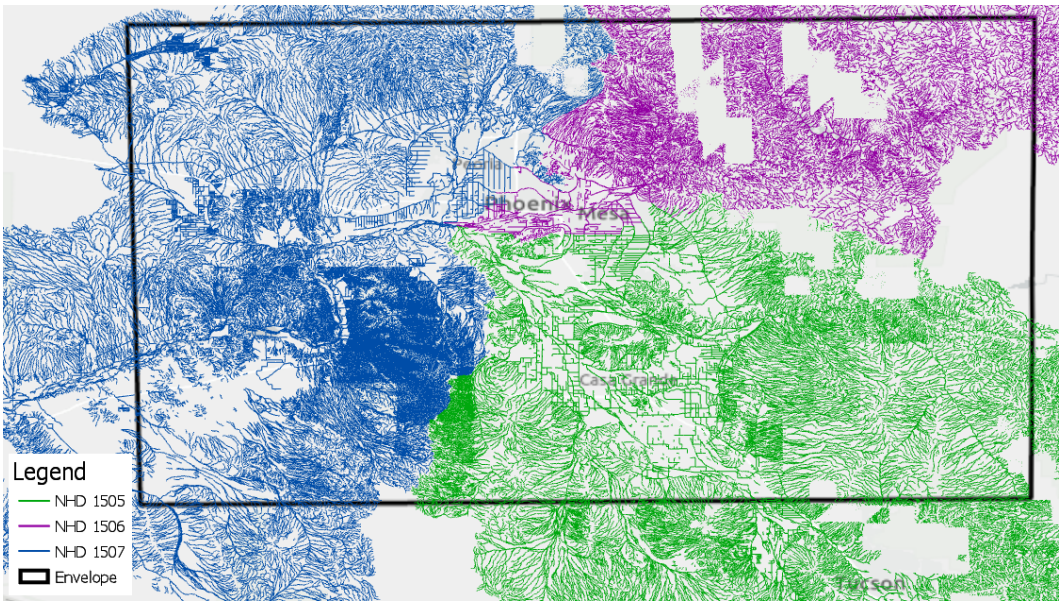

Figure 21: NHD Plus Water Network Topology Surrounding the PMA Boundary

Figure 22 demonstrates the process for translating high resolution hydrography dataset into a form usable for modelling the PMA water supply network. First, the large stream network was reduced by filtering lines outside the PMA envelope area, second, only lines of the types that include Connectors, Canal/Ditch, Pipeline, Artificial Path and with a name including “River” were retrieved—i.e., remove small washes and streams--and third, a network analysis was performed on the resulting water supply network that removed any disconnected lines. The resulting water

supply network after these three operations contained a large-size water supply network of 6,332 network lines.

This large-size water supply network was reduced to a medium-size water network by removing any leaf nodes (i.e., nodes with a single line connection) in the dendritic water network that served no purpose. First, two lines were added to complete the water supply network: a line connecting the disconnected Gila Bend Canal to the Gila River at -112.7676, 33.2294, and undeleting a line that completed the Salt River at -112.3063, 33.3816. A list of nodes was created for the large-size water supply network and four types of nodes were identified: junctions that served municipalities, junctions that served generating units, reservoirs/dams, and pumping stations. HIFLD provide water treatment plant data, however, it is secure and not publicly available. Therefore, it was assumed that each municipality is served by a single junction located nearest the municipal central location measured via Euclidean distance. Data for 31 municipalities was retrieved from 2014 Cities and Towns of the United States [National Atlas of the United States, 2013] of the type “Civil” were retrieved in the PMA envelope area. It was also assumed that each generating unit is served by a single junction located nearest via the Euclidean distance. Three reservoirs/dams were identified in the region: New Waddell Dam, Bartlett Dam, and Theodore Roosevelt Dam. Their nodes were chosen as the highest elevation nodes in their water bodies, where the elevation data for all the nodes is taken from 1/3 arc-second National Elevation Dataset provided by USGS [USGS, 2019]. Three surface water pumping plants were identified in the region: Waddell Pumping Plant, Salt-Gila Pumping Plant, and Picacho Pumping Plant. Waddell Pumping Plant was located at the outlet of Lake Pleasant (i.e., New Waddell Dam), Salt-Gila Pumping Plant was located at the combined network flows of the Salt River (downstream Theodore Roosevelt Dam) and Verde Rivers (downstream Bartlett Dam), and Picacho Pumping Plant was located just southeast of the Picacho Reservoir on Central Arizona Project (CAP) Canal. Based on these four types of nodes it was identified which leaf nodes were insignificant (served nothing) and significant (e.g., served municipality). Lines connected to nodes with at least two line connections were ignored. This resulted in a medium-

sized water supply network of 2,624 network lines and is depicted in Fig. 23 below. The list of water nodes were updated using the medium-sized water supply network.

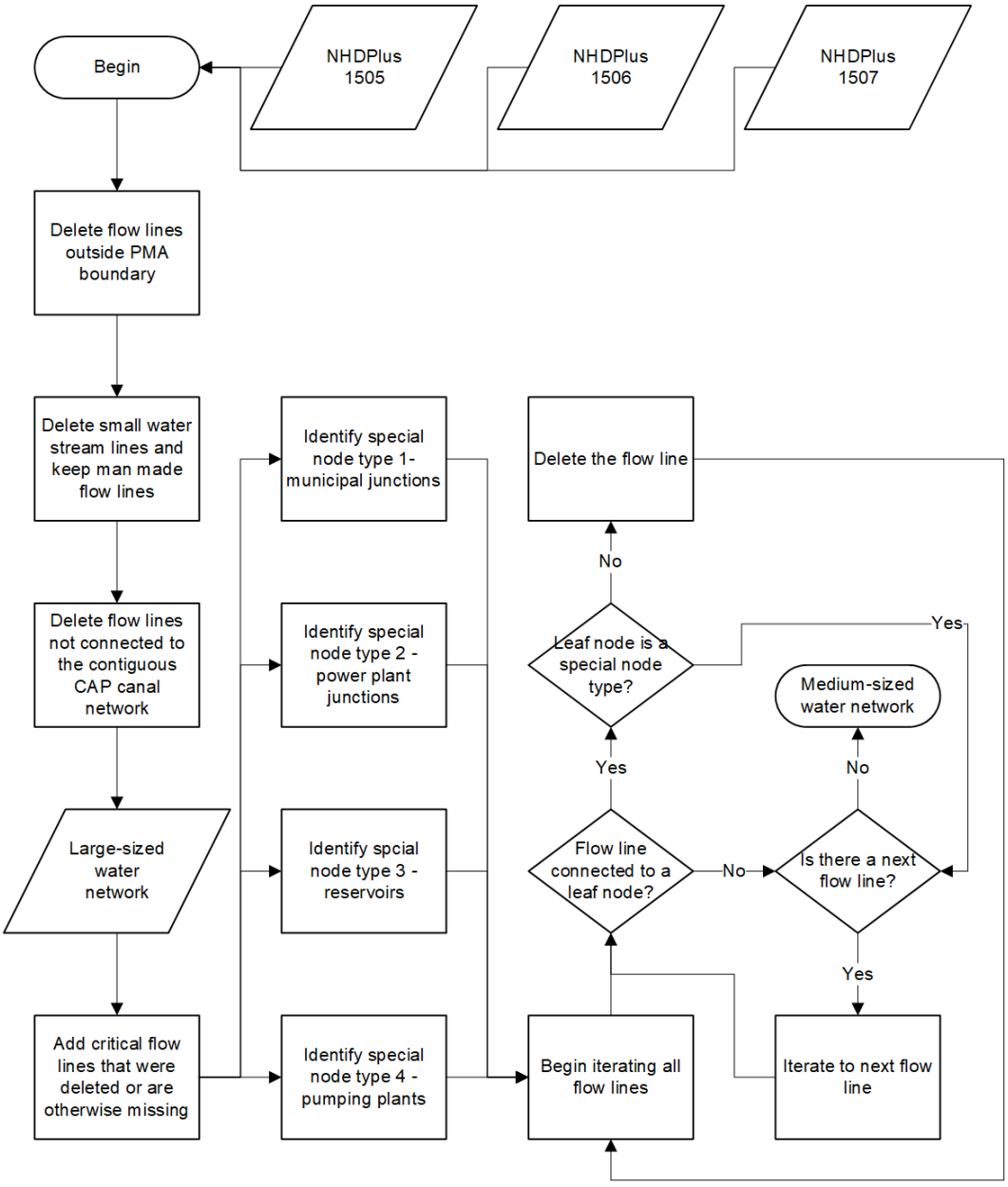

Figure 22: Process for Reducing the High-Resolution Hydrography Data Set

Methodology for assigning service areas to municipal junctions also used a top-down method with Thiessen polygons, where each municipal junction has a corresponding service area based on its Thiessen polygon. According to USGS, Maricopa county had a total public (residential, commercial, industrial) water withdrawal of 776.54 Mgal/d in 2015 and, similarly,

Pinal county had 63.24 Mgal/d in 2015 [USGS, 2018]. Tucson, which is downstream the CAP Canal, withdrew 1117,000 acre-ft from the CAP in 2016 [Tucson Water, 2016]. These values were converted into average GPM and were distributed amongst the municipal junctions proportional to the total number of household occupants (via the 2015 ACS data) in the municipal service area compared to the total number of household occupants in their respective counties, Maricopa and Pinal. The resulting distribution of water demand to each municipality and exported to Tucson are visualized as a heatmap in Fig. 68. However, the cities of Superior, Kearny, and Mammoth, AZ and the University of Arizona Biosphere 2, near Mammoth, are located upstream the Gila River (eastward) thus were assumed to not draw from the CAP Canal and were set to 0 GPM demand.

Figure 23: Medium-Sized Water Supply Network Within the PMA

The water hydraulic flow is run using the Chezy-Manning formula for modeling hydraulic head lost because the modeled water supply network is open-channel flow. Each municipal junction is modeled with an associated groundwater reservoir. Groundwater reservoirs were set to 200 ft elevation higher than their respective municipal junction, similar to the minimum observed head in the Salt River Valley [Freihoefer et al., 2009], and each groundwater reservoir has a maximum capacity of 12,399 GPM, similar to Phoenix's production of 20,000 acre-feet of groundwater per year [City of Phoenix Water Services Department, 2011]. Minimum allowable

pressure of all junctions was set to 0 PSI because they are in an open-channel water system. Water line diameters were initially determined to be 9 ft (108 in) by converting the area (62.5 sq. ft) of known rectangular channel sections into a circular pipe with the same area [Kelos, personal communication, 2015]. This rectangular channel section has an area similar to reported values for the Maricopa Canal (66.9 sq. ft), Grand Canal (59.6 sq. ft), and Indian Bend Canal (68.8 sq. ft) [USDA, 1939]. However, the water line diameters were increased to 12 ft (144 in) which was the minimum diameters that maintained zero water deficits during nominal operation at maximum total water demand.

Table 9: Hourly Water Demand in Percent of Average Day of the Season

Hour of Day	Percent of Annual Average Demand		
	Winter	Summer	Spring and Fall
12:00 AM	50	100	54
1:00 AM	45	95	51
2:00 AM	40	90	47
3:00 AM	45	100	53
4:00 AM	50	110	58
5:00 AM	58	130	68
6:00 AM	65	150	78
7:00 AM	73	175	90
8:00 AM	80	200	101
9:00 AM	73	210	103
10:00 AM	65	200	96
11:00 AM	58	175	85
12:00 PM	50	150	72
1:00 PM	45	147	69
2:00 PM	40	145	67
3:00 PM	45	170	78
4:00 PM	50	200	90
5:00 PM	58	225	103
6:00 PM	65	250	114
7:00 PM	73	263	121
8:00 PM	80	275	129
9:00 PM	73	263	121
10:00 PM	65	250	114
11:00 PM	50	100	54

The municipal water demand curve was constructed by converting annual average hourly water demand to 24-hour water demands for the average day of each season, then to 24-hour water demands for the average day of each month. Table 9 lists the 24-hour water demands (F_h^W) in percent of the average day of the seasons [Chin, 2013]—i.e., summer, spring, fall, and winter—and Table 10 lists the monthly average demands (F_m^W) in percent of seasonal average

[Mizgalewicz, 1991] that were used to calculate 288 water demand factors, $F_{m,h}^{W}$, in Eq. 24 that represent the average 24-hour demand for each month of the year.

$$F_{m,h}^{W} = F_{m}^{W} \cdot F_{h}^{W} \tag{24}$$

Table 10: Monthly Average Water Demand in Percent of Seasonal Average Demand

Season of the Year	Month of the Year	Seasonal Average Demand (%)
Winter	December	109.36
	January	94.58
	February	96.06
Spring	March	79.25
	April	101.89
	May	124.53
Summer	June	99.29
	July	108.51
	August	92.20
Fall	September	120.00
	October	100.00
	November	80.00

A.3 POWER-WATER NETWORK INTERCONNECTIONS

Power-water interconnections are modeled in two ways: generating units require water for cooling, and water pumping stations require electricity for operation. Table 11 lists the connections between 23 generating units and the corresponding coordinates of their water junctions (water junctions are not named) out of the 64 generating units in the power network, with power values in single-phase units and water withdrawal rates converted into GPM/MW [Macknick, NewMark, Heath, & Hallett, 2012]. Hydroelectric units are not included because they do not withdraw water from the canal flows and solar photovoltaic units are not included because they have no water demand. Natural gas water withdrawal rates are based on the midpoint of steam and combined cycle technologies.

Water pumping station include multiple pumps that can be installed in series and parallel configurations, depending on desired head gain and flow rate performance. Three assumptions about pumping stations performance are made due to insufficient knowledge of each station's configuration: constant head gain at all flow rates [M. Shapiro, personal communication, October 23, 2018], pump power consumption is approximated using average pumping station efficiency, and pump rotational speed is constant. Power consumption in kilowatts can then be calculated

using Eq. 12 where H_u is head gain (ft) of pump u, Q_u is flow rate (GPM), SG is specific gravity of water assumed to be 1, ϵ_u is average pumping station efficiency, and 0.7457 is the conversion factor for water horsepower to kilowatts. Table 12 lists the parameters of the 3 modelled water pumping plants [Central Arizona Project, 2012] and the electric substation that they consume power from.

$$P_u = 0.7457 \cdot \frac{H_u \cdot Q_u \cdot SG}{\epsilon_u \cdot 3960} \tag{25}$$

Table 11: Generating Unit and Water Junction Interconnections

Unit Name	Unit Type	Unit Capacity (MW)	Water Withdrawal (GPM/MW)	Junction X Coord	Junction Y Coord
Glendale Energy Power Plant	Landfill Gas	0.9	43.9	-112.308	33.536
Northwest Regional	Landfill Gas	1.1	43.9	-112.490	33.743
Agua Fria	Natural Gas	204.5	72.9	-112.221	33.545
Arizona State University CHP	Natural Gas	3.1	72.9	-111.919	33.433
Arlington Valley Energy Facility	Natural Gas	237.7	72.9	-112.795	33.300
Coolidge Generation Station	Natural Gas	242.0	72.9	-111.501	32.908
Desert Basin	Natural Gas	215.4	72.9	-111.794	32.894
Gila River Power Block 2	Natural Gas	206.3	72.9	-112.680	32.974
Gila River Power Block 3	Natural Gas	206.3	72.9	-112.680	32.974
Gila River Power Station	Natural Gas	206.3	72.9	-112.680	32.974
Harquahala Generating Project	Natural Gas	441.7	72.9	-113.091	33.508
Kyrene	Natural Gas	191.2	72.9	-111.938	33.357
Mesquite Generating Station 1	Natural Gas	230.5	72.9	-112.795	33.300
Mesquite Generating Station 2	Natural Gas	230.5	72.9	-112.795	33.300
Ocotillo	Natural Gas	111.1	72.9	-111.919	33.433
Red Hawk	Natural Gas	380.1	72.9	-112.795	33.300
Saguaro	Natural Gas	61.5	72.9	-111.303	32.588
Santan	Natural Gas	442.0	72.9	-111.751	33.329
Sundance	Natural Gas	201.7	72.9	-111.584	32.939
SunDevil Power - Gila River	Natural Gas	206.3	72.9	-112.680	32.974
West Phoenix	Natural Gas	402.5	72.9	-112.160	33.440
Palo Verde	Nuclear	1,403.2	55.1	-112.785	33.312
Solana Generating Station	Solar Thermal	93.3	3.9	-112.956	32.912

Table 12: Water Pumping Plant and Substation Interconnections

Plant Name	Substation Name	Head Gain (ft)	Capacity (cfs)	Horsepower	Plant Efficiency (%)
Picacho	Randolph	232	930	33,000	74.1
Salt-Gila	Verde	86	2,800	32,800	83.2
Waddell	New Waddell	192	1,900	43,200	95.7

APPENDIX B

TABLES

Table 13: Water System Deficits from Water Line Failure Analysis

Line ID	Deficits (GPM)	Line ID	Deficits (GPM)	Line ID	Deficits (GPM)
1038	614969	1042	71397	2488	64567
1185	614969	1064	71397	2570	64567
1379	614969	1086	71397	226	55312
1639	223648	1090	71397	71	52168
1740	223648	1121	71397	153	52168
1904	223648	1136	71397	355	52168
1969	223648	1166	71397	613	52168
2196	223648	1192	71397	1074	43290
2530	223648	1202	71397	1503	43290
2616	223648	1248	71397	1951	27543
1053	110206	1270	71397	2486	27543
1152	110206	1284	71397	1967	18372
1290	110206	1311	71397	2280	18372
1358	110206	1341	71397	1029	16761
95	107480	1349	71397	1266	16761
471	107480	1350	71397	270	15765
552	107480	1355	71397	920	15765
1763	105558	1474	71397	121	15039
2098	105558	1488	71397	950	15039
1604	104721	1542	71397	10	13822
1751	104721	2197	71397	2093	8109
2077	103657	2600	71397	2315	8109
2405	103657	192	64567	177	7563
1855	98940	787	64567	537	7563
490	92478	1605	64567	637	7563
1011	83834	1609	64567	714	7563
1013	83834	1626	64567	957	7563
1054	83834	1673	64567	2144	5306
1097	83834	1682	64567	2326	5306
1110	83834	1689	64567	1143	5098
1114	83834	1700	64567	1481	5098
1147	83834	1859	64567	1052	4470
1182	83834	1886	64567	1578	4470
1407	83834	1905	64567	2578	3461
1466	83834	2004	64567	143	1890
1485	83834	2021	64567	265	1890
1563	83834	2118	64567	268	1890
1233	78580	2173	64567	911	1890
2030	78580	2180	64567	1267	1355
1164	76931	2208	64567	1336	1355
1026	76346	2217	64567	1577	1355
1282	76346	2223	64567	1641	1049
1365	76346	2309	64567	1779	1049
128	71397	2324	64567	1288	370
194	71397	2604	64567	1460	370
262	71397	2617	64567		
1081	71397	2623	64567		

Table 14: Agricultural Items in Cropland Data Layer

Class Name	Class Name
Alfalfa	Greens
Almonds	Herbs
Apples	Honeydew Melons
Barley	Lettuce
Broccoli	Millet
Cabbage	Misc Vegs & Fruits
Cantaloupes	Oats
Carrots	Olives
Cauliflower	Onions
Celery	Oranges
Citrus	Other Crops
Corn	Other Hay/Non Alfalfa
Cotton	Other Tree Crops
Dbl Crop Barley/Corn	Pecans
Dbl Crop Lettuc/Cantaloupe	Peppers
Dbl Crop Lettuce/Barley	Pistachios
Dbl Crop Lettuce/Cotton	Potatoes
Dbl Crop Oats/Corn	Pumpkins
Dbl Crop WinWht/Corn	Radishes
Dbl Crop WinWht/Cotton	Rye
Dbl Crop WinWht/Sorghum	Sorghum
Dry Beans	Sugarbeets
Durum Wheat	Triticale
Garlic	Watermelons
Grassland/Pasture	Winter Wheat

Table 15: Interchange Weights for LDWP, CISO, IID, GRMA, TEPC

Balancing Authority	Substation	Voltage (kV)	Weight
LDWP	Westwing	500	0.241
LDWP	Hassayampa	500	0.241
LDWP	Eagle Eye	230	0.111
LDWP	Liberty	345	0.166
LDWP	Palo Verde	500	0.241
CISO	Westwing	500	0.241
CISO	Hassayampa	500	0.241
CISO	Eagle Eye	230	0.111
CISO	Liberty	345	0.166
CISO	Palo Verde	500	0.241
IID	Westwing	500	0.241
IID	Hassayampa	500	0.241
IID	Eagle Eye	230	0.111
IID	Liberty	345	0.166
IID	Palo Verde	500	0.241
GRMA	Gila River	230	1.000
TEPC	Harquahala	115	0.093

Table 16: Interchange Weights for WALC, WACM, PNM, GMA, TEPC, PACE, DEAA

Balancing Authority	Substation	Voltage (kV)	Weight
WALC	Westwing	500	0.061
WALC	Westwing	500	0.061
WALC	Silver King	500	0.061
WALC	Hassaympa	500	0.061
WALC	Harquahala	500	0.061
WALC	Saguaro	115	0.014
WALC	Saguaro	500	0.061
WALC	Hayden	115	0.014
WALC	Gavilian Peak	230	0.028
WALC	Gila River	230	0.028
WALC	Pinal Central	500	0.061
WALC	Pinnacle Peak APS	345	0.042
WALC	Pinnacle Peak APS	345	0.042
WALC	Eagle Eye	230	0.028
WALC	Tortolita	552	0.068
WALC	Liberty	345	0.042
WALC	Oracle Junction	115	0.014
WALC	Palo Verde	500	0.061
WALC	Pinal West	345	0.042
WALC	Pinnacle Peak WALC	345	0.042
WALC	Pinnacle Peak WALC	345	0.042
WALC	Dynergy Arlington	500	0.061
WACM	Silver King	500	0.197
WACM	Saguaro	500	0.197
WACM	Pinal Central	500	0.197
WACM	Pinnacle Peak APS	345	0.136
WACM	Pinnacle Peak WALC	345	0.136
WACM	Pinnacle Peak WALC	345	0.136
PNM	Silver King	500	0.813
PNM	Hayden	115	0.187
HGMA	Harquahala	500	1.00
TEPC	Hayden	115	0.093
TEPC	Tortolita	552	0.444
TEPC	Oracle Junction	115	0.093
TEPC	Pinal West	345	0.278
PACE	Westwing	500	0.139
PACE	Westwing	500	0.139
PACE	Saguaro	500	0.139
PACE	Gavilan Peak	230	0.064
PACE	Pinal Central	500	0.139
PACE	Pinnacle Peak APS	345	0.096
PACE	Pinnacle Peak APS	345	0.096
PACE	Pinnacle Peak WALC	345	0.096
PACE	Pinnacle Peak WALC	345	0.096
DEAA	Dynergy Arlington	500	1.000

APPENDIX C

FIGURES

Figure 24: Location of Water Failure Scenario 1

Figure 25: Location of Water Failure Scenario 2

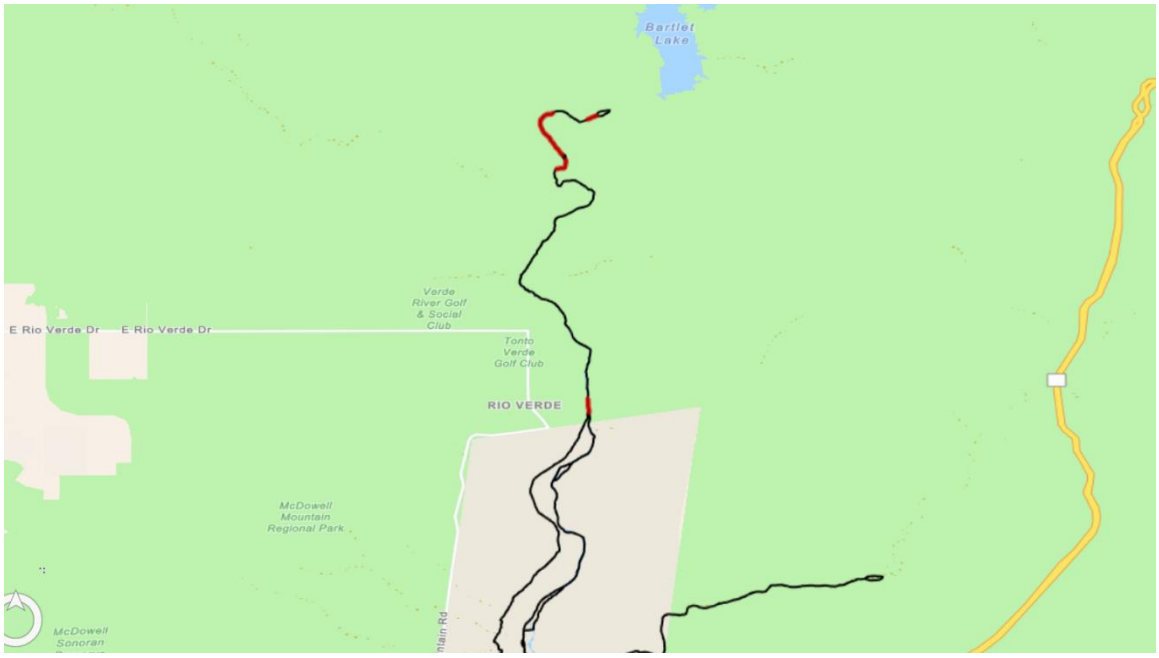

Figure 26: Location of Water Failure Scenario 3

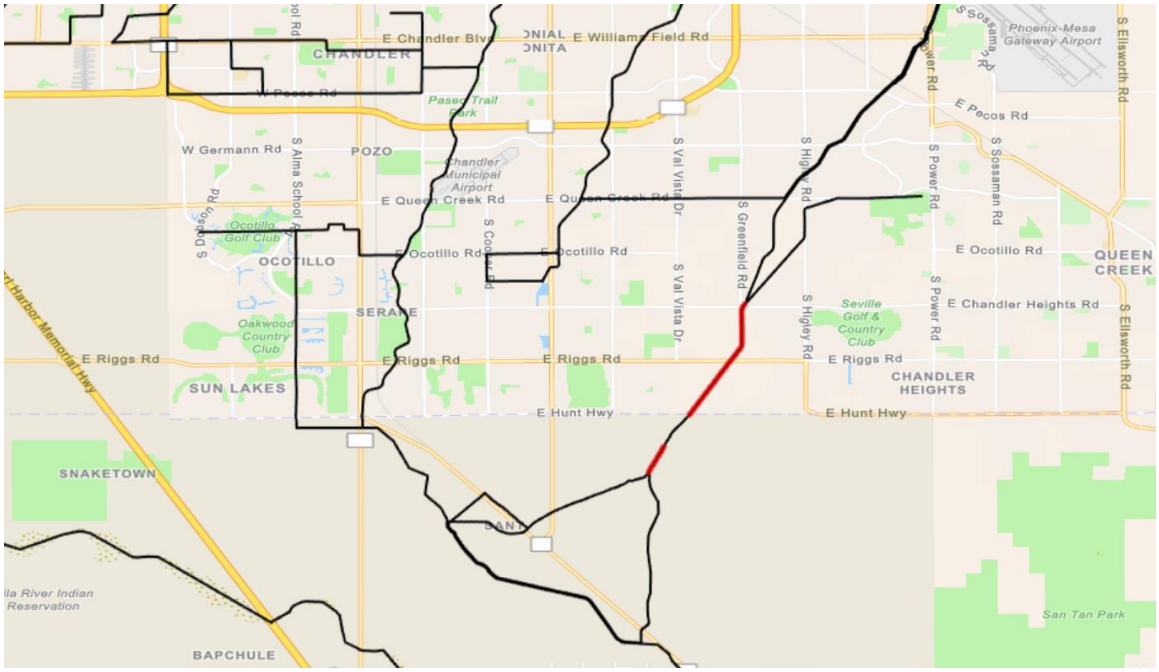

Figure 27: Location of Water Failure Scenario 4

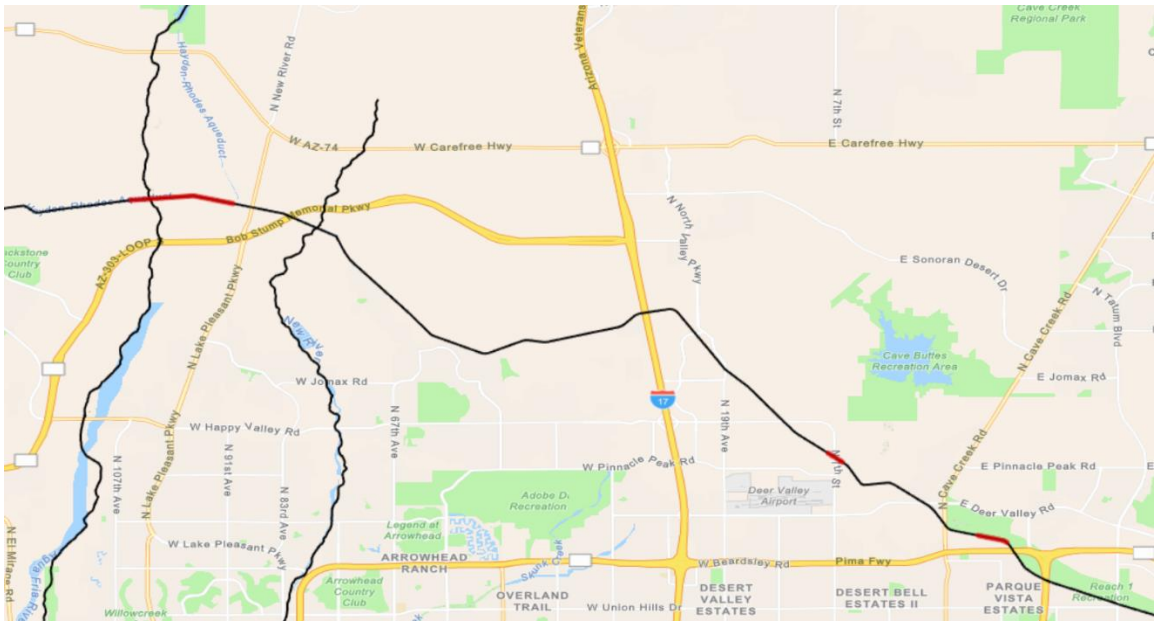

Figure 28: Location of Water Failure Scenario 5

Figure 29: Location of Water Failure Scenario 6

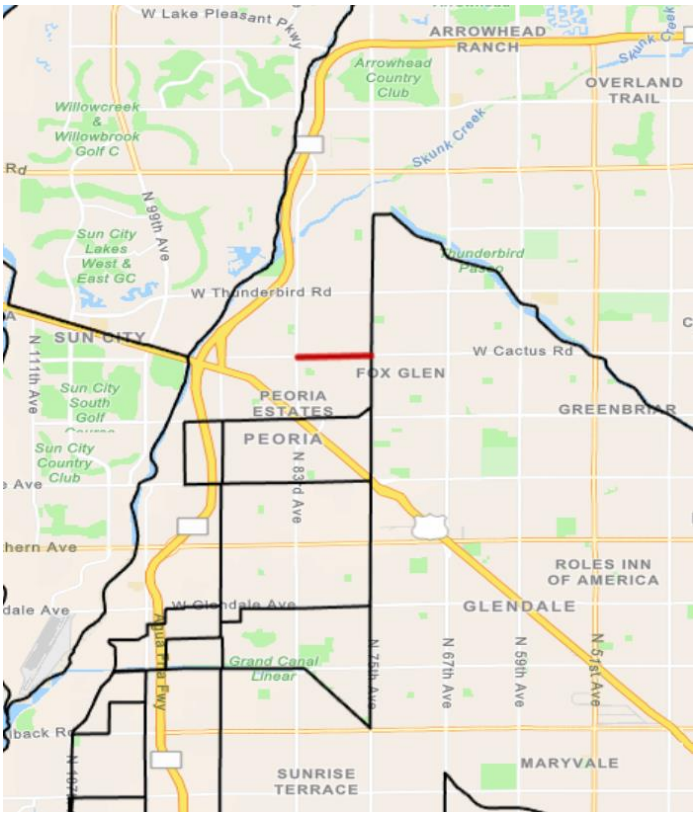

Figure 30: Location of Water Failure Scenario 7

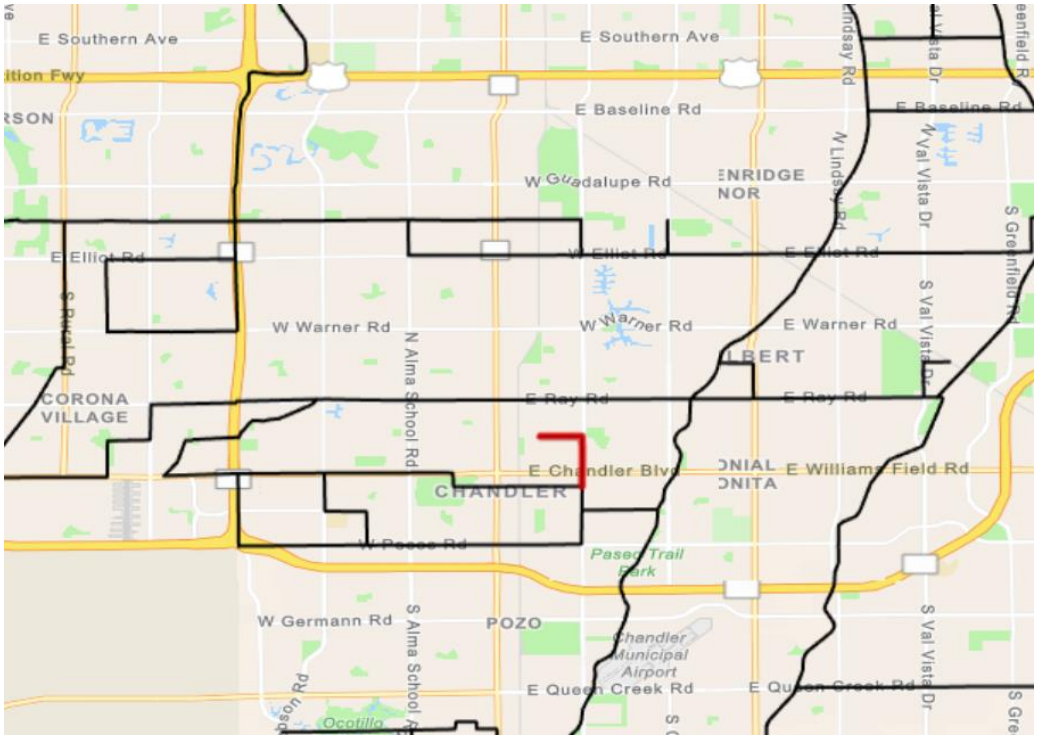

Figure 31: Location of Water Failure Scenario 8

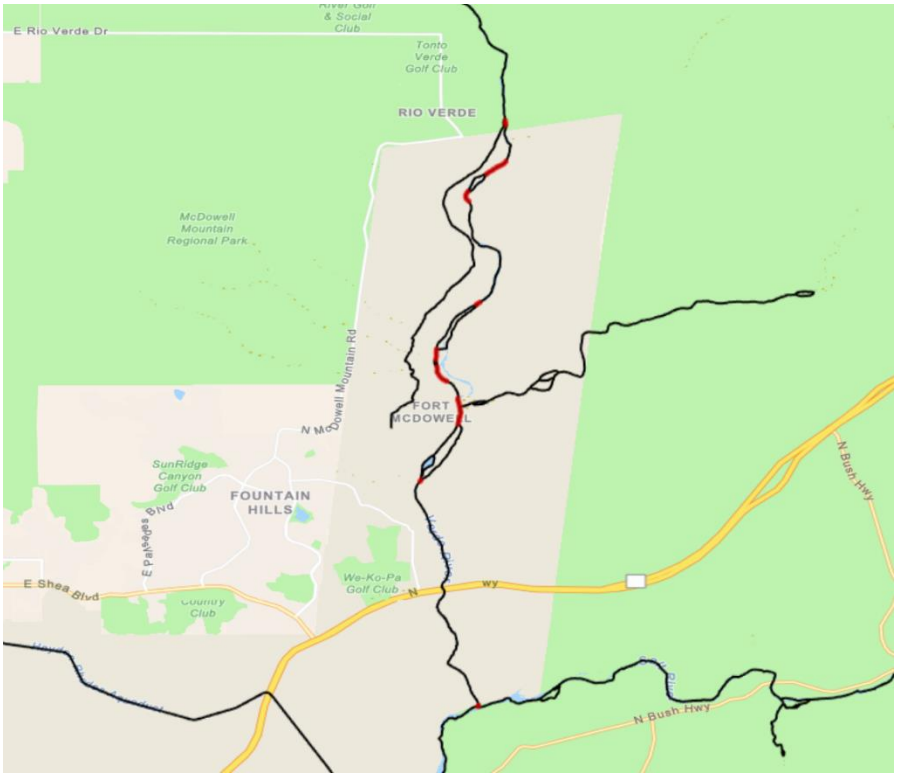

Figure 32: Location of Water Failure Scenario 9

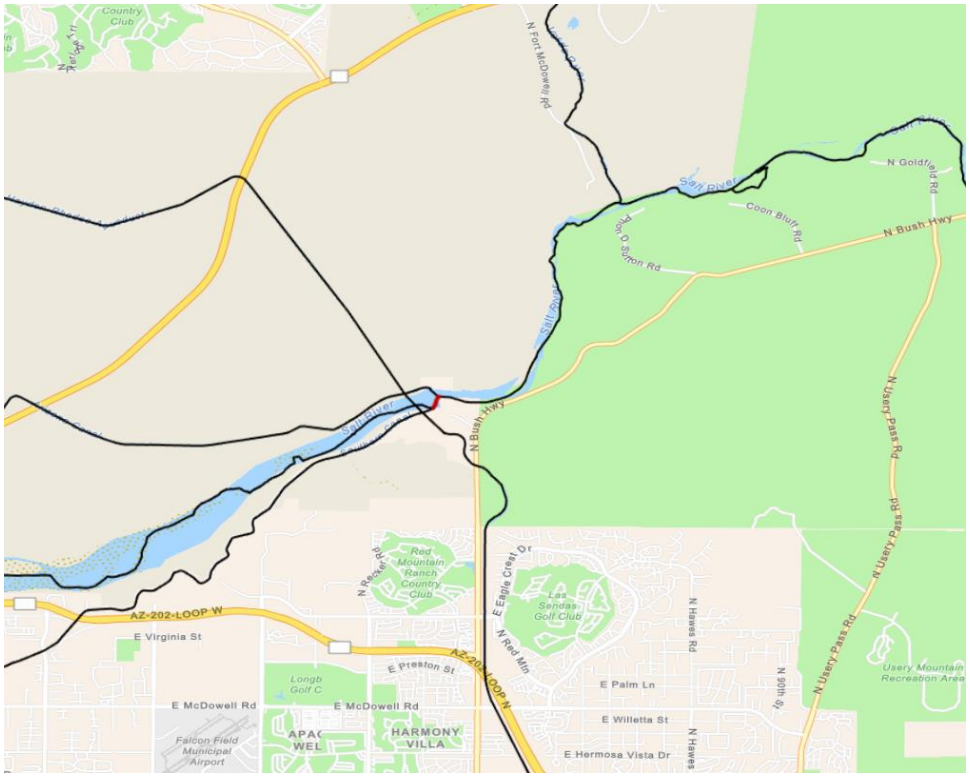

Figure 33: Location of Water Failure Scenario 10

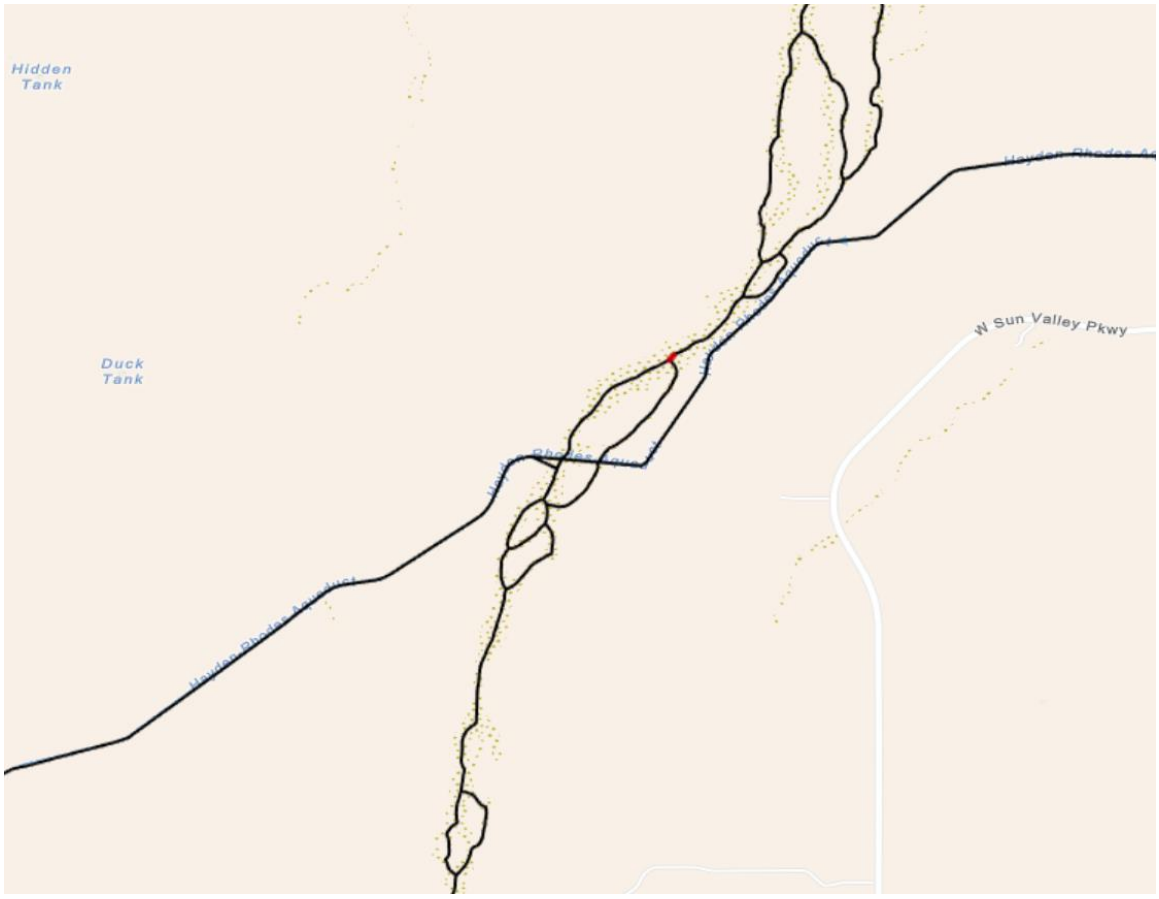

Figure 34: Location of Water Failure Scenario 11

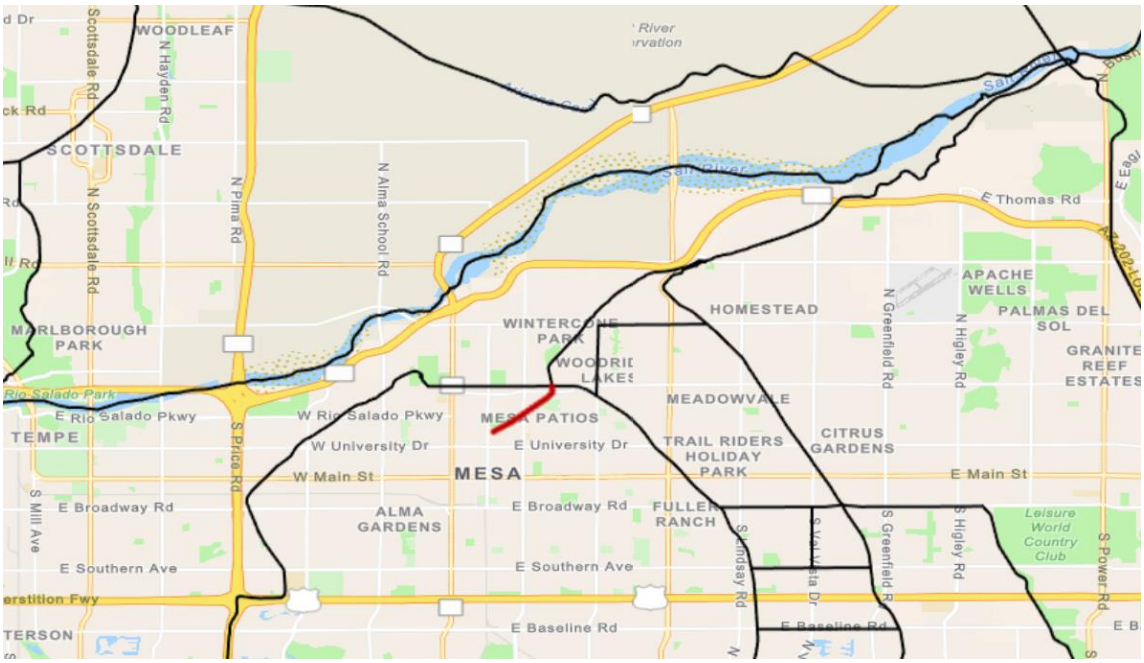

Figure 35: Location of Water Failure Scenario 12

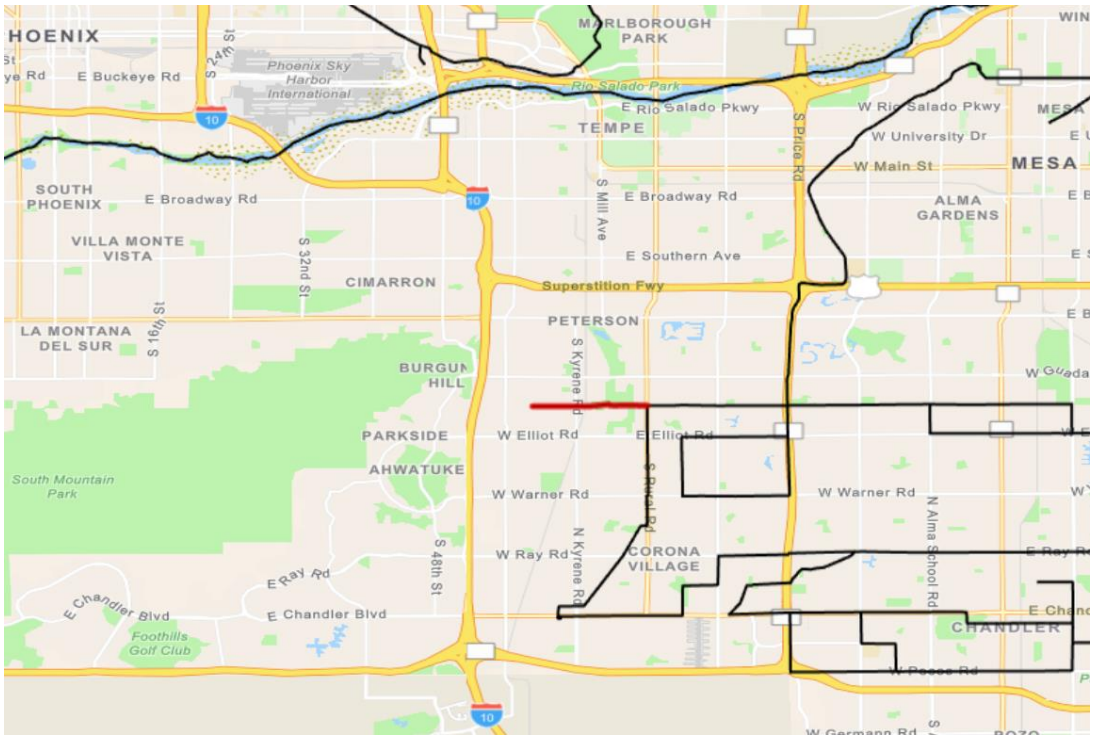

Figure 36: Location of Water Failure Scenario 13

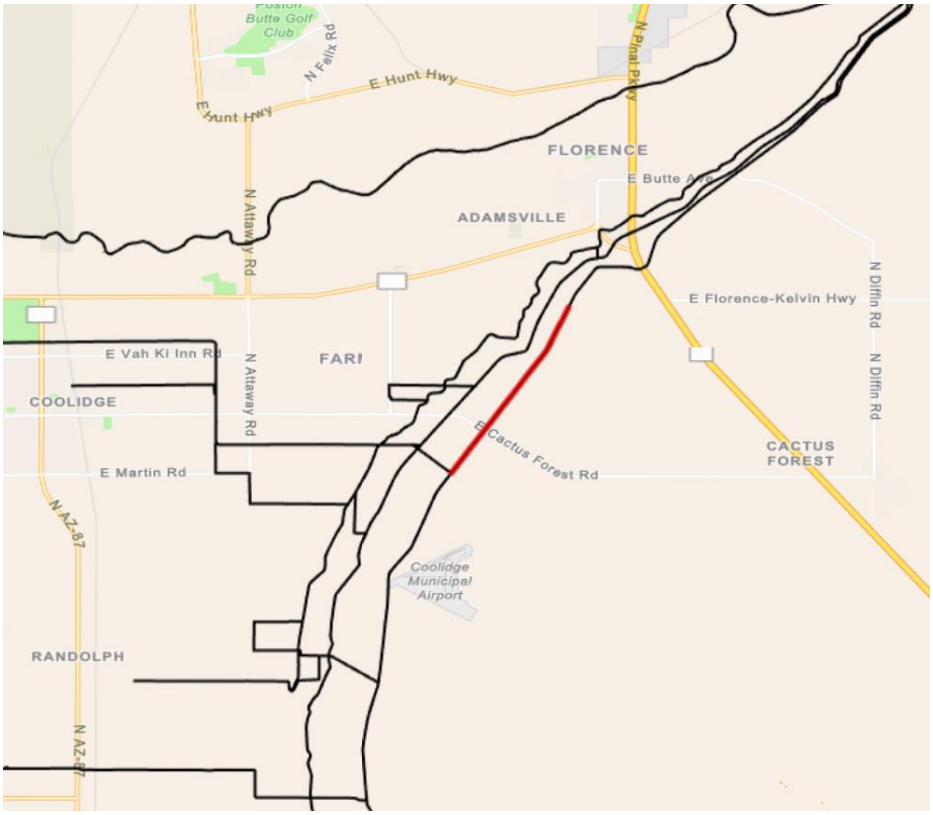

Figure 37: Location of Water Failure Scenario 14

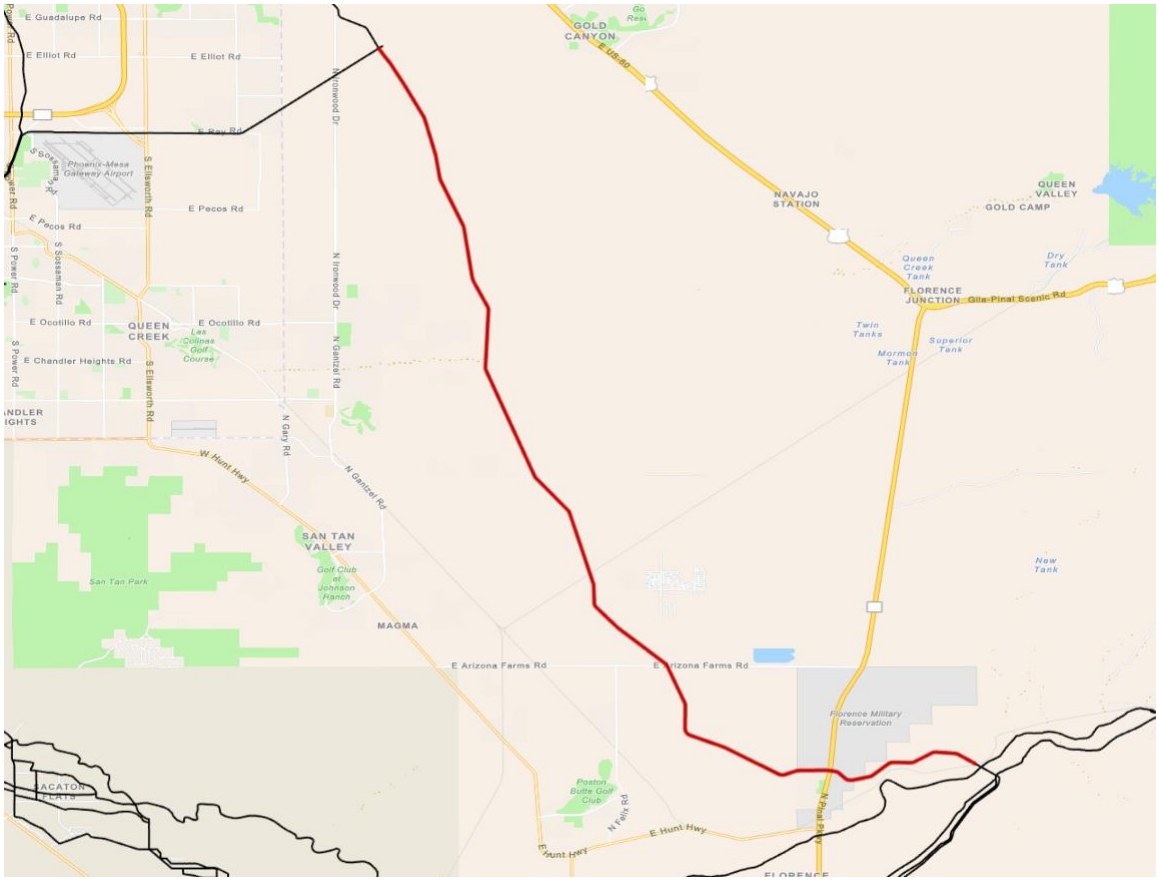

Figure 38: Location of Water Failure Scenario 15

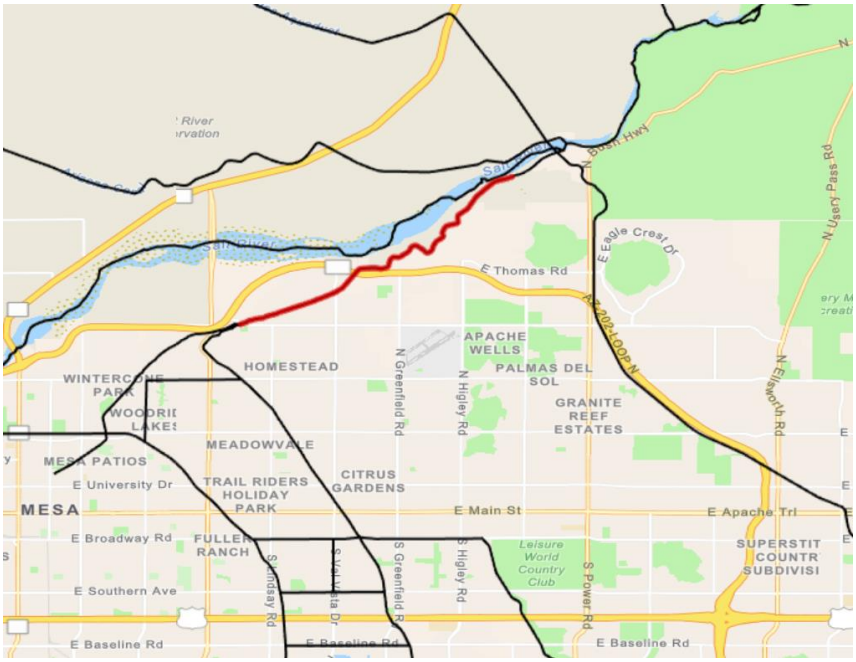

Figure 39: Location of Water Failure Scenario 16

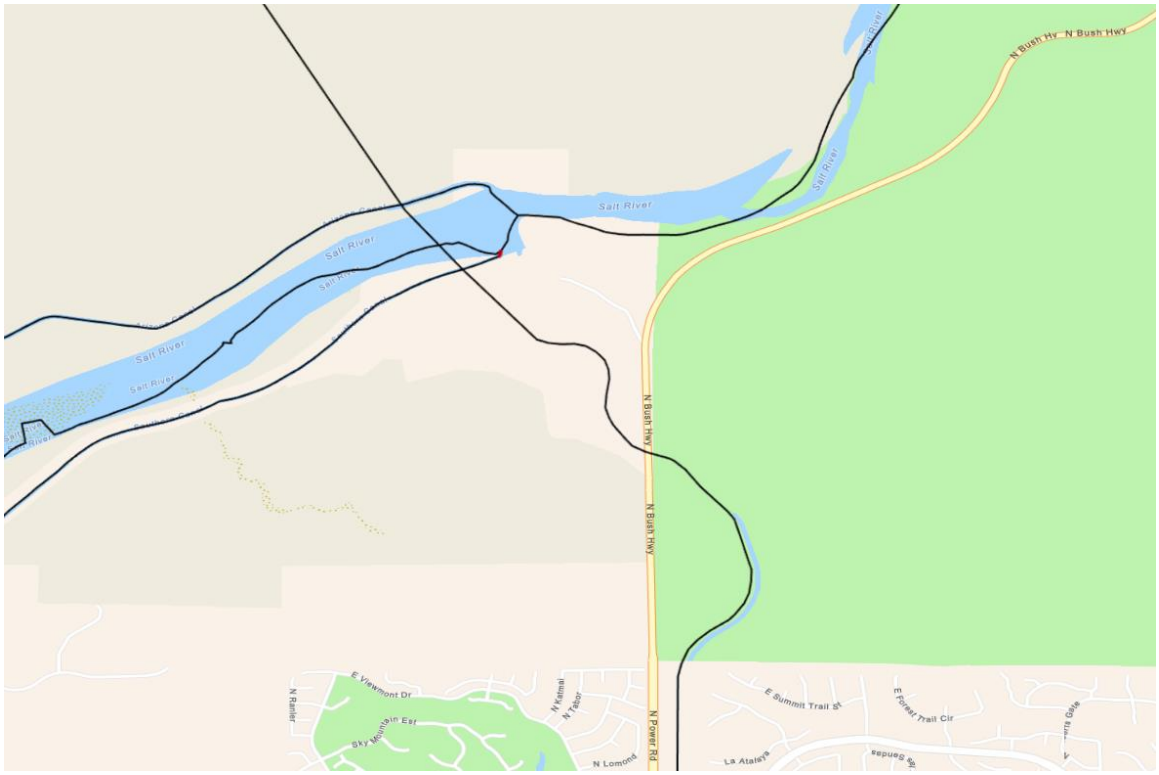

Figure 40: Location of Water Failure Scenario 17

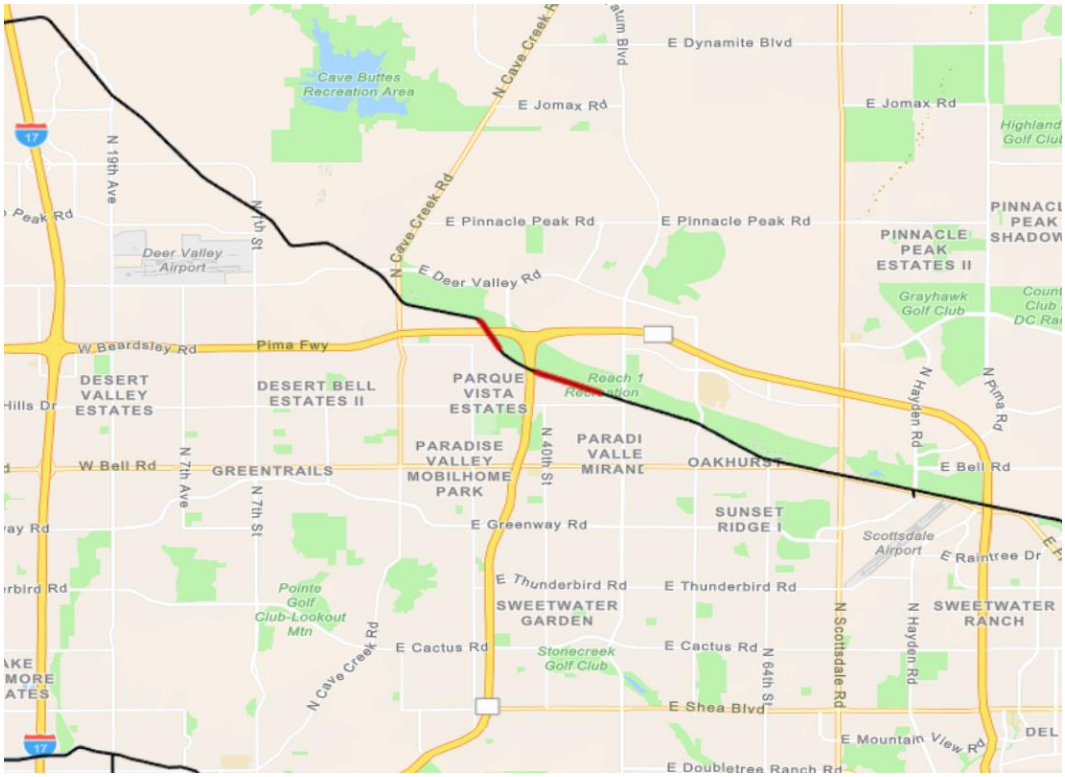

Figure 41: Location of Water Failure Scenario 18

Figure 42: Location of Water Failure Scenario 19

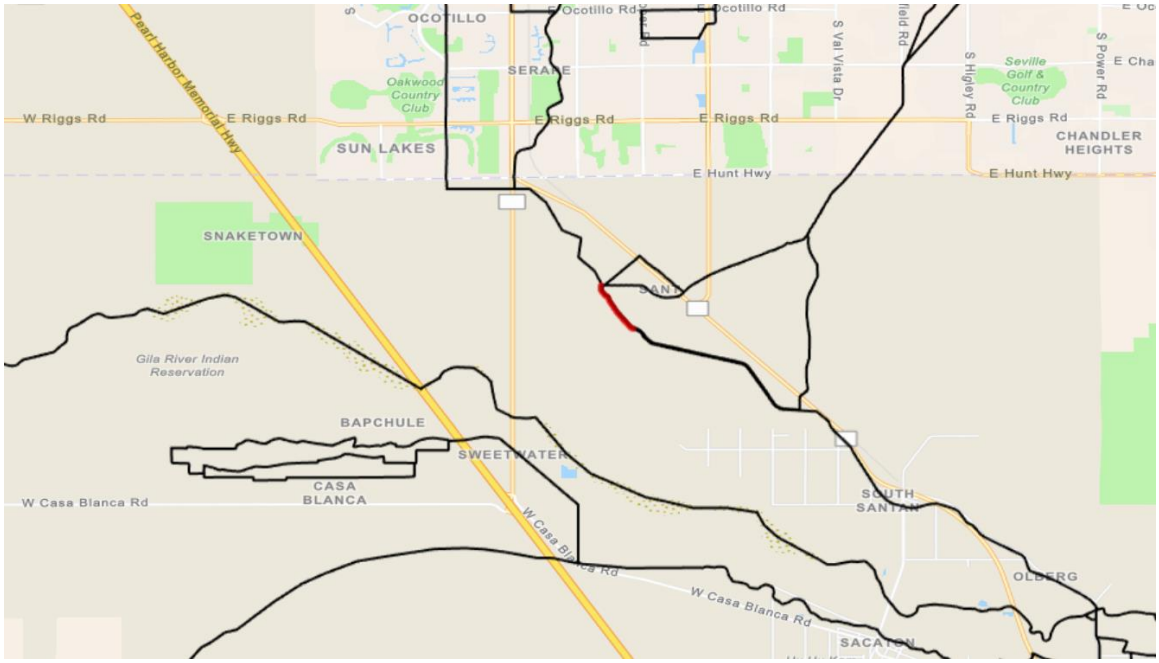

Figure 43: Location of Water Failure Scenario 20

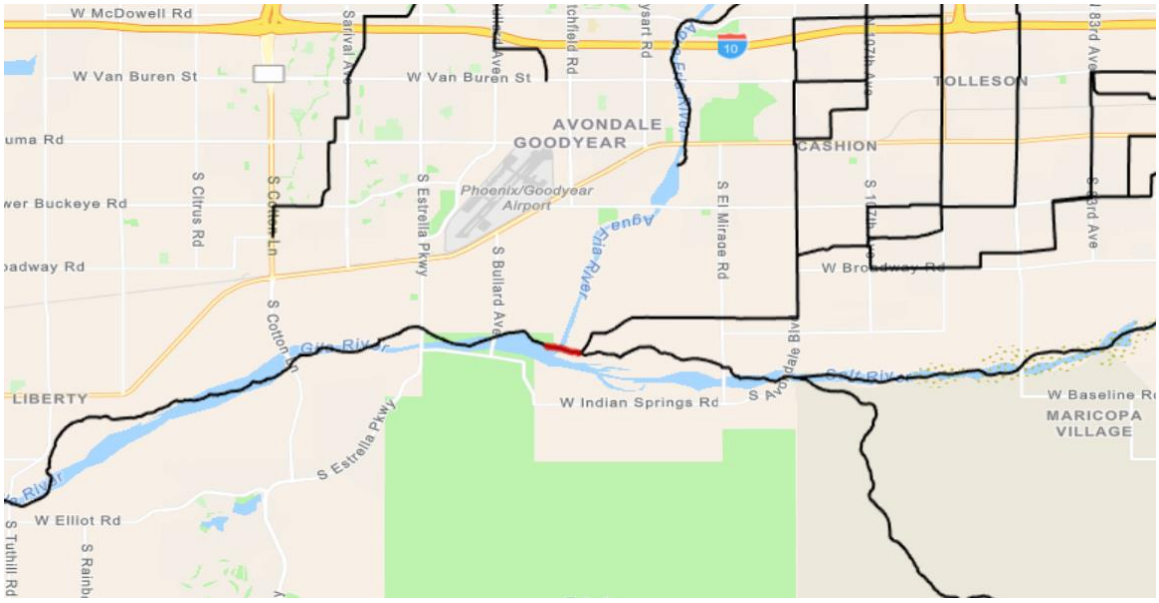

Figure 44: Location of Water Failure Scenario 21

Figure 45: Location of Water Failure Scenario 22

Figure 46: Location of Water Failure Scenario 23

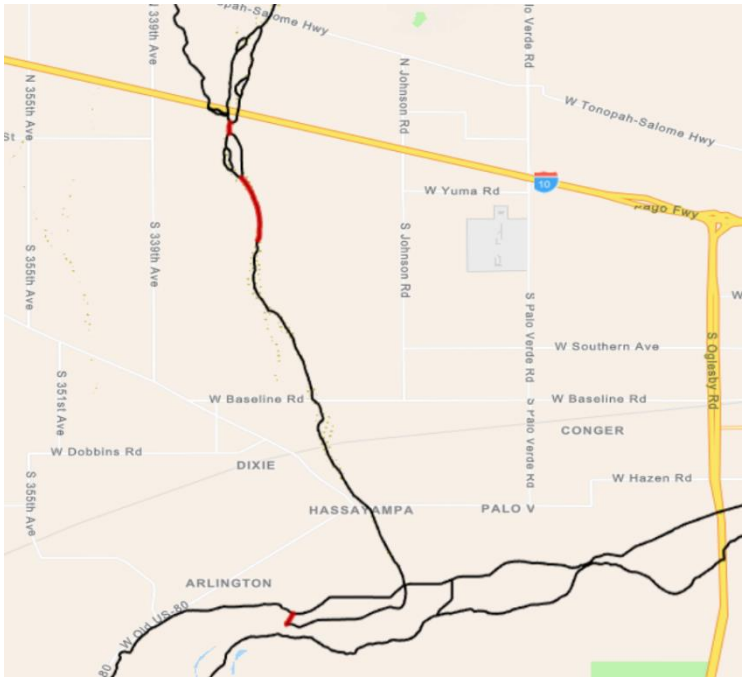

Figure 47: Location of Water Failure Scenario 24

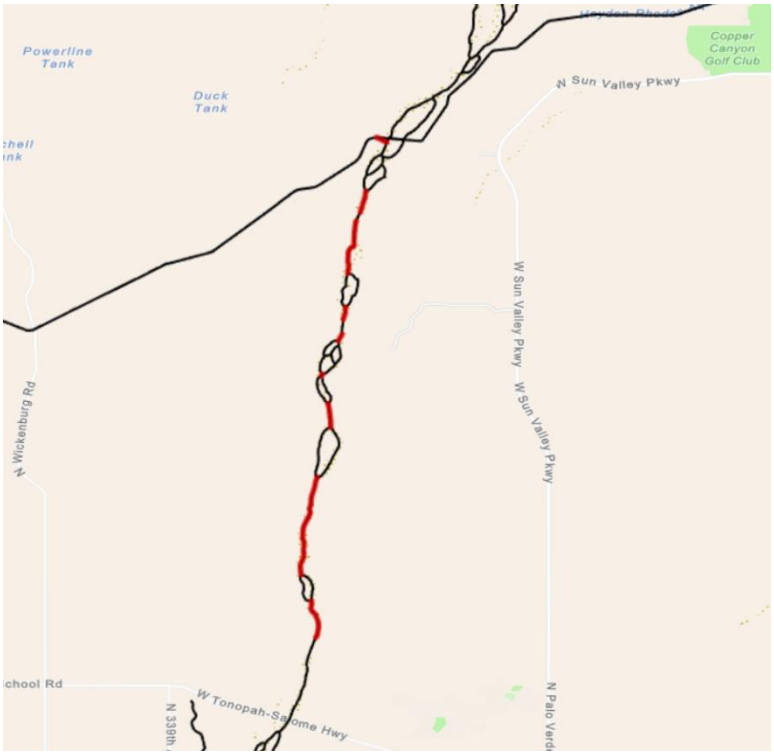

Figure 48: Location of Water Failure Scenario 25

Figure 49: Location of Water Failure Scenario 26

Figure 50: Location of Water Failure Scenario 27

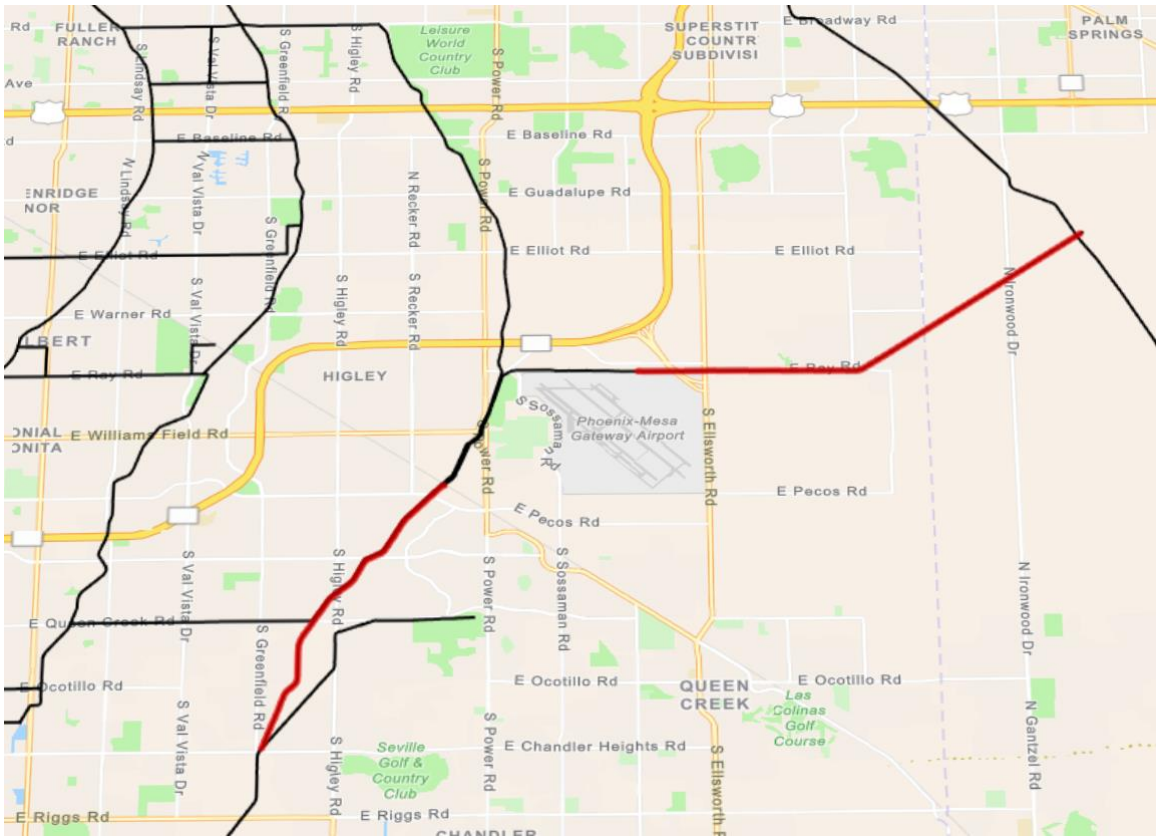

Figure 51: Location of Water Failure Scenario 28

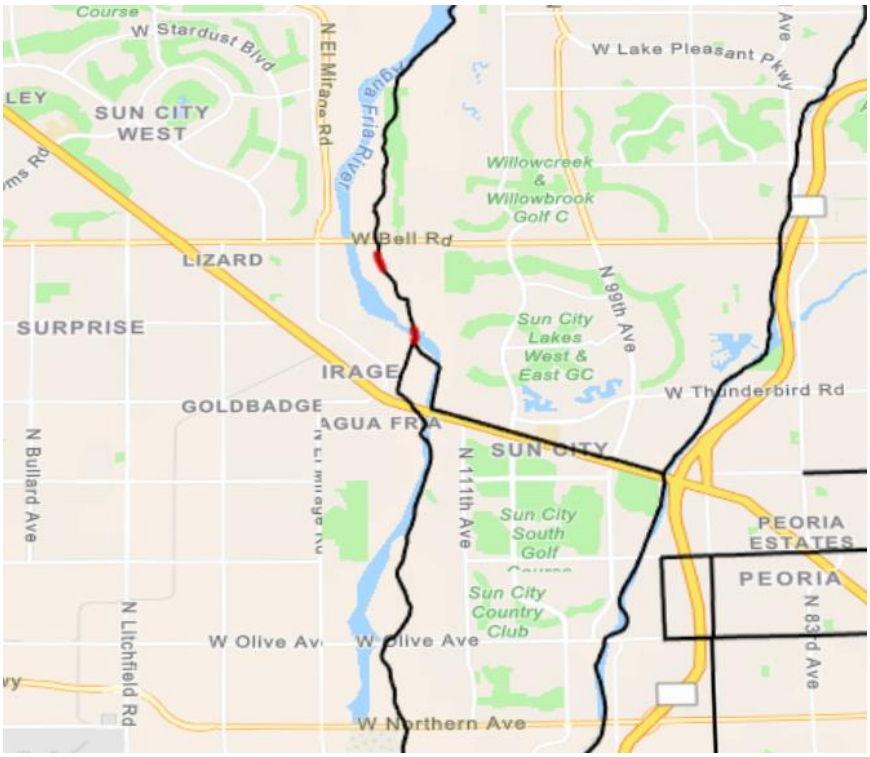

Figure 52: Location of Water Failure Scenario 29

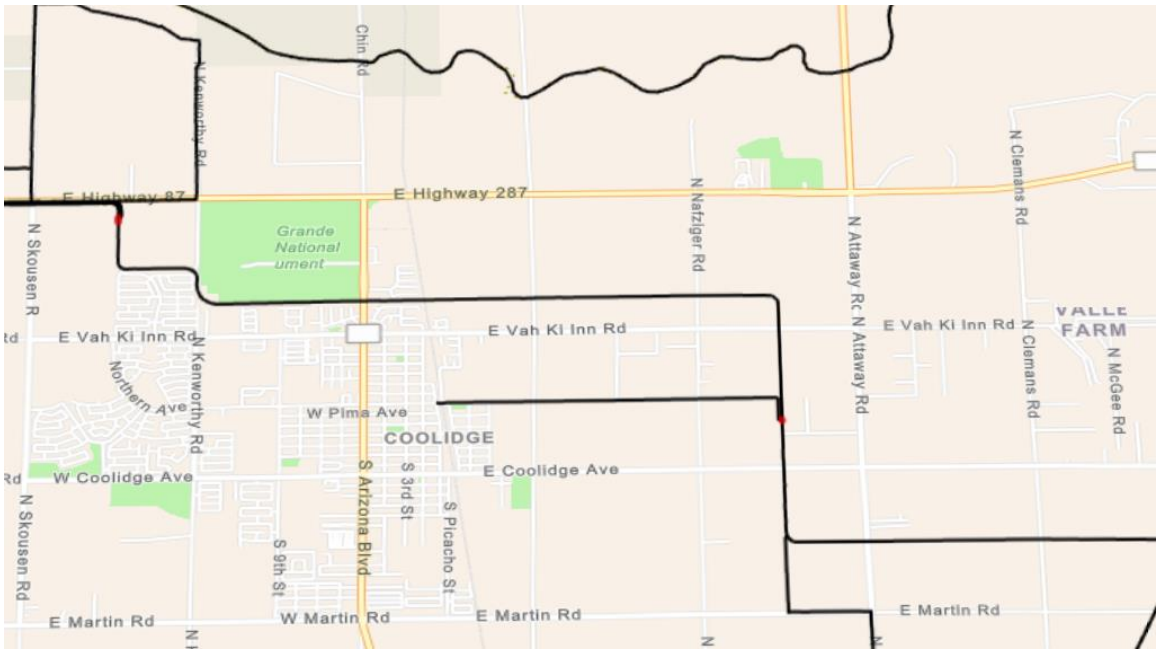

Figure 53: Location of Water Failure Scenario 30

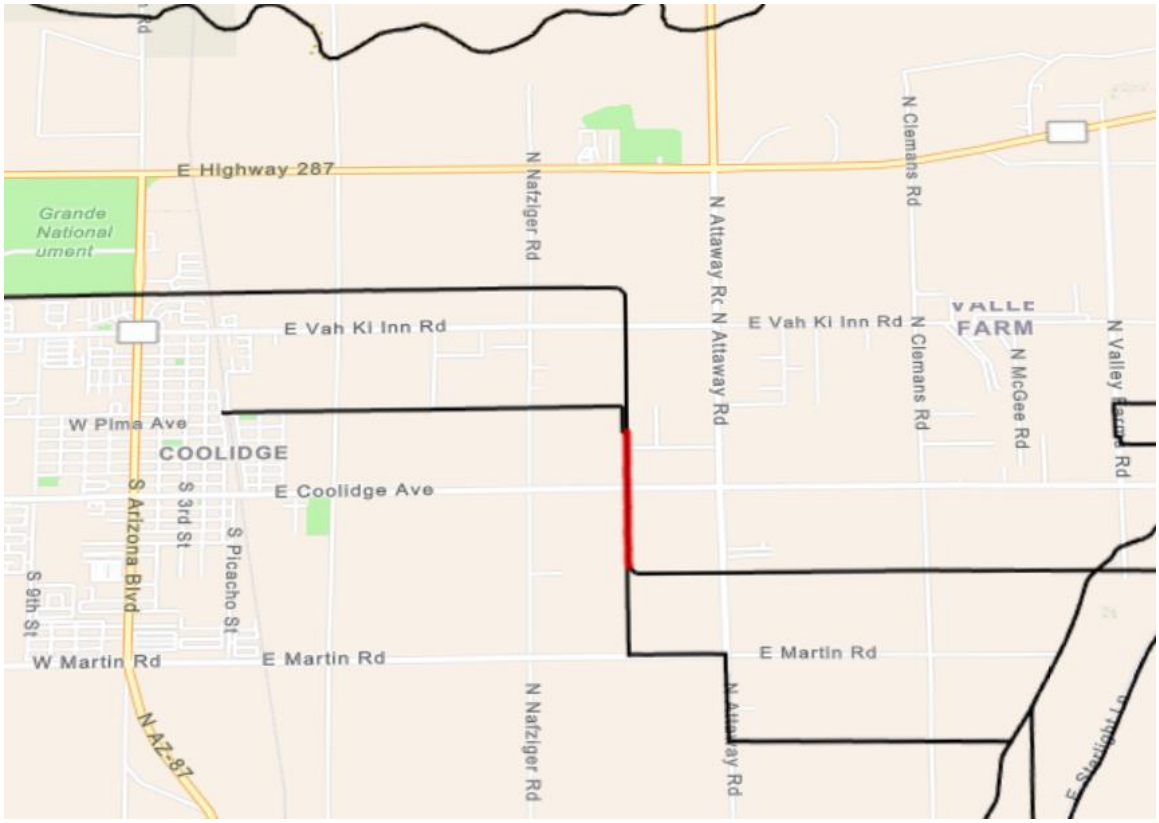

Figure 54: Location of Water Failure Scenario 31

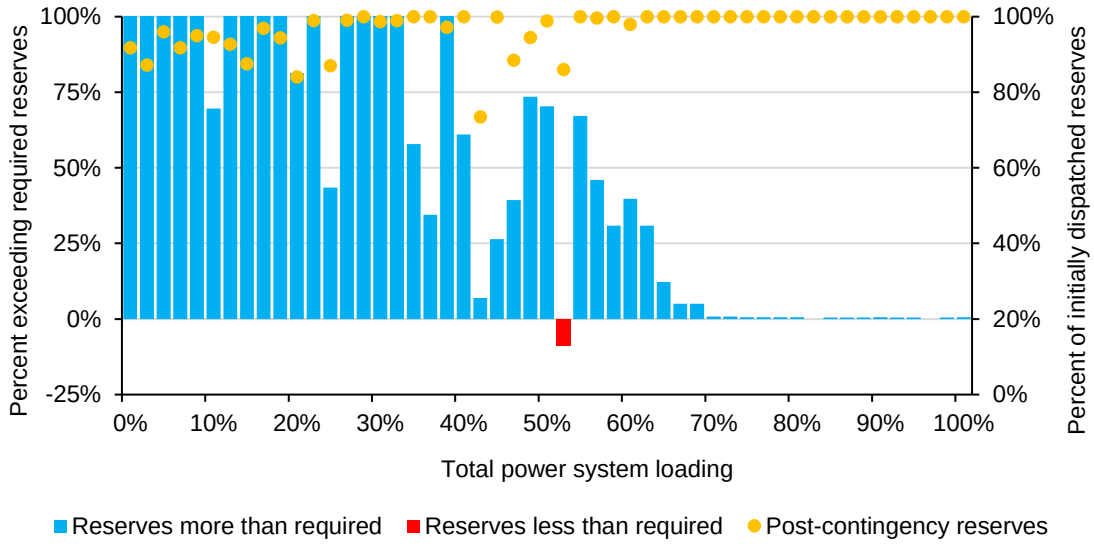

Figure 55: Contingency Reserves During Water Failure Scenario 3 at 100% Water System Demand and Assuming No Fs

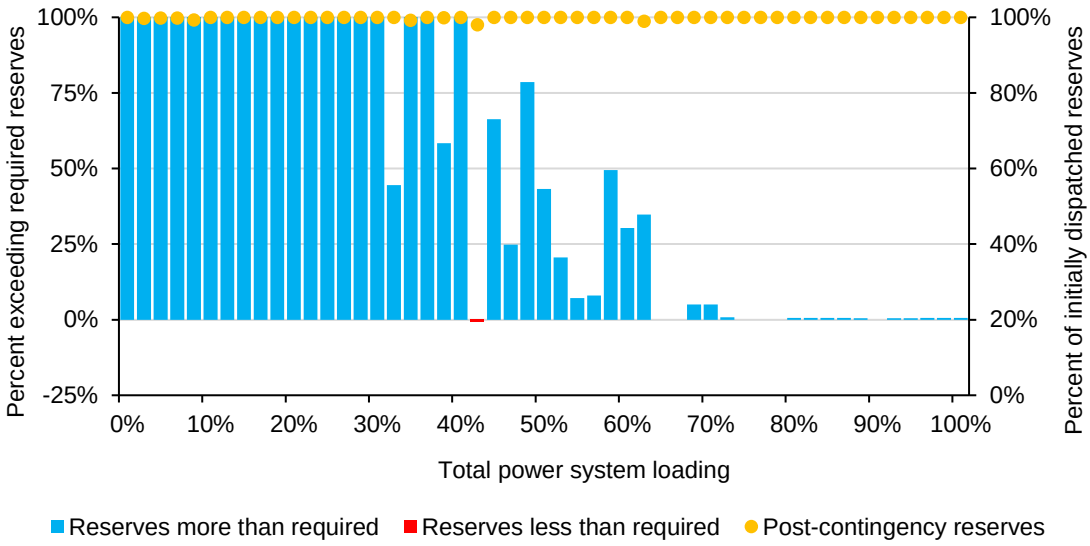

Figure 56: Contingency Reserves During Water Failure Scenario 4 at 75% Water System Demand and Assuming No Fs

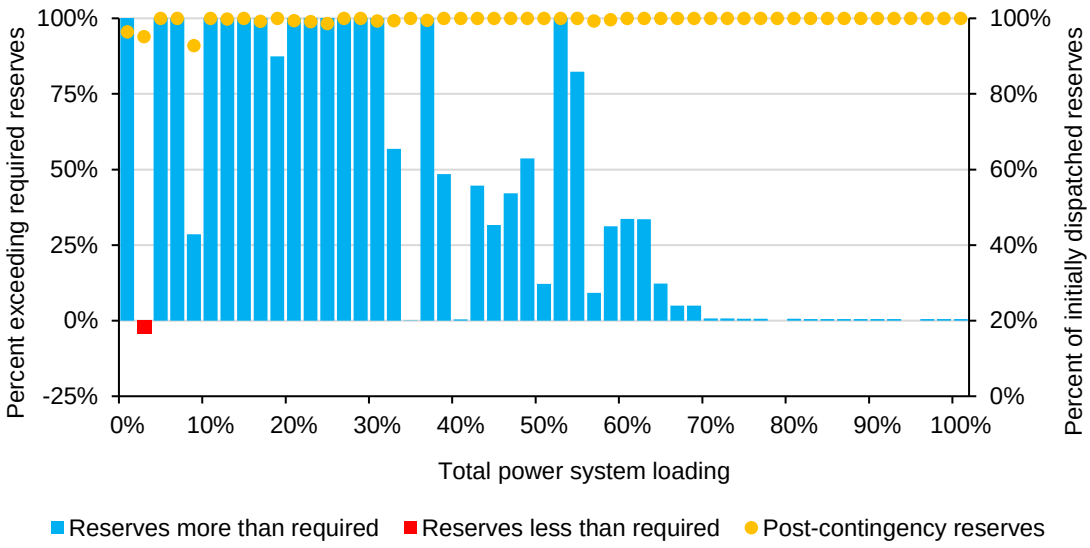

Figure 57: Contingency Reserves During Water Failure Scenario 8 at 100% Water System Demand and Assuming No Fs

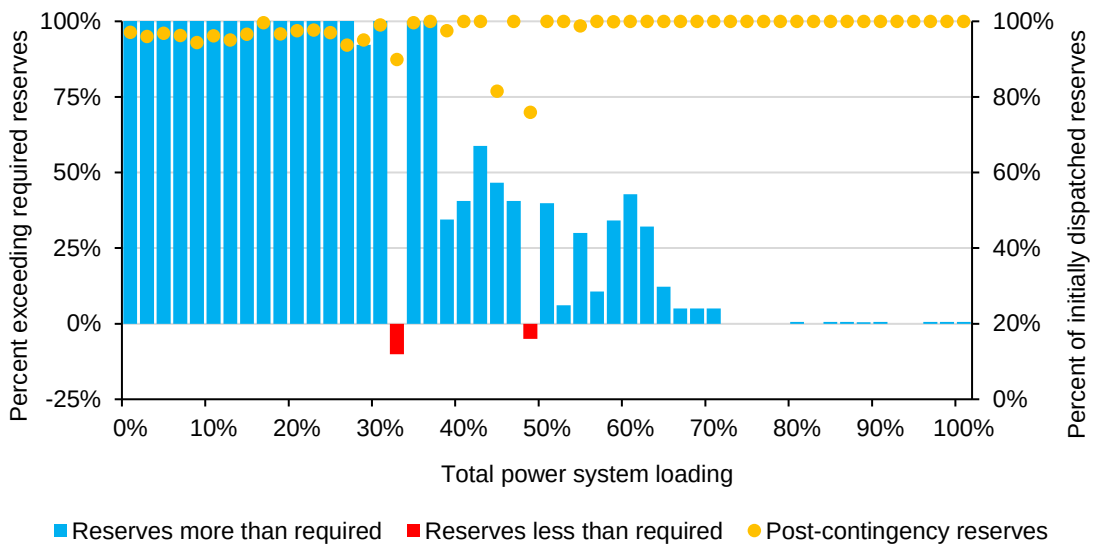

Figure 58: Contingency Reserves During Water Failure Scenario 9 at 75% Water System Demand and Assuming No Fs

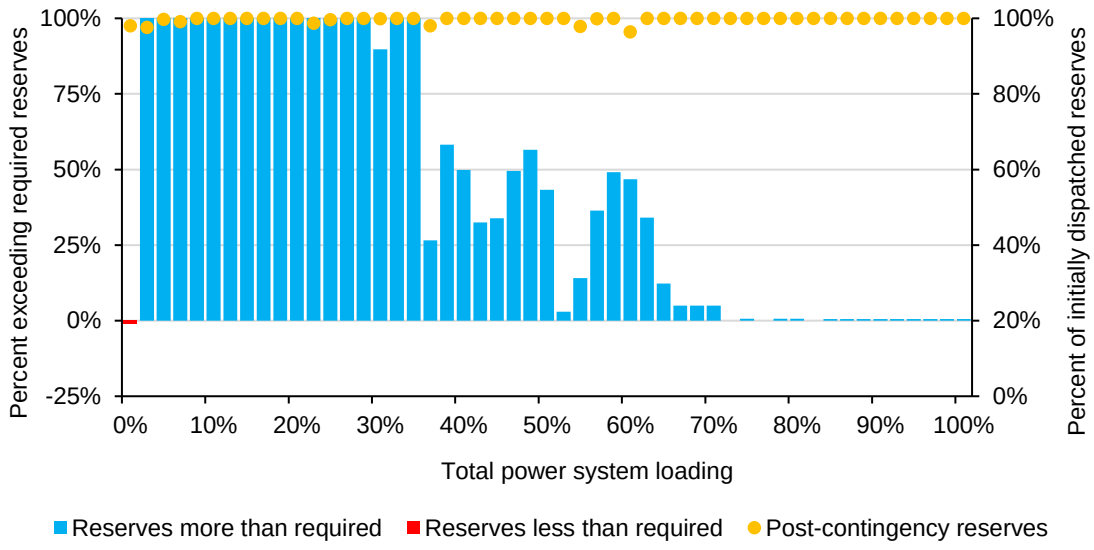

Figure 59: Contingency Reserves During Water Failure Scenario 14 at 75% Water System Demand and Assuming No Fs

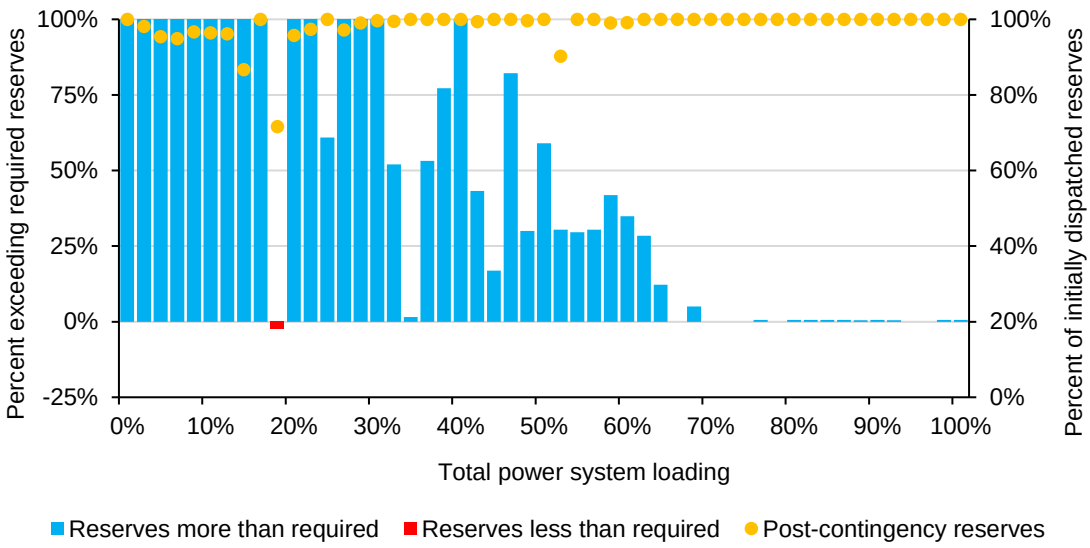

Figure 60: Contingency Reserves During Water Failure Scenario 18 at 100% Water System Demand and Assuming No Fs

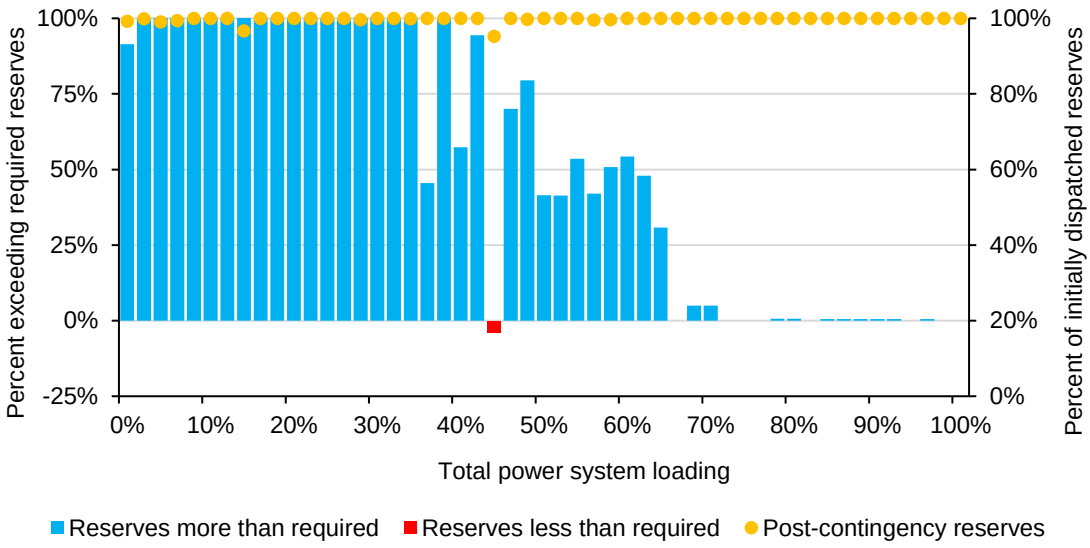

Figure 61: Contingency Reserves During Water Failure Scenario 21 at 50% Water System Demand and Assuming No Fs

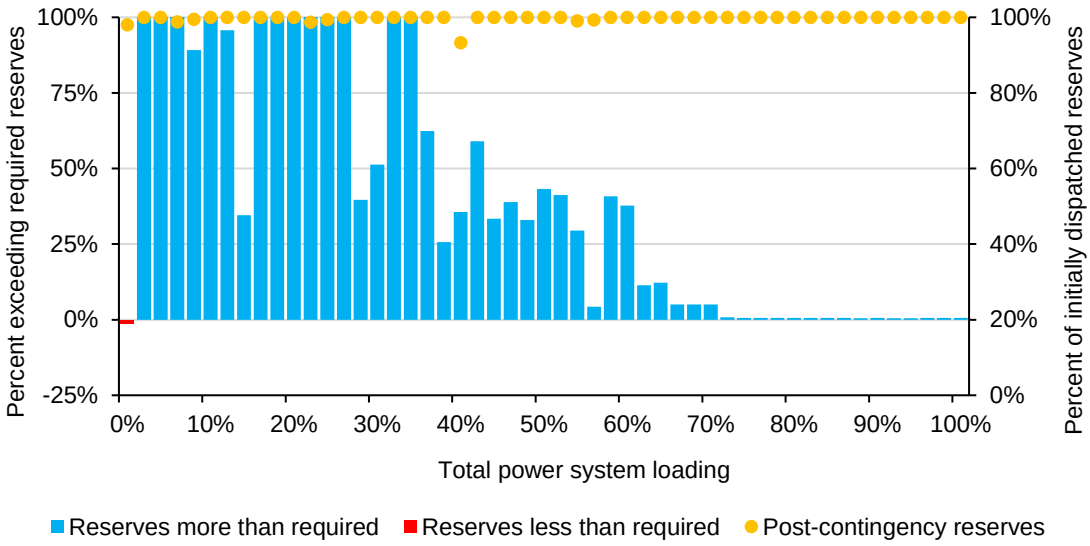

Figure 62: Contingency Reserves During Water Failure Scenario 27 at 75% Water System Demand and Assuming No Fs

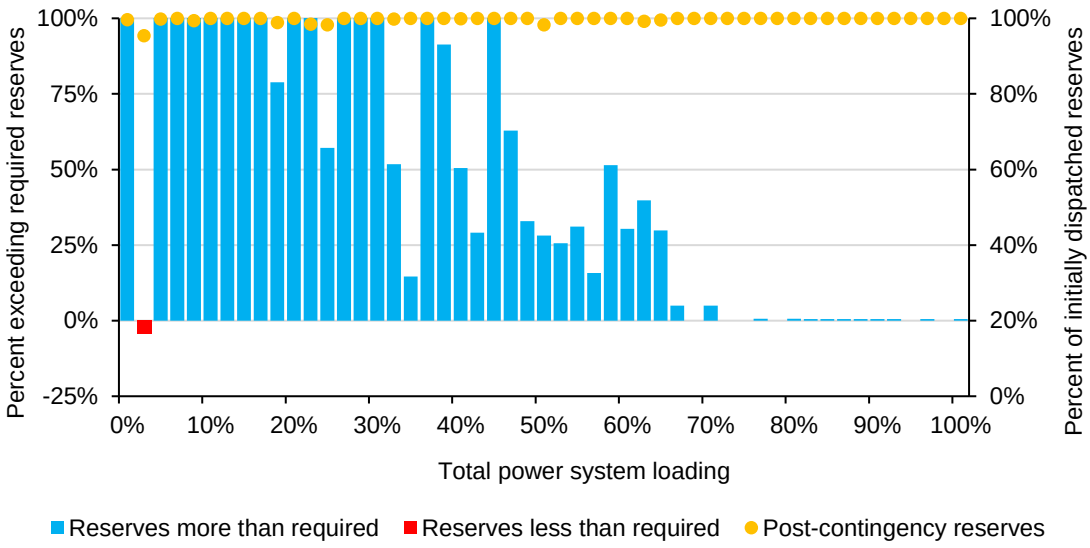

Figure 63: Contingency Reserves During Water Failure Scenario 29 at 50% Water System Demand and Assuming No Fs

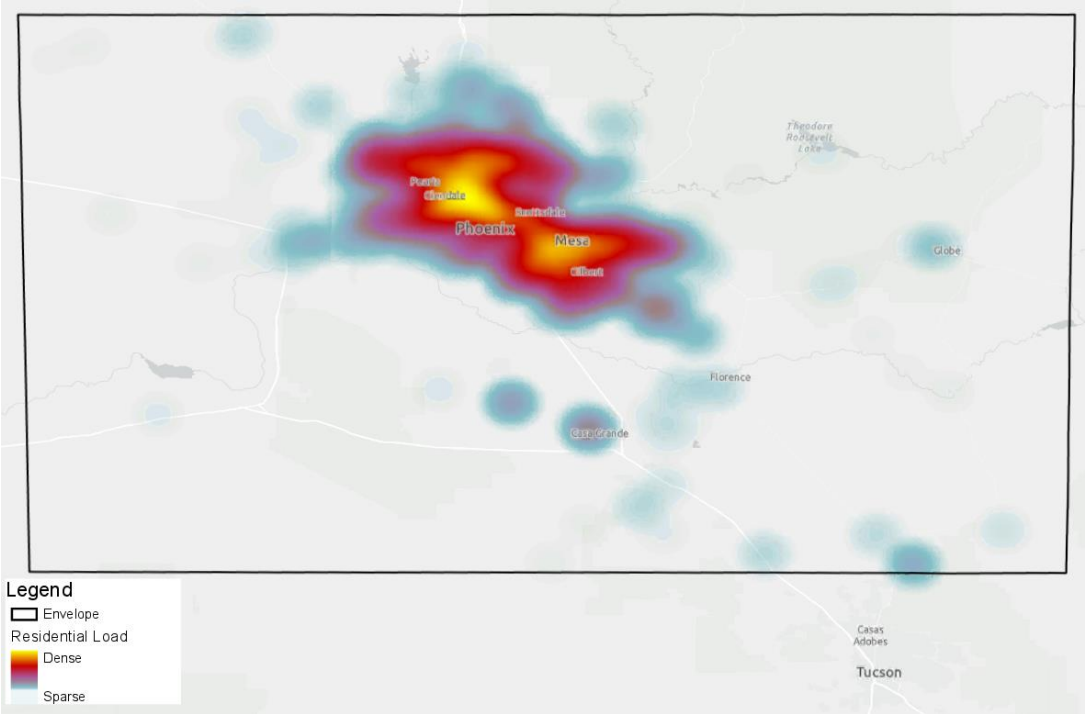

Figure 64: Relative Distribution of Residential Power Load for PMA Substations

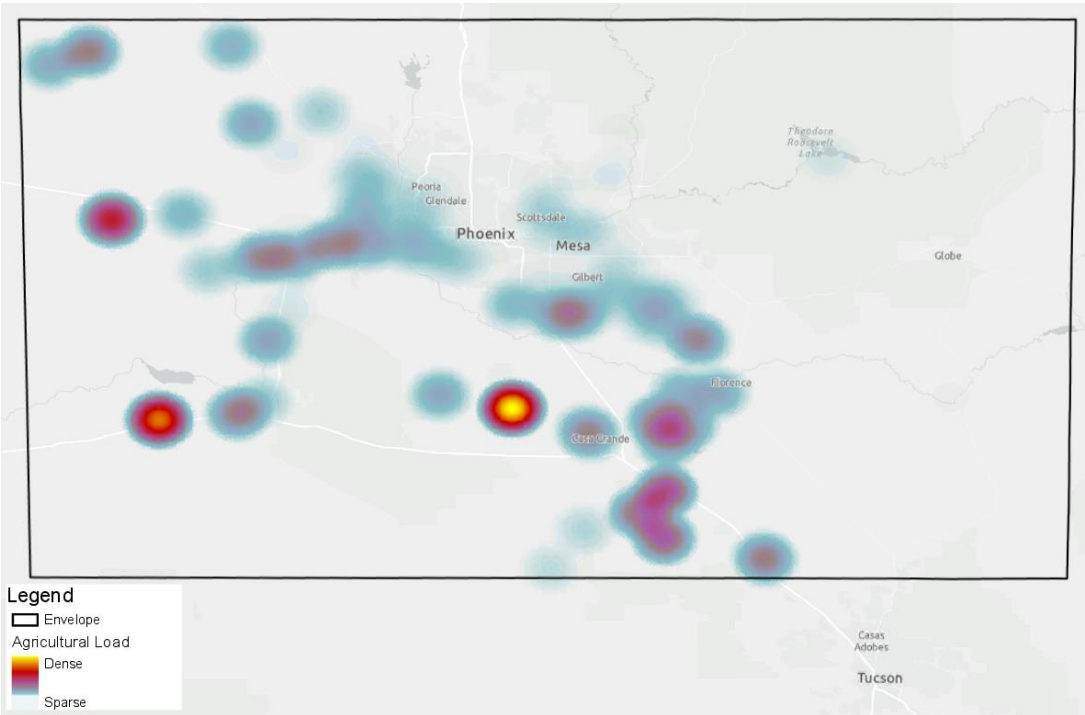

Figure 65: Relative Distribution of Agricultural Power Load for PMA Substations

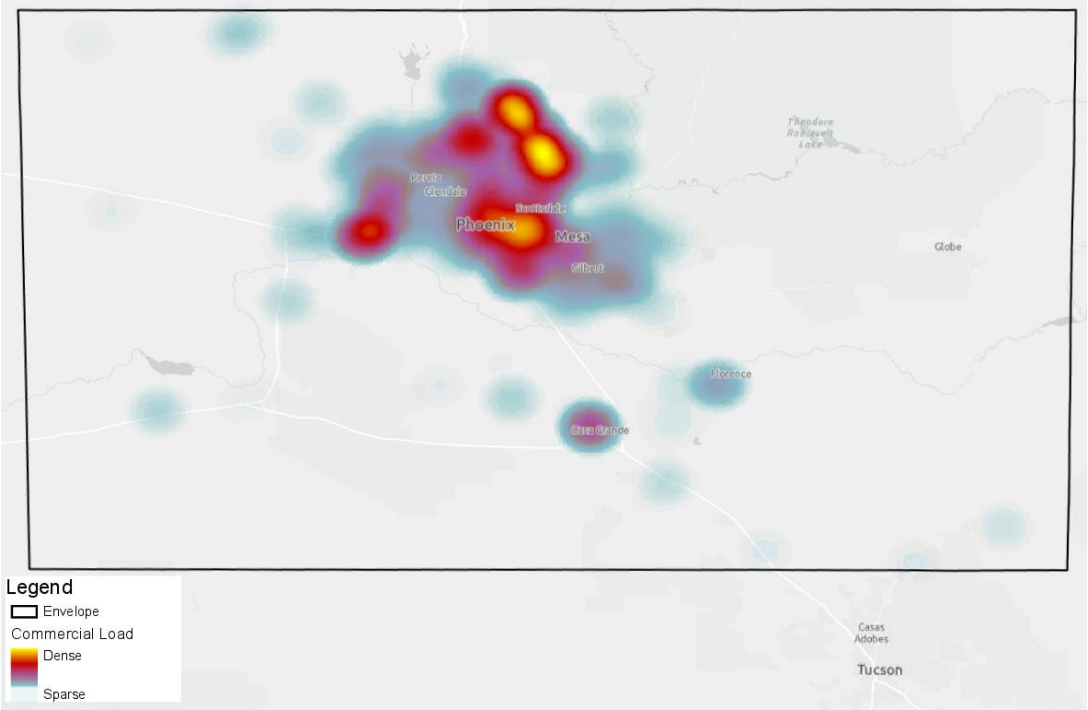

Figure 66: Relative Distribution of Commercial Power Load for PMA Substations

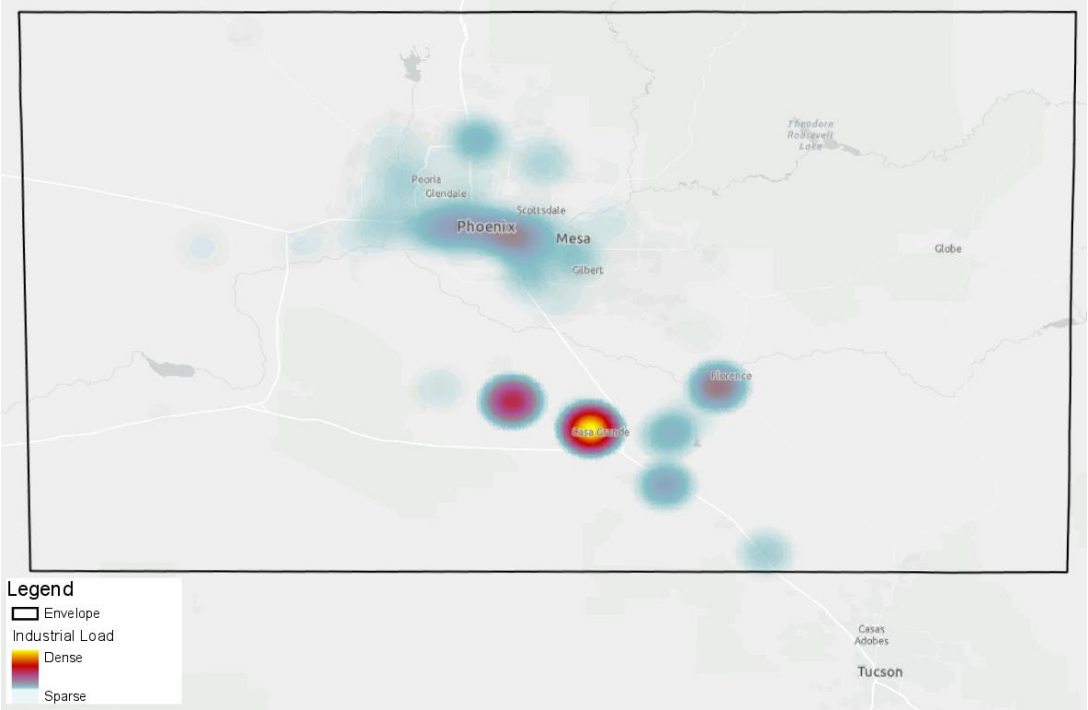

Figure 67: Relative Distribution of Industrial Power Load for PMA Substations

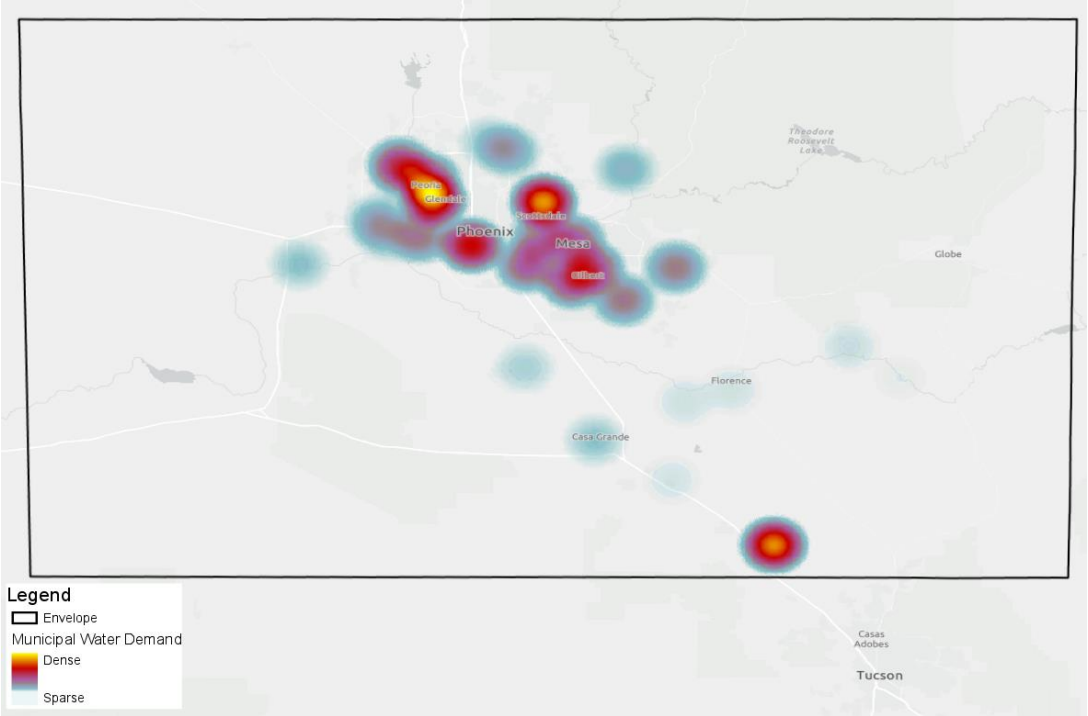

Figure 68: Relative Distribution of Water Demand for PMA Municipalities and Exports to Tucson